

A SOURCE OF POLARISED ELECTRONS FOR THE STUDY OF
POLARISATION EFFECTS IN POLARISED ELECTRON-ATOM
SCATTERING

by

Ian McGregor

Thesis submitted to the University of Stirling
for the degree of Doctor of Philosophy

Physics Department

University of Stirling

Stirling

1974

ABSTRACT

A source of polarised electrons suitable for use in a crossed-beam electron/atom scattering experiment has been built. The electrons were polarised by scattering them elastically from mercury atoms in a crossed-beam experiment. The electron polarisation was investigated for electron energies between 6 eV and 44 eV in the angular range from 30° to 130° . Spin analysis was performed by means of a 100 keV Mott scattering experiment from a gold target at a scattering angle of 120° . The intensity of the polarised electron beam was monitored simultaneously with the polarisation measurements.

A maximum polarisation of $(67.2 \pm 8.2)\%$ was obtained for an incident electron energy of 14 eV at a scattering angle of 95° . However, as a source of polarised electrons, the optimum conditions were obtained when the electron energy was 13 eV at a scattering angle of 95° . Under these conditions an electron polarisation of $(62.7 \pm 8.0)\%$ was measured with an electron current in the alkali interaction region of 3.10^{-12} A.

Comparison with the results of previous theoretical and experimental studies of electron polarisation in low energy scattering from mercury show good agreement with the polarisation values and differential cross-sections.

TABLE OF CONTENTS

CHAPTER 1	PAGE
Introduction	1
CHAPTER 2	
2.1 Sources of Polarised Electrons	7
2.1.1 Mott scattering	9
a) High energy Mott scattering	9
b) Low energy Mott scattering	10
2.1.2 Photoionisation of Alkali Atoms	10
a) Photoionisation of polarised alkali atoms	11
b) Fano effect	12
2.1.3 Spin Exchange	13
2.1.4 Ionisation of Metastable Atoms	14
2.1.5 Resonance Scattering	14
2.1.6 Additional Sources	15
2.2 Electron Spin Analysers	16
CHAPTER 3	
Theory of Electron-Atom Scattering When Spin Effects are Included	18
3.1 Methods of Determining Scattering Amplitudes in Mott Scattering	19
a) Scattering excluding exchange	23
b) Scattering including exchange	27
3.2 Determination of Conditions for Complete Polarisation	27
3.3 Determination of Scattering Amplitudes for Electron Alkali Scattering	29
3.4 Types of Scattering Experiments	31
a) Mott scattering	31
b) Electron alkali scattering	36

CHAPTER 4	PAGE
Triple Scattering Experimental Arrangement	41
4.1 The Design Constraints	42
4.2 The Vacuum System	45
4.3 The Large Turntable	48
4.4 The Small Turntable	49
4.5 The Electron Gun	50
4.6 The Electron Collector	54
4.7 The Mercury Filter Lens System	55
4.8 The Alkali Filter Lens and Injector System	56
4.9 The Mercury Oven	58
4.10 The Mercury Collector	60
4.11 The Temperature Controller for the Mercury Boiler	61
4.12 The Helmholtz Coils	62
 CHAPTER 5	
The Electron Spin Analyser	65
5.1 Mott Scattering Theory As Applied to the Measurement of Electron Polarisation	65
5.2 Experimental Arrangement of Spin Analyser	67
5.3 The Mott Scattering Chamber	68
5.4 The Electron Accelerator	72
5.5 Mounting for Detectors and Foils	74
5.6 The Gold Foil	75
5.7 The Detectors	76
5.8 The Detector Electronics	77
a) Detection and amplification	78
b) Optical telemetry	81
c) Data acquisition system	85

CHAPTER 6	PAGE
Calibration Methods	86
6.1 Optimum Thickness for Gold Foil	86
6.2 The Gold Foil Thickness	87
6.3 Determination of the Sherman Function	88
6.4 Determination of the Angular Settings	90
6.5 The Mercury Beam Density	92
6.6 Determination of the Interaction Energy	94
a) Using the resonance structure in mercury	94
b) Using the 19.3 eV resonance in helium	97
c) Equilibrium between ions and electrons	99
d) Experimental determination of potential depression	100
 CHAPTER 7	
The Measured Asymmetries	103
7.1 Instrumental Asymmetries	103
a) Using low electron energy	105
b) By varying scattering energy	106
c) Using a low-Z scatterer	106
d) Using a thick scatterer	107
7.2 Effect on the Spin of an Electron of a Homogeneous Field	108
7.3 Mercury Filter Lens Performance	110
7.4 Performance of Electron Collector	111
7.5 Linearity of Count Rate with Beam Densities	113
7.6 Flural Scattering Depolarisation	118

CHAPTER 8	PAGE
Results of Polarisation Measurements	121
8.1 The Error in Electron Polarisation Measurements	121
8.2 Differential Cross-Section and Scattered Intensity	126
8.3 Results	128
8.4 Discussion of Results	129
8.5 Determination of Polarised Electron Current	129
8.6 Optimum Operating Settings	130
CONCLUSION	134
Acknowledgements	135
Appendix 1	136
Appendix 2	138
Appendix 3	142
Appendix 4	144
References	146

CHAPTER 1

INTRODUCTION.

From the beginning of this century the importance of the study of the scattering mechanism when two, or more, particles are in collision has been realised. Such studies have developed considerably since then and have provided a fruitful source of the details governing those interactions.

In 1911 Rutherford proposed a model for the atom in which the positive charge and all of the mass is concentrated in a small region called the nucleus. Using this model, a relation between the deflection angle and the scattered intensity of β - particles incident on thin foils could be obtained which was consistent with the experimental results. Since then scattering processes have been used successfully to increase our knowledge of the nature of matter. Such methods have led among others to a better understanding of atmospheric and astrophysical processes.

As the nature of collisions is probed experimentally in greater detail, the comparison with more extensive theories is possible. Experiments are now being designed to investigate spin effects in a collision, and it is necessary that for a full theoretical description spin effects are included.

In the case of electrons scattered from single electron atoms the cross-section is given by

$$\sigma(\theta) = \frac{3}{4} |F_3|^2 + \frac{1}{4} |F_1|^2 \quad (1 - 1)$$

if no spin-orbit effects are considered. The two amplitudes F_3 , triplet, and F_1 , singlet, are a consequence of the Pauli exclusion principle.

There is an equivalent way to describe the collision in terms of the direct and exchange amplitudes. In this form the cross-section is given by (Kleinpoppen, 1971)

$$\sigma(\theta) = \frac{1}{2} |f|^2 + \frac{1}{2} |g|^2 + \frac{1}{2} |f - g|^2 \quad (1 - 2)$$

where f is the direct amplitude, and g is the exchange amplitude. In this form the cross-section is seen as the sum of three terms, each corresponding to a different process.

Using unpolarised atoms and electrons a cross-section measurement produces only a measurement of one of the parameters describing the interaction, viz. the incoherent sum of the different scattering amplitudes given by equations (1 - 1) or (1 - 2).

Another case to consider is when electrons are in collision with heavy atoms and explicitly spin dependent forces play an important role. Here the spin-orbit effect is related to the additional magnetic field which an electron moving in an electric field experiences. This effect although relativistic in origin, exists even when the incident electron is moving at non-relativistic velocities.

The concept of the electron possessing an intrinsic angular momentum, or spin, was first introduced in 1925 to

provide a fourth quantum number which could explain the observed atomic energy levels. It was not however till Dirac developed his relativistic theory, that the existence of the electron spin and its properties emerged in a logically consistent way, as a necessary consequence of the fundamental principles of a relativistic quantum theory.

At this time the spin of the electron had only been observed on electrons bound to atoms, and the question was asked whether it was possible to prepare a beam of polarised electrons. An argument proposed by Bohr (Mott and Massey, 1965, p.215) showed that the Stern-Gerlach method could not be used to produce completely polarised electrons. This is a consequence of the uncertainty principle.

The first definitive prediction that the spin of free electrons could produce an observable effect was given by Mott (1929, 1932). His theoretical investigation of the spin dependence of elastic scattering from heavy nuclei at high energies (greater than 50 keV) showed that an experiment involving two identical scatterings would produce an asymmetry for the number of electrons scattered to the left and to the right at the second scattering. It was not for a further fourteen years before this was shown experimentally to be the case.

The degree of polarisation of an electron beam is defined by equation (1- 3) :

$$P = \frac{N_{\uparrow} - N_{\downarrow}}{N_{\uparrow} + N_{\downarrow}} \quad (1 - 3)$$

N_{\uparrow} and N_{\downarrow} correspond to the number of electrons which have their spins aligned in the direction parallel, and anti-parallel, respectively, to a given quantisation axis.

The aim of this thesis is to build up an apparatus which could be used to investigate spin effects in collision experiments between electrons and one electron atoms. An intense beam of polarised electrons at low energy is produced by cross-firing a beam of mercury atoms with a low energy (less than 50 eV) electron beam. Spin analysis of the primary scattered electron beam is performed using Mott scattering at high energy (100 keV). (The design of the apparatus used is fully discussed.)

The polarisation of the electrons is investigated over the angular range of 30° to 130° and at various energies from 6.5 eV to 44 eV. This provides a calibration of the polarised electron source and identifies the optimum operating conditions. To this end, calibration of the Mott spin analyser is also carried out.

With an electron beam of known polarisation then available, the proposal was to scatter the polarised electrons from polarised hydrogen atoms. This was later changed, and an atomic alkali beam will be used instead. The main reason for this is the ease in producing an intense alkali beam. It has also recently been shown (Drukarev and Ob'edkov, 1971) that on theoretical grounds hydrogen is not as promising as the alkalis for a study involving exchange processes. An experiment to scatter a polarised electron beam from a polarised potassium beam is at present underway using the apparatus described here.

This experiment can be characterised by three competing processes. Shown below are the cases when both beams are completely polarised either parallel or anti-parallel with each other.

- (1) $e(\uparrow) + A(\uparrow) \rightarrow e(\uparrow) + A(\uparrow)$ (f - g) or (F_3)
interference
or triplet scattering
amplitude
- (2) $e(\uparrow) + A(\downarrow) \begin{cases} \rightarrow e(\uparrow) + A(\downarrow) & (f) \text{ direct scattering} \\ & \text{amplitude} \\ \rightarrow e(\downarrow) + A(\uparrow) & (g) \text{ exchange} \\ & \text{scattering amplitude} \end{cases}$

A relative measure of the triplet amplitude can be obtained even when the two beams are not completely polarised.

In the next chapter the reasons for choosing low energy Mott scattering, from a mercury beam, is discussed. This is followed by an explanation of the choice of high energy Mott scattering, from a gold foil, as the spin analyser. In chapter III the matrix formalism is shown in the context of polarisation. It is used to determine the types of experiments which can be carried out. This follows a discussion of the theoretical models used in low energy scattering from mercury.

In chapters IV and V the experimental arrangement is fully discussed, with the calibration procedures and values required for the mercury scattering process and the spin analyser being evaluated in chapter VI. The cross-section results and polarisation values obtained over an energy range of up to 44eV are given and compared with theoretical values and results of other experimental groups where applicable.

In the conclusion the settings for optimal polarisation conditions are given. Further improvements are suggested.

It should be noted that the polarisation measurements entail a double scattering experiment and can be classified as "difficult" because of the problems associated with small intensities. On the otherhand the cross-section measurements which only require a single scattering can be classified as "easy".

CHAPTER 11

2.1 SOURCES OF POLARISED ELECTRONS.

The idea of producing a beam of polarised electrons has been considered ever since the electron spin was first proposed in 1925. The first method which proved successful was when electrons with an energy of 400 keV, were scattered through 90° , from thin gold foils (Shull, Chase and Myers, 1943). Since then other sources of polarised electrons have been discovered.

Two categories of polarised electron sources exist. In the first, electrons bound to an atom (possibly in a solid), can be prepared in a specific spin state, and a process which allows them to be released still in their well defined spin state is used to produce a beam. Such sources include ionisation of polarised atoms and field emission from ferro-magnetic materials. In the second, unpolarised electrons undergo an interaction in which preferential selection of electrons in a definite spin state is allowed. Also in this category is the situation where the initially random population of spin states is converted to one in which one of the spin states dominates. These sources include elastic scattering in a coulomb field where spin-orbit coupling introduces a spin dependence and exchange scattering from a polarised atom beam. The usefulness of any source depends on the operational requirements imposed on it.

An electron beam with polarisation P and a current I corresponds to a completely polarised beam current I_{eff} given by

$$I_{\text{eff}} = I P^2$$

The initial beam of energy E_0 , minimum beam radius r and an angular spread θ , must pass through a lens system which can only pass electrons with an energy of E (or less). Such a beam has a maximum effective brightness given by

$$B_{\text{eff}} = \frac{P^2 I E}{r^2 (\theta)^2 E_0} \quad (2 - 1)$$

From this it can be seen that E/E_0 should be as large as possible. Since the source is to be used for low energy alkali scattering (<10 eV), the brightness falls off rapidly with increasing source energy. This is purely a result of electron optics.

Also from electron optics, Raith (1969) shows that electrons produced in a strong axial magnetic field will take up skewed trajectories if they are used outside of this field, and vice versa. Since the final experiment requires a low magnetic field the ideal source will not involve a strong magnetic field.

Some of the more successful methods shall be reviewed briefly here, with attention paid to the electron energy and the presence of large magnetic fields. For other reviews on the subject see Marago (1965), Raith (1969), Messler (1969), and Jost (1972).

2.1.1. MOTT SCATTERING.

This method can also be split into two types. The first, originally proposed by Mott (1929, 1932) and verified by Shull, Chase and Myers (1943) is high energy scattering from heavy atoms. The second was a proposal by Massey and Mohr (1941) that polarisation effects should also appear in low energy scattering processes. This was shown to be the case by Deichsel (1961), when he elastically scattered electrons of low energy (1 - 2 keV) from atomic beams of mercury in a double scattering experiment and observed an asymmetry, which was dependent on electron energy and scattering angle.

Since these early experiments at both low and high energies, much progress has been made towards producing a usable polarised electron beam by these methods.

2.1.1.(a) HIGH ENERGY MOTT SCATTERING.

Considerable development has gone into this method, especially with a view to developing an efficient and reliable analyser of the degree of polarisation of a transversely polarised electron beam. One instance of it being used for a source of polarised electrons is described by Van Duinen and Alders (1968), who scattered a primary unpolarised electron beam (of 50 μA) with an electron energy of 261 keV from a 300 $\mu\text{g}/\text{cm}^2$ gold foil supported on a 200 $\mu\text{g}/\text{cm}^2$ aluminium backing. Using a scattering angle of 105° , a

transversely polarised beam of 1.5nA was obtained which had a polarisation of 30%. This polarised electron source was in fact used in the only experiment in which a triple scattering process has been studied.

2.1.1. (b) LOW ENERGY MOTT SCATTERING.

Since the first measurements of Deichsel (1961), further results have been obtained, and almost the entire range has been covered from 3 eV up to several keV, for electrons elastically scattered from mercury. These results are discussed in review articles by Kessler (1969) and by Eckstein (1970). The polarisation can change rapidly from positive to negative and can reach very high values at particular scattering angles if the angular resolution is small enough (85% with an angular resolution of $\pm 1^\circ$, Jost & Kessler, 1966). The polarisation always occurs near minima in the cross-section (Buhring, 1968).

One of the best conditions being obtained for electrons of energy 6.75 eV scattered elastically from mercury at a scattering angle of 95° . An electron beam with a 27.5 degree of polarisation at an electron current of about 10 nA has been obtained (Milners, Haug & Deichsel, 1969).

2.1.2. PHOTOIONISATION OF ALKALI ATOMS.

As early as 1930 a proposal to produce polarised electrons by photoionisation from polarised alkali atoms was put forward. The photoionisation process of an

alkali atom is predominantly an electric dipole transition from the $n_0^2 S_{\frac{1}{2}}$ ground state to a continuum $P_{\frac{1}{2}, \frac{3}{2}}$ state. As has been emphasised recently, the complete theory of alkali photoionisation must also take into account the spin orbit perturbation (Fano, 69A, 69B) of the continuum P state.

This results in two different approaches to the problem. One method uses polarised alkali atoms and unpolarised light, and the other, known as the Fano effect, uses unpolarised alkali atoms and circularly polarised light.

2.1.2 (a) PHOTOIONISATION OF POLARISED ALKALI ATOMS.

That this effect produces longitudinally polarised electrons was verified conclusively by Long, Raith and Hughes in 1965. It has been extensively studied since then, with the aim of producing a prototype injector of polarised electrons for a high energy accelerator (see Hughes, Long, Lubell, Posner & Raith, 1972, Corifet, 1967, and Baum & Koch, 1969).

A beam with a polarisation of 78% in 1.5 μ s pulses containing 2×10^8 electrons has been produced using a polarised Li^6 beam and a UV light source. The alkali beam is polarised by passing it through a hexapole magnet. Afterwards the beam undergoes an adiabatic transition to a longitudinal magnetic field of 100 gauss in the ionisation region. The light source was a high voltage spark discharge between tungsten electrodes in an atmosphere of argon or xenon. The maximum pulse rates were 10 per second. A high pressure Xe - Hg arc lamp was used as a continuous

source of a UV radiation, but the photoelectron current was reduced to about 6×10^7 electrons /sec. The electrons were extracted from the ionisation region by an anode at 100 keV potential.

Polarised electrons were also produced using the same apparatus from polarised potassium atoms. However, the maximum current using a continuous radiation source was a factor of ten lower than with lithium. The electron polarisation obtained with potassium is also reduced giving a value of 58% electron polarisation.

2.1.2. (b) FANO EFFECT.

In 1969 Fano published a theory which included spin orbit effects for the photoionisation of electrons from alkali atoms (in particular cesium atoms). He predicted, that the photoelectrons could have a large degree of polarisation ($> 85\%$) even when the alkali atom is unpolarised if circularly polarised light is used for the ionisation process. The wavelength of the light should correspond to the wavelength region in the vicinity of the Cooper minimum (Cooper, 1962) in the photoionisation cross-section. This is because it is near minima in the ionisation cross-section that the difference in ionisation probability for electrons of opposite spin is significant. (c.f. Mott scattering, section 2.1.1.)

The group at Yale university, by looking at the ions produced, confirmed the general predictions of Fano. (Lubell & Raith, 1969, Baum, Lubell & Raith, 1972). The

polarisation of the electrons was determined shortly afterwards by Kessler & Lorenz, (1970) (see also Heinzmann, Kessler & Lorenz 1970 (a), 1970(b)) thus giving complete confirmation to the proposal of Fano. In this experiment a mercury high pressure arc lamp was used in conjunction with a caesium atomic beam. The photoelectrons were extracted with a weak electric field ($\sim 10\text{V/cm}$) in a direction at right angles to the two incident beams. An average polarisation of 81% was obtained with currents of $3 \times 10^{-11}\text{A}$. Extraction voltages of about 400V were used with a field penetration system to reduce the number of background electrons.

Baum, Lubell & Raith, (1971) have also detected a polarisation of 65% with a current of about 10^{-9}A .

Both methods of photoionising alkali atoms can produce comparable electron currents and polarisations. The first method uses a pulsed source whereas the second utilises a continuous source.

2.1.3. SPIN EXCHANGE

Electrons are trapped for up to 20 ms by a combination of an electrostatic potential well (1.8 V deep) and a uniform magnetic field (10mT). A beam of polarised potassium atoms passes along the axis of the electron trap, allowing an exchange interaction to occur, with the atomic beam polarisation exponentially being transferred to the trapped electron cloud. Polarisation of the electron beam of up to 50% has been detected with a current

of about 10^{-13} A at electron energies of about 1 eV. (Campbell, Brash & Farago 1971, 1972 and Farago & Siegmann 1969).

2.1.4. IONISATION OF METASTABLE HELIUM.

A source of polarised electrons obtained from an optically pumped helium discharge is described by McCusker, Hatfield & Walters (1969, 1972).

In this source, a conventional helium optical pumping apparatus is used, consisting of a cell containing gas subjected to an electrical discharge, irradiated by polarised 1.08μ . ($2^3S - 2^5P$) resonance light. The cell was however, modified by attaching a base plate through which the electrons could be extracted. A magnetic field of 5 gauss in the direction of the incident light was applied to provide a unique quantisation axis. The electrons, which were extracted with voltages on the extraction plates of about 2000 V, were longitudinally polarised. The maximum polarisation detected was 10% with currents of $0.2 \mu A$ although under different conditions a polarisation of 8% at currents of up to $4 \mu A$ could be detected. A polarisation value of 17% was detected for electrons extracted in the late afterglow of a pulsed discharge. This source has a large energy distribution in the beam (10eV).

2.1.5. RESONANCE SCATTERING.

It has been shown theoretically that appreciable

polarisation effects can exist in the neighbourhood of resonances due to spin orbit effects. Franzen & Gupta (1965) did an analysis for neon in the vicinity of the resonance at about 16 volts.

Reichert & Deichsel (1967) (see also Heindorff, Höfft, & Reichert, 1973) confirmed the presence of polarisation effects in the vicinity of the resonance.

For resonance effects to be significant the energy resolution must be very good, thus the electron currents are small but the angular acceptance can be quite large with only a slight degradation on the polarisation peaks.

2.1.6. ADDITIONAL SOURCES.

Other sources which can yield a polarised beam are field and photo-emission from solids. With field emission a polarisation of 18% at 10 to 100 nA has been obtained from poly-crystalline tungsten tips cooled to 80°K with magnetic fields up to 25 kilogauss. (Regenfus & Sutsh, 1974). In the case of photo-emission up to 20% polarisation at 10 nA has been reached from thin films of ferromagnets evaporated on to a liquid helium cooled surface. A mercury xenon arc is used in conjunction with large electric and magnetic fields for the release of the electrons (Busch, Campagne & Siegmann, 1970, 1971).

Both of these methods above have been developed out of an interest in the band structure in solids rather than as sources of polarised electrons.

Two other sources are β -decay from radio-active substances (usually low intensities and high energies) and electron - electron Møller scattering (very energetic electrons).

It can be seen that of the sources available only low energy Mott scattering and the Rano effect present a good value for the brightness. At the start of this experiment the Rano effect had just been proposed so its feasibility in this context could not be considered. Low energy Mott scattering has the additional advantage in that it is possible to make it compact, allowing easier rotation about the alkali beam axis (see following chapter).

2.2. ELECTRON - SCATTER ANALYSIS.

The most widely used technique for the measurement of the degree of electron polarisation is high energy Mott scattering. Low energy Mott scattering has also been used. Use has also been made of electron - electron (Møller) scattering in studies of β -decay electrons but requires extremely high energies ($\geq 1\text{MeV}$).

The fall of parity conservation gave great impetus to high energy Mott scattering, and it is well understood both theoretically and experimentally. It is normally used with electrons of energies in the range 50 keV - 1 MeV and requires foils (usually of gold) to be thin to ensure that depolarisation effects do not dominate the process. The overall detection efficiency can be made fairly large

(0.01%). A thorough study has been made of this type of analyser by Van Klinken (1965).

Low energy (300 eV) scattering from mercury has been used by a group at Mainz University for spin analysis. They have developed a compact analyser using an atmosphere of mercury (Gehenn, Haug, Wilmers & Deichsel, 1969) as well as a more conventional analyser using a mercury beam (Deichsel, Reichert & Steidl, 1966).

Mott scattering is sensitive to transverse polarisation only, but in connection with spin rotators, longitudinal polarisation can be measured as well.

It can be seen from equation (2 - 1) that although low energy Mott scattering may be useful for the production of polarised electrons, high energy Mott scattering is better as a spin analyser.

A high energy Mott scattering method was chosen for the spin analyser since a considerable study has already been made of it. Calibration of its analysing power can rely on values confirmed by experiment and theory, without requiring further extensive study as would be the case in low energy scattering. The instrumental asymmetries can be checked upon with relative ease in the high energy case, but are more difficult to detect in low energy scattering. A disadvantage is however the high voltage at which the detection electronics must be floated.

CHAPTER III

THEORY OF ELECTRON - ATOM SCATTERING WHEN SPIN
EFFECTS ARE INCLUDED.

A considerable amount of theoretical effort has gone into the evaluation of scattering theories which are able to predict correctly changes in the polarisation state of the interacting partners. The present state of these theories is surveyed, in particular for scattering from mercury and gold.

The quantities which can be observed, before and after scattering, and their relationship are dealt with using the Stokes vectors. This enables a description of the different interactions involving spin to be considered independently of the detailed form of the scattering amplitudes.

3.1 METHODS OF DETERMINING THE SCATTERING AMPLITUDES IN MOTT SCATTERING.

Detailed information about a scattering process can be obtained once the scattering amplitudes are known (see section 3.4). To include spin effects explicitly in the calculation of the scattering amplitudes the relativistic Dirac equation is used. This is necessary even when the electron energy is only a few eV, due to the important role played by spin-orbit coupling. The spin-orbit interaction of an electron with a field of electrostatic potential $V(r)$ is given by

$$V_{so} = \frac{\hbar}{m^2 c^2 r} \left(\frac{dV}{dr} \right)$$

For a low energy electron incident on a neutral atom the importance of V_{so} increases rapidly with Z .

Less sophistication has been used with relativistic calculations, when compared with their non-relativistic counterparts, due to the greater complexity of the system. For each non-relativistic state there is in general two relativistic angular momentum states, and for each of those a coupled pair of equations must be solved. In addition, for heavy atoms there is a greater possibility for electron exchange to occur. The electron is regarded as being scattered by a central electrostatic potential, chosen to include the nuclear charge and possible screening by the atomic electron cloud. The distortion of the electron by the incident electron and electron exchange may also be included.

The wave function ψ which describes the scattered electron beam has four components ψ_λ , $\lambda = 1 - 4$. The asymptotic forms of the two large components of ψ_λ are given by

$$\left. \begin{aligned} \psi_3 &\sim e^{ikz} + \frac{e^{ikr}}{r} f_1(\theta, \phi) \\ \psi_4 &\sim \frac{e^{ikr}}{r} g_1(\theta, \phi) \end{aligned} \right\} A$$

$$\left. \begin{aligned} \psi_3 &\sim \frac{e^{ikr}}{r} g_2(\theta, \phi) \\ \psi_4 &\sim e^{ikz} + \frac{e^{ikr}}{r} f_2(\theta, \phi) \end{aligned} \right\} B \quad (3-1)$$

for the two cases when the electron spin is aligned parallel (A) and anti-parallel (B) with the direction of motion (along the z-axis). f_1, f_2 and g_1, g_2 are the scattering amplitudes to be determined.

The equation governing the elastic scattering of an electron by an atom such as mercury, which consists of closed shells*, is given by†

$$(H_1 - E + V)\psi - W - X = 0 \quad (3-2)$$

where H_1 is the one electron Dirac hamiltonian

$$H_1 = ic\underline{\alpha} + \beta c^2 - \frac{Ze^2}{r}$$

* Closed shells refer to an atom which when specified by quantum numbers n, j, s , has all possible states in a group filled. The three quantum numbers shall be denoted by the letter A.

† The convention $\hbar = m = 1$ is used here.

with

$$\underline{\alpha} = \begin{pmatrix} 0 & \underline{\sigma} \\ \underline{\sigma} & 0 \end{pmatrix}, \underline{\sigma} \text{ are the } 2 \times 2 \text{ Pauli spin matrices}$$

$$\underline{\beta} = \begin{pmatrix} \text{I} & 0 \\ 0 & \text{I} \end{pmatrix}, \text{I is the unit } 2 \times 2 \text{ matrix.}$$

E is the energy of the incident electron with the contribution to the potential from the atomic electrons given by

$$V = \sum_A \int \phi_A^*(r_2) \frac{e^2}{r_{12}} \phi_A(r_2) dr_2$$

with ϕ_A denoting the bound state wave function.

The exchange term is given by

$$W = \sum_A \phi_A(r_1) \int \phi_A^*(r_2) \frac{e^2}{r_{12}} \psi(r_2) dr_2$$

and the last term X is a function representing any lack of orthogonality between the scattered wave functions and the bound state wave functions. For a unique set of solutions, the wave functions are usually taken to be orthogonal, so X is zero, and this is ensured throughout the calculations.

The one electron wave functions can be represented by central field wave functions of the form

$$\psi = \begin{pmatrix} i \frac{P(r)}{r} \chi_{k,m} \\ \frac{Q(r)}{r} \chi_{-k,m} \end{pmatrix} \quad (3-3)$$

where $\chi_{\pm k, m}$ are angular momentum state eigenfunctions with $k = -(j + \frac{1}{2})a$, j is the total angular momentum and $a = \pm 1$ on substituting equation (3 - 3) into equation (3 - 2) a coupled pair of equations for the radial components of the scattered wave function can be obtained.

$$\left. \begin{aligned} \frac{dP_k}{dr} + \frac{kP_k}{r} + \frac{1}{c} (E + V(r) + c^2) Q_k &= W_Q(r) \\ \frac{dQ_k}{dr} - \frac{kQ_k}{r} - \frac{1}{c} (E + V(r) - c^2) P_k &= -W_P(r) \end{aligned} \right\} (3 - 4A)$$

where $V(r)$ is the screened potential of the atom.

These equations are subject to the asymptotic condition that for large r

$$\lim_{r \rightarrow \infty} \left(\frac{P_k}{r} \right) \longrightarrow j_1(kr) \cos \delta_1^\pm - n_1(kr) \sin \delta_1^\pm$$

Here δ_1^\pm is the scattering phase shift for the given values of l and a and $j_1(kr)$ and $n_1(kr)$ are the spherical Bessel and Neumann functions respectively.

Other large Z atoms such as gold ($Z = 79$) have been treated similarly for large interaction energies even though they do not form closed groups. The potential in such cases has been taken as the unscreened coulomb potential with exponential screening terms added, rather than using a Hartree potential.

a) Scattering Excluding Exchange.

The case where exchange is not of critical importance shall be considered first (energies greater than 500 eV).

Here $w_Q = 0 = w_p$ in equation (3 - 4A)

(this is later referred to as equation (3 - 4B)) and it can, by eliminating $Q(r)$ and letting

$$P(r) = \eta^{1/2} G(r), \quad \eta = (E + V + c^2)/c^2$$

be reduced (Mott and Massey, 1965, p 227) to

$$\frac{d^2 G}{dr^2} + (k^2 - \frac{1(1+1)}{r^2} - U_k(r)) G(r) = 0 \quad (3 - 5)$$

$$U_k(r) = \frac{2E}{c^2} V - \frac{V^2}{c^2} + \frac{k\eta'}{r\eta} + \frac{1}{2} \frac{\eta'^2}{\eta} - \frac{1}{2} \frac{\eta''}{\eta}$$

Equation (3 - 5) is of the same form as the non-relativistic Schrödinger equation but is dependent on the incident electron energy and spin. Numerical integration methods are required to solve equation (3 - 5) from which the phase shifts are determined.

For energies high enough that the atom can be considered as a bare nucleus, Mott (1929, 1932) obtained by a suitable combination for ψ_3 and ψ_4 in equation (3 - 1)

$$\begin{aligned} f_1(\theta, \vartheta) &= f_2(\theta, \vartheta) = f(\theta) \\ g_1(\theta, \vartheta) &= g(\theta) e^{i\vartheta} \quad \text{and} \quad g_2(\theta, \vartheta) = -g(\theta) e^{-i\vartheta} \end{aligned}$$

with

$$\begin{aligned} f(\theta) &= \frac{1}{2ik} \sum_{l=0}^{\infty} [(1+1)(\exp(2i\delta_1^+) - 1) \\ &\quad + 1(\exp(2i\delta_1^-) - 1)] P_l(\cos \theta) \\ g(\theta) &= \frac{1}{2ik} \sum_{l=1}^{\infty} [\exp(2i\delta_1^-) - \exp(2i\delta_1^+)] P_l'(\cos \theta) \end{aligned} \quad (3 - 6)$$

where $P_1(\cos \theta)$ and $P_1'(\cos \theta)$ are the Legendre and associated Legendre polynomials respectively. Equation (3 - 5) has been used by Holtzwarth and Meister (1964) for electron scattering from gold and mercury atoms in the energy range from 200 eV to 290 keV.

Other transformations such as

$$P_k = A_k \cos \delta_k$$

$$Q_k = A_k \sin \delta_k$$

have been used in equation (3 - 4B) by Lin, Sherman and Percus (1963), and Lin (1964) for high energies and by Bunyan and Schonfelder (1965) and Schonfelder (1966) for scattering between 1 keV and 2 keV.

Buhring (1965, 1968) has expressed equation (3 - 4B) as a power series, so that the errors in the solution are associated with the accuracy of the summation, rather than being dependent on the method of numerical integration as in above methods. Results for mercury at energies of 46 keV to 204 keV are in excellent agreement with those in Lin (1964) whilst disagreeing to some extent with those of Holtzwarth and Meister (1964).

For low energies the sum in equation (3 - 6) is truncated and only a few partial waves are considered. However at high energies many terms must be included and used (Walker, 1971) to speed convergence. In the case of fast electrons, the atom is essentially a bare nucleus and the slow decrease of the coulomb potential with distance modifies the asymptotic form of the function P_k and the phase shifts can be calculated explicitly.

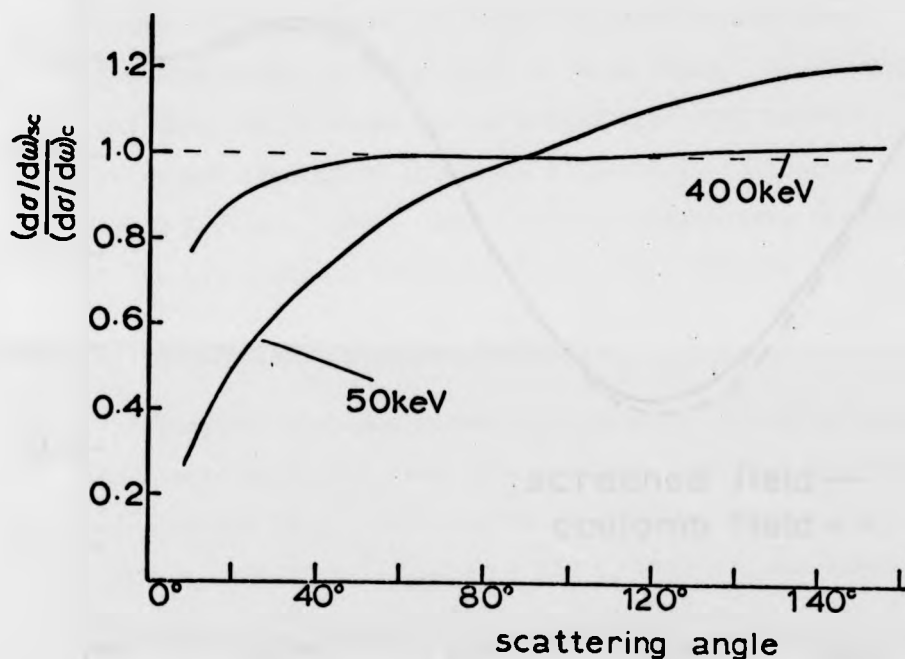


Figure 1. The effect on the differential cross-section when screening of the gold nucleus is included. Incident electron energy of 50 keV & 400 keV. (Lin, 1964)

In equation (3 - 2) the screening of the nucleus was included and the importance of this term can be seen in Figure 1 where the results for scattering from gold at energies of 50 keV and 400 keV are shown for the unscreened coulomb field and for the screened coulomb field. It may be seen that screening is most important at smaller angles, but is of lesser importance as the energy is increased. From Figure 2, which depicts the polarisation value with a screened and with an unscreened potential, the agreement is good even at 50 keV. Thus the differential cross-section is much more sensitive to screening than is the polarisation effect.

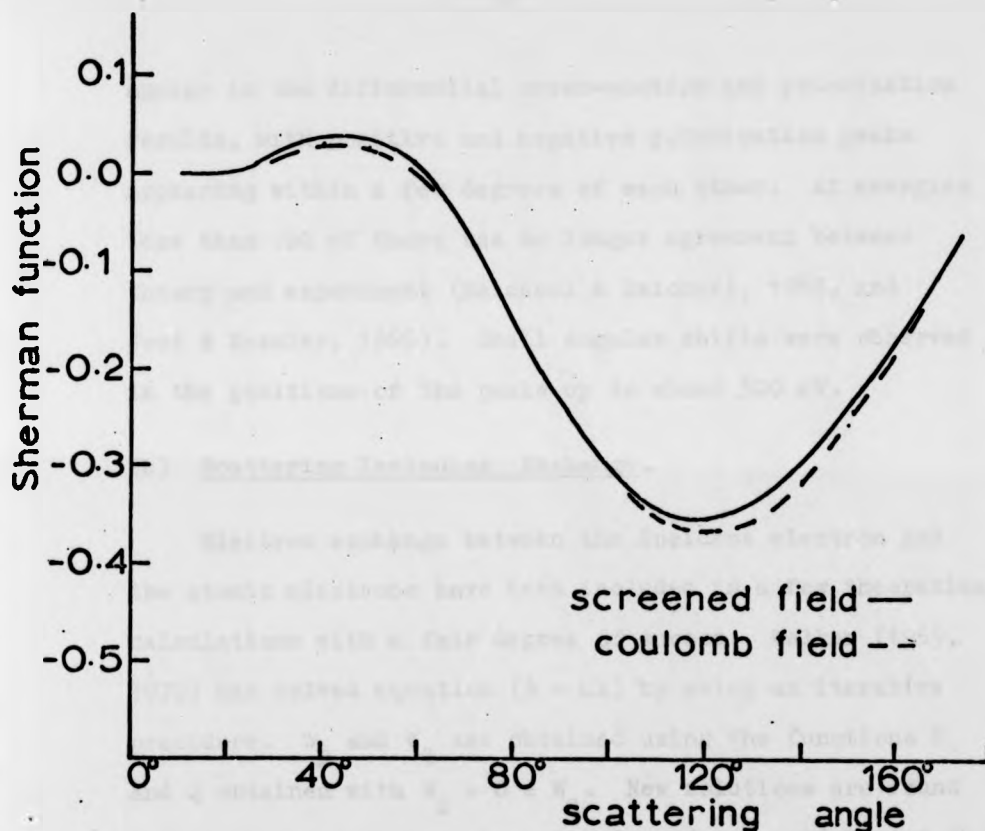


Figure 2. The effect on the Sherman function when screening of the gold nucleus is included. Incident electron energy of 50 keV (Lin, 1964).

It was noted by Massey and Mohr (1941) and Mohr and Tassie (1954) that polarisation effects were to be expected at low electron energies as well as at high energies. Several authors have studied interactions with energies less than 3 keV, and shown that fair agreement with experiment could be obtained at least to about 100 eV. (Bunyan, 1963, Bunyan & Schonfelder, 1965, Schonfelder, 1966, Holtzworth and Meister, 1964, and Buhning, 1968).

At these low energies considerable structure did

appear in the differential cross-section and polarisation results, with positive and negative polarisation peaks appearing within a few degrees of each other. At energies less than 100 eV there was no longer agreement between theory and experiment (Deichsel & Reichert, 1965, and Jost & Kessler, 1966). Small angular shifts were observed in the positions of the peaks up to about 500 eV.

(b) Scattering Including Exchange.

Electron exchange between the incident electron and the atomic electrons have been included in a few theoretical calculations with a fair degree of success. Walker (1969, 1970) has solved equation (3 - 4A) by using an iterative procedure. W_p and W_q are obtained using the functions P and Q obtained with $W_p = 0 = W_q$. New solutions are found for P and Q using the improved values for W_p and W_q and the process repeated until W_p and W_q converge. Good agreement has been obtained by this method with experiment down to energies of 25 eV, except in the peaks, before significant discrepancies appear. A contour plot of polarisation values obtained as above is shown in Figure 3.

3.2 DETERMINATION OF CONDITIONS FOR COMPLETE POLARISATION.

Total polarisation ($P = \pm 1$) may be expected where the complex scattering amplitude $f(Z)$ is zero (Buhning, 1968). At this position minima in the differential cross-section will occur. Expressions for the maximum (and minimum) polarisation and their position can be obtained from functions of the complex scattering amplitudes, which are

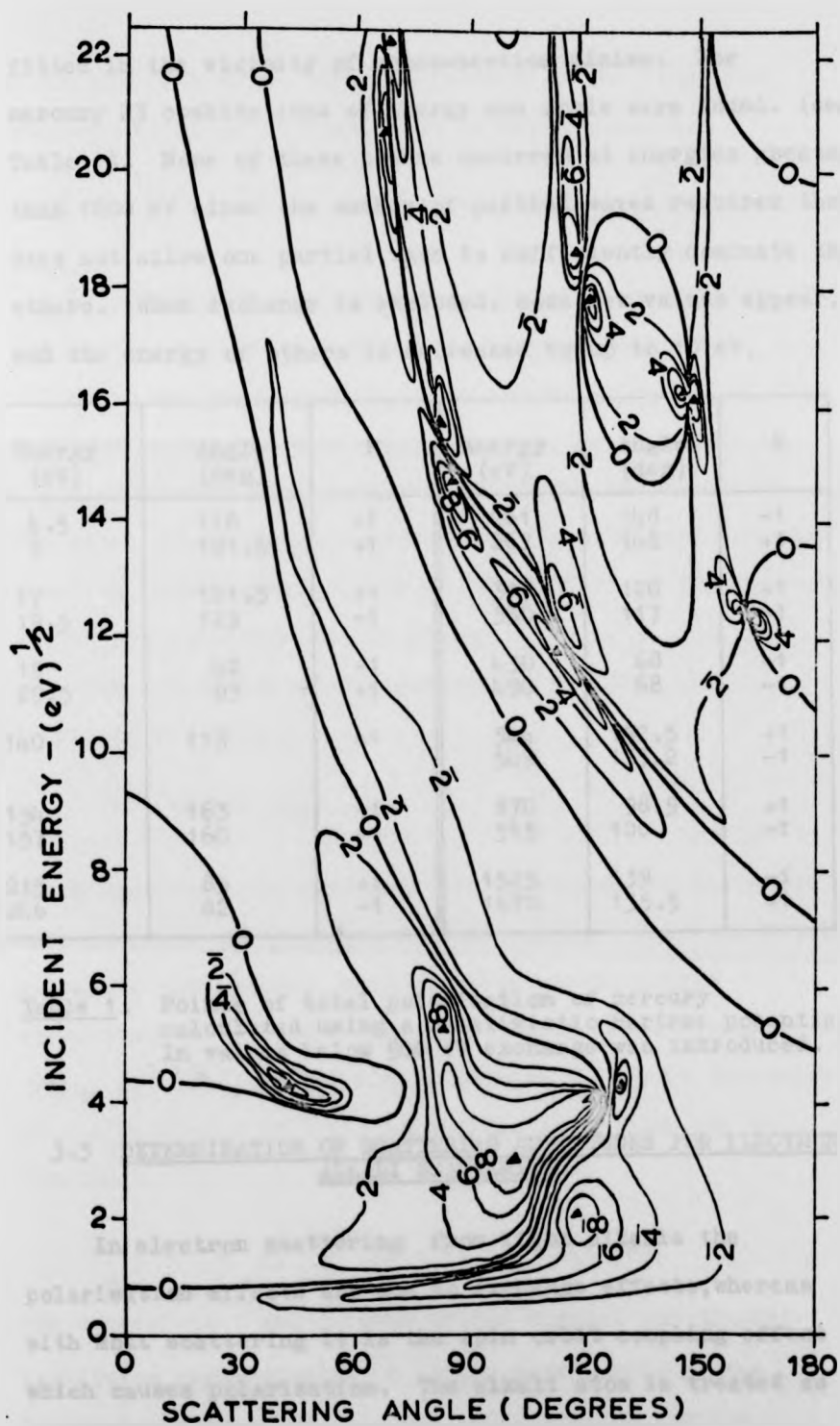


Figure 3. A contour plot of polarisation against angle and energy. Contours in intervals of $P = 0.2$ (Walker 1971).

fitted in the vicinity of cross-section minima. For mercury 23 combinations of energy and angle were found. (see Table 1). None of these points occurred at energies greater than 1800 eV since the number of partial waves required then, does not allow one partial wave to sufficiently dominate the others. When exchange is excluded, some new values appear, and the energy of others is decreased by up to 10 eV.

Energy (eV)	Angle (deg)	P	Energy (eV)	Angle (deg)	P
4.5	118	-1	261	148	-1
9	101.5	+1	267	146	+1
17	121.5	+1	317	120	+1
19.5	129	-1	350	117	-1
19	42	-1	430	68	+1
29.5	83	+1	490	68	-1
140	113	+1	544	152.5	+1
			549	153.2	-1
154	163	+1	870	98.5	+1
157	160	-1	915	100	-1
215	85	+1	1525	139	-1
246	82	-1	1670	135.5	+1

Table 1. Points of total polarisation of mercury calculated using a relativistic Hartree potential. In values below 500 eV exchange was introduced.

3.3 DETERMINATION OF SCATTERING AMPLITUDES FOR ELECTRON ALKALI SCATTERING.

In electron scattering from light alkalis the polarisation effects are due to exchange effects, whereas with Mott scattering it is the spin orbit coupling effect which causes polarisation. The alkali atom is treated as

a one electron atom. The Hamiltonian of the atom plus incident electron is considered as being given by

$$H = -\frac{1}{2} \nabla_1^2 - \frac{1}{2} \nabla_2^2 + V(r_1) + V(r_2) + \frac{e^2}{r_{12}}$$

The first two terms represent the kinetic energies of the atomic and incident electrons respectively, the following two terms represent the potential energy of each electron in the field of the atom, and the last term is the electrostatic interaction between the two electrons. The total orbital angular momentum, the total spin angular momentum, their z-components and the parity of the combined system are constants of the motion.

For a solution of the scattering problem, the "Schrodinger equation

$$(H - E) \psi(\underline{r}_1, \underline{r}_2) = 0$$

which describes the system of both electrons by the exact wave function $\psi(\underline{r}_1, \underline{r}_2)$, must be solved. E is the total energy of the system. This equation can be solved approximately by considering a few terms in an expansion for $\psi(\underline{r}_1, \underline{r}_2)$, and the transition matrix, T, may be determined. From a knowledge of T the scattering amplitudes may be obtained:

$$F_{1,3}(\theta) = \frac{1}{2k} \sum_1 (2l + 1) T_{l,3}^{1,3} P_l(\cos\theta)$$

The subscripts 1 and 3 refer to the singlet and triplet amplitudes respectively. k is the wave number of the incident electron and l is the total orbital angular momentum.

Using a four state (3s - 3p - 4s - 3d) close coupling method, Moores and Norcross, (1972) have obtained the singlet and triplet amplitudes for elastic and inelastic scattering from sodium. A variational calculation for scattering of electrons from lithium, sodium and potassium (Sinfallam & Nesbet, 1973), at energies below the first excitation threshold, is in good agreement with a two state (3s - 3p) close coupling calculations of Norcross (1971), and the four state close coupling calculations of Moores & Norcross (1972) for sodium.

3.4 TYPES OF SCATTERING EXPERIMENTS.

In appendix I relations between the Stokes vectors, the polarisation components and the scattering intensity have been outlined. This matrix formalism will now be used to demonstrate what effects can be expected from an electron scattering experiment. Initially the case of Mott scattering, which is the subject matter of this thesis, is treated and afterwards the method is illustrated when applied to electron scattering from a one electron atom. This illustrates the useful experiments which can be done with a beam of polarised electrons.

a) Mott Scattering.

The form of the asymptotic solutions of Dirac's wave function can be written in the general form for arbitrary spin direction as (cf., equation (3 - 1)).

$$\psi_{\lambda} = b_{\lambda} e^{ikz} + \frac{e^{ikr}}{r} u_{\lambda}(\theta, \varphi) \quad (\lambda=1-4)$$

and if only the two large components of this function are

considered

$$\left. \begin{aligned} u_3(\theta, \vartheta) &= Af(\theta) - Bg(\theta) \exp(-i\vartheta) \\ u_4(\theta, \vartheta) &= Bf(\theta) + Ag(\theta) \exp(i\vartheta) \end{aligned} \right\} (3-7)$$

with $f(\theta)$ and $g(\theta)$ defined in equation (3-6).

From equation (3-7) the scattering matrix, M , can be obtained (Mott and Massey, 1965, p250).

$$M = \begin{pmatrix} f & -ge^{-i\vartheta} \\ ge^{i\vartheta} & f \end{pmatrix} \quad (3-8)$$

The transfer matrix, T , of the Stokes vectors (see appendix I) in polarisation space is given by (Byrne, 1971, McMaster, 1961)

$$T = \begin{pmatrix} U & 0 & 0 & V \\ 0 & R & -S & 0 \\ 0 & S & R & 0 \\ V & 0 & 0 & U \end{pmatrix} \quad (3-9)$$

where

$$\begin{aligned} U &= |f|^2 + |g|^2 & V &= -i(f^*g - g^*f) \\ R &= |f|^2 - |g|^2 & S &= fg^* + f^*g \end{aligned}$$

In the determination of the above matrix the scattering centre is considered as the origin of the co-ordinate system. The 1 - axis of this co-ordinate system is defined by the wavevector, \underline{k} , of the incident electron. The 3 - axis is defined as being normal to the scattering plane and the 2 - axis is such as to form an orthogonal triad. Representing the scattered electron direction with the wavevector \underline{k}' gives

$$\begin{aligned}
 \underline{e}_1 &= \underline{k} / |\underline{k}| \\
 \underline{e}_3 &= \underline{k} \times \underline{k}' / |\underline{k} \times \underline{k}'| \\
 \underline{e}_2 &= \underline{e}_3 \times \underline{e}_1
 \end{aligned}
 \tag{3 - 10}$$

The transfer matrix given by equation (3 - 9) does not however represent the complete transfer matrix since it is necessary to rotate the coordinate system such that the \underline{e}_1' - axis again lies along the direction of the (scattered) beam. The rotation matrix for the old to the new coordinates in the space of the Stokes vector is given by

$$R = \begin{pmatrix} 1 & 0 & 0 & 0 \\ 0 & \cos \theta & \sin \theta & 0 \\ 0 & -\sin \theta & \cos \theta & 0 \\ 0 & 0 & 0 & 1 \end{pmatrix}$$

The transfer matrix to be used is obtained from

$$T' = RT \tag{3 - 11}$$

All the properties relating to the scattering are contained in the transfer matrix given by equation (3 - 11). The final outcome, as given by the Stokes vector of the scattered beam, \underline{S}^f , is also dependent on the initial conditions as given by the initial Stokes vector, \underline{S}^i . Equation (A1 - 13) gives the relationship

$$\underline{S}^f = T' \underline{S}^i \tag{A1 - 2}$$

These equations above hold for either relativistic or non-relativistic energies if the appropriate scattering amplitudes f and g are used. The main difference caused by the energy of the electron is that at low energies the polarisation vector and the spin angular momentum vector

are equivalent, but at relativistic energies this is in general no longer true.

A normalised incident beam will be considered henceforth, so $S_0 = 1$. An unpolarised incident beam will be represented by

$$\underline{S}^i = \begin{pmatrix} S_0 \\ S_1 \\ S_2 \\ S_3 \end{pmatrix} = \begin{pmatrix} 1 \\ 0 \\ 0 \\ 0 \end{pmatrix} \quad (3 - 12)$$

and an incident beam, polarised along the 2 - axis is given by

$$\underline{S}^i = \begin{pmatrix} 1 \\ 0 \\ a \\ 0 \end{pmatrix}$$

where the polarisation component is obtained using equation (A1 - 1)

$$P_2 = \frac{S_2}{S_0} = a$$

For an incident unpolarised beam the result from equations (3 - 11), (A1 - 2) and (3 - 1) is

$$\begin{aligned} S_0^f &= US_0^i = |r|^2 + |g|^2 \\ S_2^f &= VS_0^i = -i(f^*g - g^*f) \\ S_1^f &= 0 = S_2^f \end{aligned}$$

These are the results of Mott scattering. An initially unpolarised beam undergoing a single scattering

becomes polarised, in the direction normal to the plane of scattering, and with a magnitude of

$$P_3 = S_3^f / S_0^f = V / U = \frac{-i(f^*g - g^*f)}{|f|^2 + |g|^2}$$

P_3 is often referred to as the Sherman function after his extensive calculations (1956) of its value for electrons scattered from mercury, cadmium and aluminium with velocities from 0.2c to 0.9c.

If double scattering is to be considered, then for the most general case a rotation of coordinate system for the second scattering through an azimuthal angle of ϕ should also be considered. The Stokes vector of an initially unpolarised beam of electrons after a double scattering through angles $(\theta_1, 0)$ and (θ_2, ϕ) is given by

$$\underline{S}^f = T'(\theta_2) R(\underline{e}_1, \phi) T'(\theta_1) \underline{S}^i$$

with

$$R(\underline{e}_1, \phi) = \begin{pmatrix} 1 & 0 & 0 & 0 \\ 0 & 1 & 0 & 0 \\ 0 & 0 & \cos \phi & \sin \phi \\ 0 & 0 & -\sin \phi & \cos \phi \end{pmatrix}$$

which results in

$$S_0^f = U(\theta_1) U(\theta_2) (1 + \delta \cos \phi) \quad (3 - 13)$$

$$\text{with } \begin{pmatrix} V(\theta_1) \\ U(\theta_1) \end{pmatrix} \begin{pmatrix} V(\theta_2) \\ U(\theta_2) \end{pmatrix} = \delta$$

This equation will be referred to in a later chapter when the conditions for greatest sensitivity of a Mott

analyser are investigated. The double scattering case can be considered alternatively of as a single scattering of a polarised beam where the degree of polarisation is given by

$$P = \frac{V(\theta_1)}{U(\theta_1)}$$

If the scattering process determines an asymmetry in intensity for scattering to $+\theta_2$ and $-\theta_2$, it is possible to determine the value of P if $V(\theta_2)/U(\theta_2)$ is known. Since the polarising power and the analysing power, for the same scattering angle, are represented by the same expression, they must be equal.

The effect of a single scattering for a beam polarised in the plane of scattering is to cause a rotation of the Stokes components in the scattering plane through an angle given by

$$\chi = \tan^{-1} \left(\frac{R \sin \theta - S \cos \theta}{R \cos \theta + S \sin \theta} \right)$$

The investigation of the ratio R/S requires a triple scattering experiment since a scattering is required to polarise the initial beam, to rotate the polarisation vector, and to analyse the final polarisation. The only such experiment to have been reported (Van Duinan and Aalders, 1968) used 265 keV electrons scattered from gold.

b) Electron Alkali Scattering.

The special case of the polarisation, P^t , of the alkali beam being parallel with its direction of motion (i.e. along the e_3 direction) is considered. If this is now cross fired by an electron beam which has the e_3 direction

as the direction of the normal to the scattering plane, the transfer matrix for the Stokes vector of the electrons in polarisation space is given by (Byrne, 1971).

$$T = \begin{pmatrix} k(\theta) & 0 & 0 & P^t m(\theta) \\ 0 & n(\theta) & P^t q(\theta) & 0 \\ 0 & -P^t q(\theta) & n(\theta) & 0 \\ P^t q(\theta) & 0 & 0 & n(\theta) \end{pmatrix} \quad (3 - 14)$$

where

$$\begin{aligned} k(\theta) &= \frac{1}{4} \sqrt{3} |F_3|^2 + |F_1|^2 \\ n(\theta) &= \frac{1}{4} \sqrt{3} |F_3|^2 - |F_1|^2 \\ m(\theta) &= \frac{1}{2} \sqrt{3} |F_3|^2 + \operatorname{Re} F_3^* F_1 \\ p(\theta) &= \frac{1}{2} \sqrt{3} |F_3|^2 - \operatorname{Re} F_3^* F_1 \\ q(\theta) &= \frac{1}{2} \operatorname{Im} F_3^* F_1 \end{aligned}$$

The intensity after scattering is (from equation A1 - 2)

$$S_0^f = k(\theta) S_0^i + P^t m(\theta) S_3^i \quad (3 - 15)$$

from which the differential cross-section is given by

$$\sigma(\theta) = \frac{S_0^f}{S_0^i} = k(\theta) + P^t P_3^e m(\theta)$$

where $P_3^e = S_3^i / S_0^i$ (from equation A1 - 1)

It can be seen that if either P^t or P_3^e is zero then the cross-section is independent of spin effects and is given by

$$\sigma(\theta) = \frac{1}{4} |F_3|^2 + \frac{1}{4} |F_1|^2 \quad (3 - 16)$$

However if both beams are polarised the cross-section is

$$\begin{aligned} \sigma(\theta, P^e, P^t) &= \frac{1}{4} |F_3|^2 \sqrt{3} + P^t P_3^e \\ &\quad + \frac{1}{4} |F_1|^2 \sqrt{1 - P_3^e} \end{aligned} \quad (3 - 17)$$

It can be seen from equation (3 - 17) that if both beams could be completely polarised, then a measurement of this cross-section, $\sigma(\theta, P_3^e, P^t)$ gives the triplet scattering amplitude directly. Experimentally this is not possible to perform at the present time, however, if it is combined with a measurement of $\sigma(\theta)$ an expression can be obtained for the triplet scattering amplitude. By combining equations (3 - 16) and (3 - 17):

$$\frac{\sigma(\theta, P_3^e, P^t)}{\sigma(\theta)} = (1 - P^t P^e) + \frac{P^t P^e |F_3|^2}{\sigma(\theta)}$$

Such an experiment could be carried out at present using a double scattering arrangement.

Returning to the Stokes vector (equation A1 - 2) then

$$P_3^{ef} = \frac{S_2^f}{S_0^f} = \frac{1}{\sigma(\theta)} [P^t p(\theta) + P^e n(\theta)] \quad (3 - 18)$$

Treating the case when $P^t = 0$ and using the relations for the direct and exchange amplitudes in terms of the singlet and triplet amplitudes

$$\begin{aligned} F_3 &= f - g \\ F_1 &= f + g \end{aligned}$$

where f and g are the direct and exchange amplitudes respectively. Equation (3 - 18) can be simplified to

$$\frac{P_3^{ef}}{P_3^e} = 1 - \frac{|g(\theta)|^2}{\sigma(\theta)} \quad (3 - 19)$$

This would involve a triple scattering experiment and is not possible to contemplate at the moment.

If now $P_3^e = 0$ then equation (3 - 17) reduces to

$$\frac{P_3^{ef}}{P^t} = 1 - \frac{|f(\theta)|^2}{\sigma(\theta)} \quad (3 - 20)$$

A double scattering experiment to determine the relative direct scattering amplitude has been carried out (Hils, McCusker, Kleinpoppen & Smith, 1972).

If equation(3 - 15) is considered and intensity measurements are made when P^t (or P_3^e) has both positive and negative values then

$$\begin{aligned} \frac{s_0^f(+)}{s_0^f(+)} - \frac{s_0^f(-)}{s_0^f(+)} &= P^t P_3^e m(\theta) / k(\theta) \\ &= P^t P_3^e \frac{|F_3|^2 - |F_1|^2}{|F_3|^2 + |F_1|^2} \\ &= P^t P_3^e \left(\frac{|f|}{\sigma(\theta)} \right)^{\frac{1}{2}} \left(\frac{|g|}{\sigma(\theta)} \right)^{\frac{1}{2}} \cos v \end{aligned}$$

where v is the phase angle between the amplitudes f and g . This measurement requires a knowledge of f and g however.

Similar expressions could have been obtained with the transfer matrix relating to electron polarisation and if the Stokes vectors representing the atom spin states had been used. The information obtained by that method would be complementary to that obtained above for any particular case. Experiments have been performed to determine

$|g(\theta)|^2/\sigma(\theta)$ (compare equations 3 - 19 and 3 - 20) by spin analysing the scattered atoms.

CHAPTER IV

TRIPLE SCATTERING EXPERIMENTAL ARRANGEMENT.

The aim of the present experiment is to produce a source of polarised electrons, of known polarisation, suitable for use in a crossed beam experiment with an alkali (potassium) beam. A method of analysing the polarisation state, as well as that of producing a polarised beam is required. The present state of affairs regarding sources and analysers of polarised electrons was investigated (see Chapter II), and it was decided to use as a polariser low energy Mott scattering from a mercury beam and as an analyser high energy Mott scattering from a gold foil.

Although the term triple scattering is used above it refers to the geometry of the apparatus, and it should not be interpreted that a triple scattering experiment will actually be performed, but rather that the ability exists for doing any of the three possible double scattering experiments, viz:-

- (1) unpolarised electrons scattered from mercury atoms and subsequently scattered from unpolarised alkali-atoms - the resultant intensity being measured.
- (2) unpolarised electrons scattered from mercury and subsequently scattered from a gold foil - measure the up-down intensity asymmetry.
- (3) unpolarised electrons scattered from (un)polarised

alkali atoms and subsequently scattered from gold foil - measure the up-down intensity asymmetry.

A description of the general constraints on the experimental arrangement will be given now, followed by a more detailed description of the actual components.

4.1 Design Constraints

A conventional single scattering experiment consists of an incident electron beam (and source), a scattering target (which may be in the form of another beam), and a scattered beam (and detectors).

Usually the incident beam or the scattered beam can be rotated about some fixed direction. In this experiment however, there are two such variable angles (see Figure 4) and the ability to rotate two of the following systems is required:

- (1) a primary electron beam
- (2) an asymmetry detection apparatus floating at high voltage.
- (3) an alkali beam apparatus
- (4) a mercury beam apparatus.

Normally a crossed beam apparatus would made use of differential pumping and collimating apertures for the atomic beams involved, and so even to rotate one such system involves considerable difficulties. Rotating a detection system, which by its nature should be fairly large and involve voltages in the region of 100 kV (see Chapter 5), would present some considerable insulation problems.

In Figure 4(1) there is a schematic diagram of an arrangement with the two atomic beams fixed in position

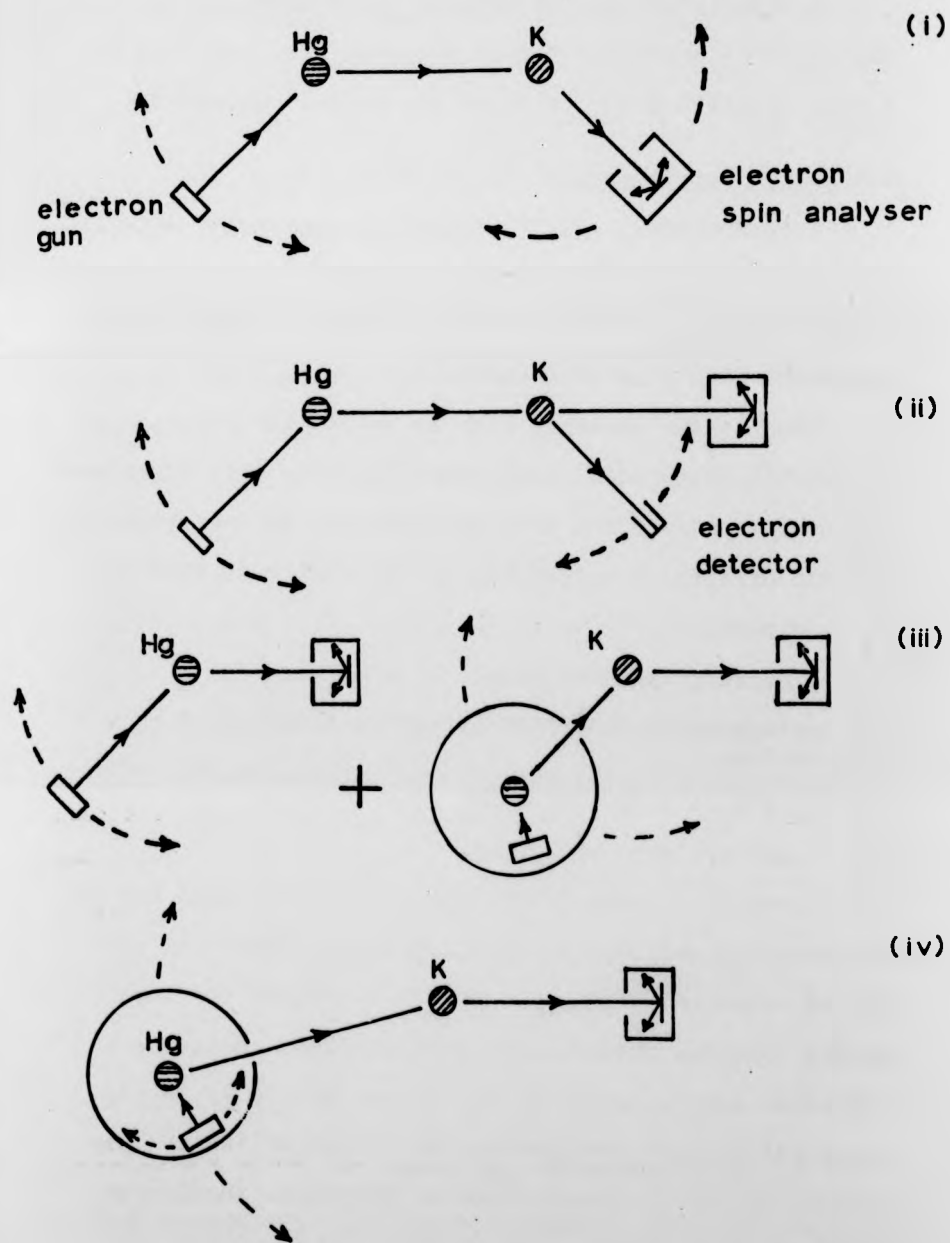


Figure 1. A Schematic representation of four possible experimental arrangements (see text for details).

(i)

(i.e. rotating the primary electron beam direction and the secondary scattered beam direction), in which differential pumping would be possible. This would require up to four separate vacuum chambers. This would be the type of system most analogous to a single scattering experiment. This scheme would allow recycling of the alkali and of the mercury extending the maximum possible duration of a single run.

ysers

A further advantage of this method is that before and after the mercury scattering, space would not be a limitation regarding the use of electron lenses to filter out

(ii)

inelastically scattered electrons and to focus the electron beam. However, these advantages do not outweigh the disadvantages of rotating the Mott analyser (Some of these problems would be overcome if instead of high energy Mott scattering, the analysing method was low energy Mott scattering (see section 2.2)).

(iii)

Figure 4 (ii) illustrates another variant, which would be to fix the Mott analyser direction as well as those of both the atomic beams, and include an additional detector, which did not employ scattering after the alkali scattering. This would allow continuous monitoring of the polarisation of the primary scattered beam, but would not permit the angular variation of the polarisation of the secondary scattered beam to be determined.

(iv)

Another method is to fix the potassium beam axis and the Mott scattering assembly, while the mercury beam system rotates around the alkali beam. There are two alternatives with this scheme. The first (see Figure 4(iii)) would have the primary electron beam making a fixed angle with the

TABLE 2 SUMMARY OF POSSIBLE SCATTERING ARRANGEMENTS

Method	Rotate Primary Electron Beam	Rotate Mercury Oven	Rotate Potassium Oven	Rotate Mott Analyser	Spin Analysis of Scattered Beam
1	Yes	No	No	Yes	Yes
2	Yes	No	No	No	No
3	No*	Yes	No	No	Yes
4	Yes	Yes	No	No	Yes

* requires a separate experiment to determine polarisation of primary beam.

primary scattered beam, whose polarisation would have been previously determined by an additional independent experiment. This would not use the actual double scattering conditions for the polarisation determination, but the mechanical problems would be considerably simplified. The second alternative (see figure 4(iv)) is to be able to rotate the electron beam independently of the second rotation. This would require two independent rotations, one operating inside the other.

These last two methods have the disadvantage that the potassium scattering must take place in the same chamber in which the mercury beam is operating. The mercury background would need to be kept as low as possible, and the potassium beam might require to be chopped, with phase

sensitive detection being used for the doubly scattering signal. The mercury system could not be recycled or have much done in the way of collimation without increasing the difficulties.

These four methods are shown schematically in figure 4 and are summarised in table 2. There are of course, several further variants from these four methods, e.g. as regards the necessity of differential pumping.

Method 4 was the basic design finally chosen. Just what is involved in this decision can be seen in Table 3.

4.2 Vacuum system

A system of three vacuum chambers is used. (see plate 1). There is a large chamber which houses the double turntable arrangement. Offset from the centre of the large turntable is the mercury system, with the electron gun mounted on a small turntable. The alkali oven is contained in a second chamber with the beam direction coinciding with the axis of rotation of the large turntable. The Mott scattering is done in a third chamber. The electron scattering plane is parallel to the turntables.

The main scattering chamber is in the shape of a cuboid with inner dimensions of 900 mm x 900 mm x 300 mm. One of the rectangular sides can be completely removed, forming a large flange on which the turntable support is mounted. The scattering plane is aligned with the median plane of the chamber. There is a NW350 flange on each of the large faces of the chamber, and smaller flanges on the others.

The alkali oven chamber is a cylinder of diameter 350 mm

TABLE 3 ADVANTAGES AND DISADVANTAGES OF THE CHOSEN
EXPERIMENTAL SCHEME

ADVANTAGES

- (1) Mott analyser fixed in position lessens insulation problems.
- (2) Alkali beam fixed in position.
 - (a) allows differential pumping of alkali
 - (b) can produce well collimated beam
 - (c) can recycle alkali
- (3) Primary scattered beam can have its polarisation measured directly.
- (4) Space available for efficient filtering, collimating and focusing lens system between alkali interaction region and Mott scattering chamber.
- (5) Needs only three vacuum systems.

DISADVANTAGES

- (1) Mercury system rotating
 - (a) difficult to recycle
 - (b) difficult to collimate
 - (c) cannot differentially pump
- (2) will require efficient mercury collector which must also rotate, or be very large.
- (3) Due to mercury background, will require to chop alkali beam and use phase sensitive detection.
- (4) Require one rotation inside and independent of a second rotation.
- (5) Lack of space for primary electron beam focusing and collimating.
- (6) Lack of space for filtering lens system between mercury and alkali interaction regions.
- (7) One of the vacuum systems must be large to help compensate for (5) and (6) above.

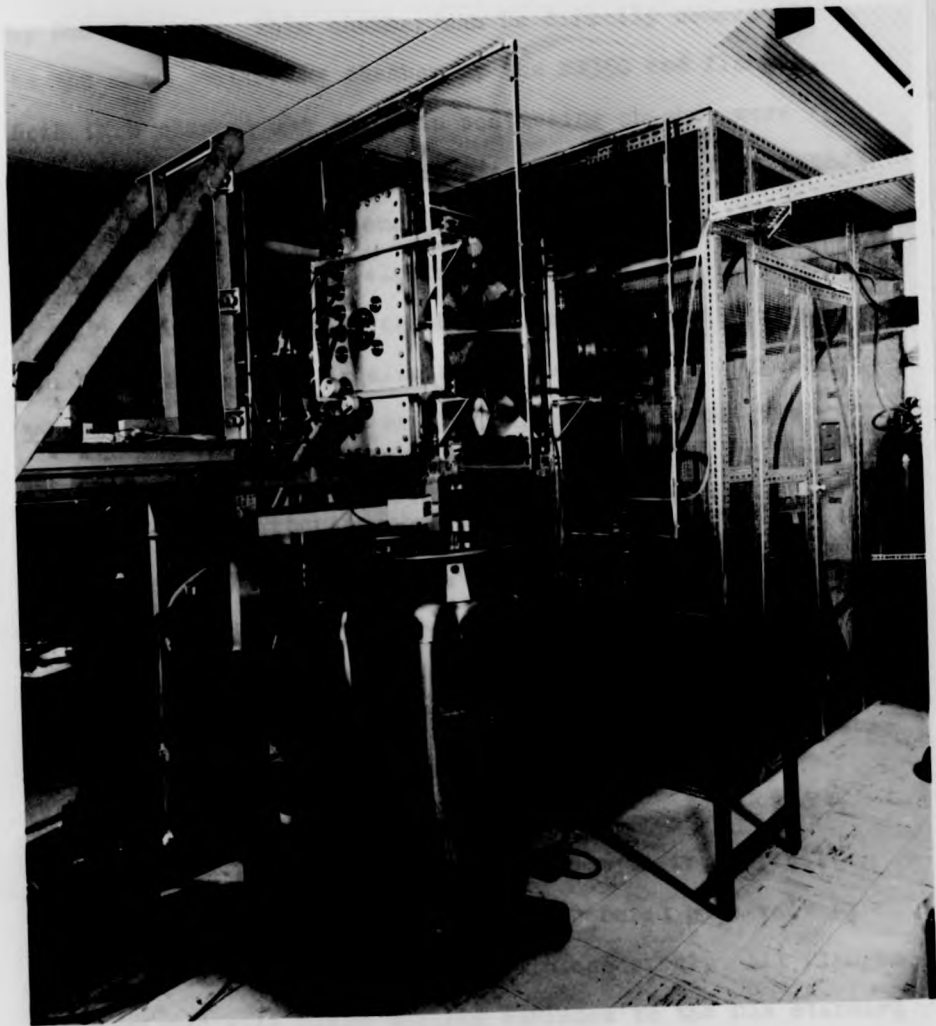


Plate 1. General View of Apparatus.

The following description of the apparatus is based on the
report of the author, which is published in the
Journal of the Royal Society, London, 1931, p. 100.

The apparatus is described in the following
sections: (1) The apparatus; (2) The method of
operation; (3) The results.

The apparatus is described in the following
sections: (1) The apparatus; (2) The method of
operation; (3) The results.

by 600 mm long. This chamber can be directly connected to the main scattering chamber by the NW350 end flanges. Both this chamber and the main scattering chamber were manufactured from non-magnetic stainless steel (type EN58J) since with low electron energies any stray magnetic fields can play havoc with the electron trajectories.

The Mott scattering chamber is manufactured from an aluminium alloy with an aluminium liner. It is a cylinder 350 mm in diameter x 350 mm long and is pumped out via the main scattering chamber.

The main scattering chamber is pumped with an Edwards 9M3A 9" mercury diffusion pump which with liquid nitrogen trap and refrigerated baffle gives a pumping speed of 400 l/sec. A similar pumping arrangement is used for the alkali oven chamber, except that an Edwards 12M3, 12" mercury diffusion pump is used, resulting in a pumping speed of 750 l/sec.*

Both systems can be closed off from their respective pumping systems using pneumatically operated gate valves, manufactured from non-magnetic stainless steel. All flanges are designed with plain sealing surfaces to the DIN standard for NW flanges. Viton 'O' ring gaskets are used throughout. The backing lines have either stainless steel or mercury protected alloy components and are both pumped through a zeolite trap by a Balzers two stage rotary pump. There is also an electro-magnetic isolating valve in the common part of the backing line.

The vacuum chambers are supported on a welded duraluminium framework with the diffusion pumps hanging from the chambers.

* The large pumping speeds are used because one of the original suggestions had been to do the experiment with an atomic hydrogen beam, rather than an alkali beam.

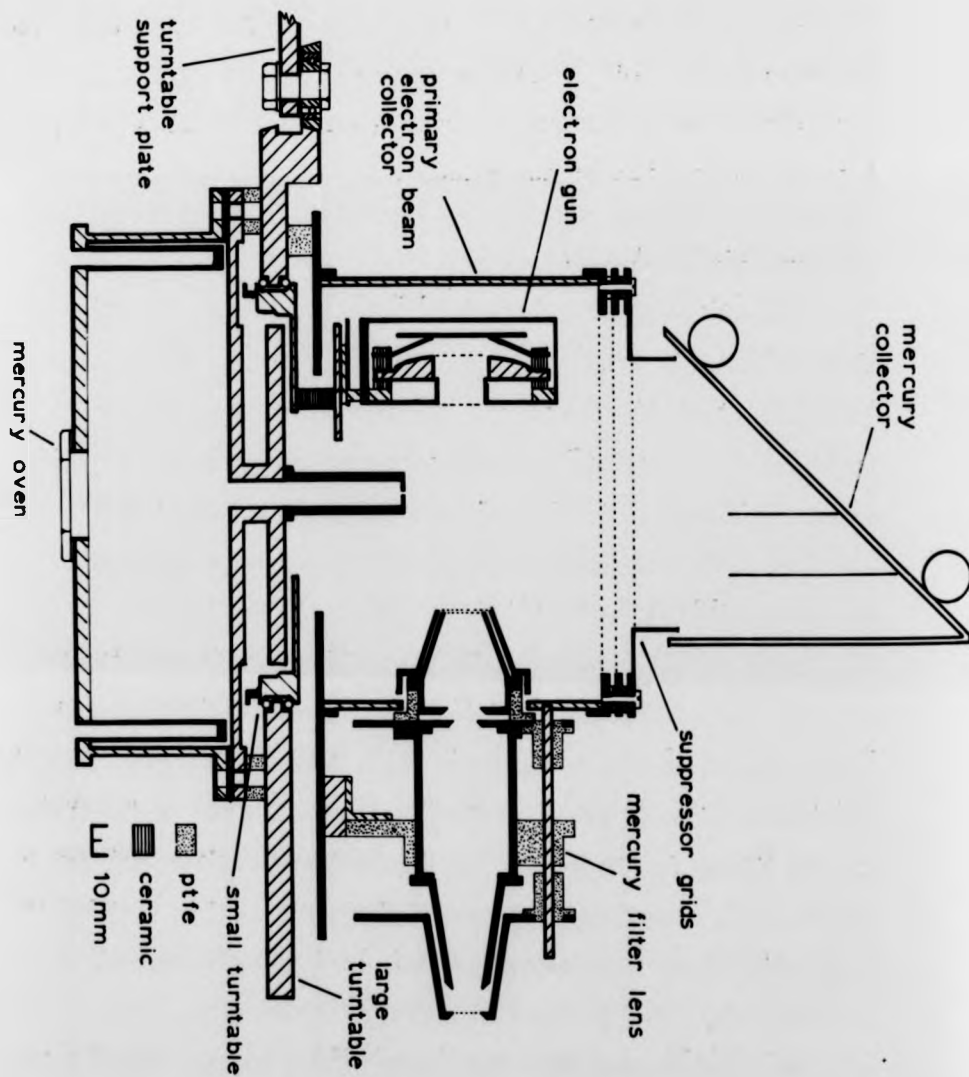


Figure 5. The mercury system including the electron gun and filter lens.

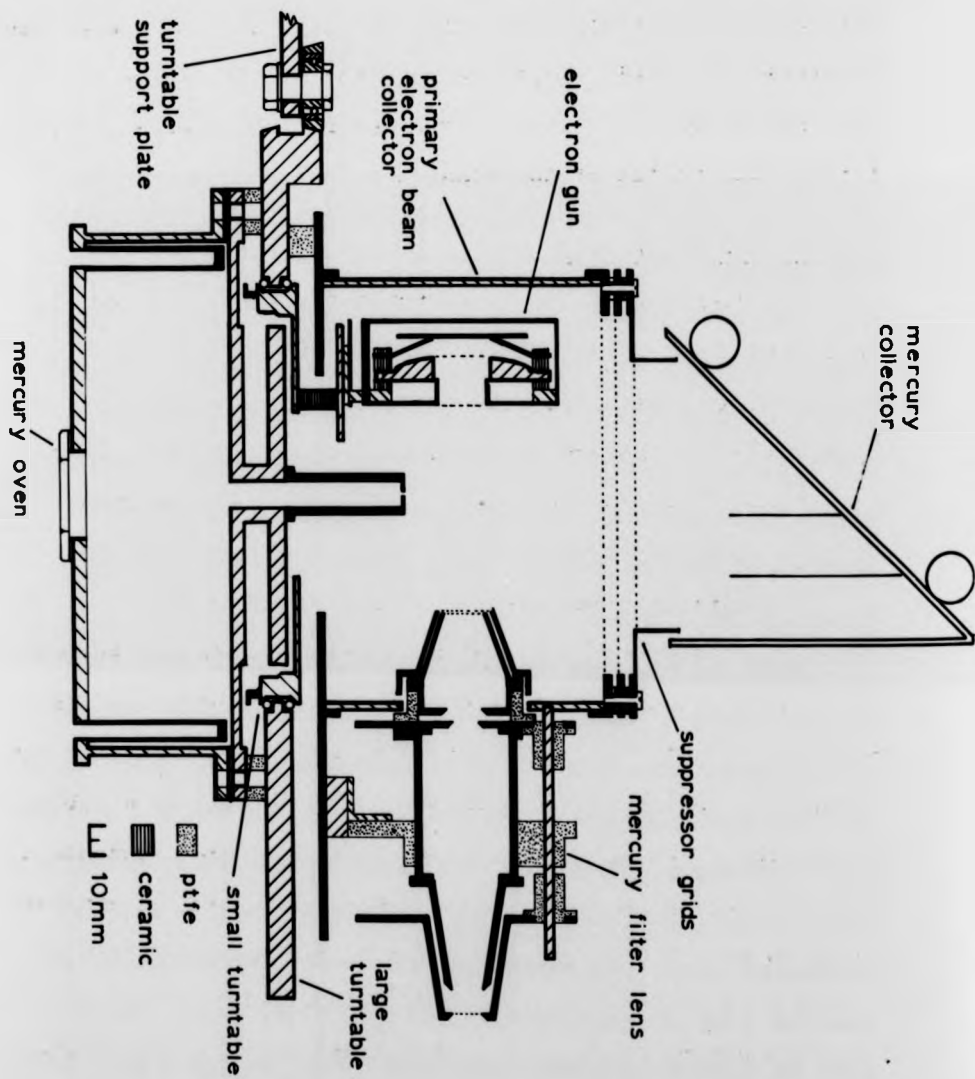


Figure 5. The mercury system including the electron gun and filter lens.

The whole assembly is manufactured from non-magnetic components.

The large end flange could be bolted to a trolley and the flange, support plate, turntable and all components can then be wheeled along the framework, till all the components are easily reached. Positive location of the flange is obtained by means of two tapered dowel pins located at the top and the bottom of the flange.

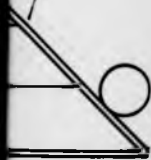
4.3 The Large Turntable.

The diameter of the large turntable is 670 mm and it is recessed on one side to reduce its weight. It is supported at sixteen points on its tapered circumference by means of 1" tapered bearings mounted on eccentric bolts (see figure 5). The eccentric bolts permit slight radial adjustment of the turntable.

The turntable is rotated using a two-wire drive arrangement coupled to a system of gears, which are turned using a Vacuum Generators vacuum rotary feedthrough. The wire drive lies in a channel cut in the circumference of the turntable, and is anchored on the turntable and on a cable drum. The gears have a reduction ratio of 120:1, and use a phosphor bronze gear with a stainless steel worm to decrease friction when under vacuum. Slack on the wire is taken up by means of a small pulley at the anchor point.

The rotary feed-through is calibrated in 5° intervals but, in addition, a scale was inscribed in degrees on the circumference of the turntable. This scale is visible through a glass window on the large flange, and can be read to $\pm 0.2^\circ$

mercury
collector



electron gun

by use of a reference line on the support plate. The turntable is capable of rotating through slightly more than $\pm 180^\circ$ from zero degree position. Due to problems with friction in the small turntable drive system the angular motion of the large turntable is restricted to $\pm 50^\circ$. This turntable, all the lens elements, and all components mounted on it, are manufactured from Firth Vickers Immaculate V stainless steel.

4.4 The Small Turntable.

This turntable has a diameter of 145 mm and is located 210 mm off-centre from the large turntable. It is supported by means of a large number of $\frac{1}{8}$ " stainless steel ball bearings held in a channel by a clamp ring.

This turntable is also driven by a two wire arrangement coupled to a similar system of gears, as the large turntable. With this turntable the wire has to be enclosed in a wire coil sleeving. This outer sleeving defines the length of pulley wire required, being anchored near the turntable on the gear support* and is flexible enough to pass round a cable drum. As the large turntable revolves this outer winds itself up on the drum, still permitting the inner wire to move and turn the small turntable. As the large turntable is rotated in the opposite direction, the outer sleeving unwinds itself. The small turntable can be turned at all positions of the large turntable through an angle of more than $\pm 180^\circ$ ($\pm 140^\circ$ when the other components are in place) from an in line position.

*Tension of the inner cable could be adjusted using screw adjusters on the terminal points of the outer sleeving.

With this drive it was found that friction in the gears (between the stainless steel worm and the phosphor-bronze gear) was great enough to cause them to seize up. Several dry lubricants were tried unsuccessfully before Santovac 5, a very low vapour pressure oil used on diffusion pumps, was used and found to be completely successful at removing trouble from this source.

The angular setting of the turntable is determined by using a potentiometer wire set into an annulus of PTFE, which is located around the small turntable on the mercury boiler side of the large turntable. A beryllium copper slider, attached to the small turntable, shorts the potentiometer to earth at this point. The resistance of either end of the potentiometer wire to earth is a measure of the angular setting of the small turntable.

4.5 The Electron Gun.

The space available for this gun is a compromise reached between, the electron gun, the filter lens, and the physical sizes of the large turntable and the main scattering chamber. These constraints mean that the overall size of the gun must be as small as possible. On the other hand the maximum current possible is required, since this is a double scattering experiment.

One way of trying to maximise the scattered current is to utilise as much of the mercury beam as is possible. An electron gun which is rectilinear rather than cylindrical will allow some increase which does not run into space

problems since there is more space available in this dimension.

Kuyatt & Simpson (1963 A) discuss low voltage electron guns using a multi-staging principle, which because of their extended size cannot be considered as contenders in the present experiment. In another paper Simpson & Kuyatt (1963 B) deal with the limitations on beam density of unipotential guns. They obtain the following expression relating the cathode temperature T (in $^{\circ}\text{K}$), the electron convergence angle at the anode, θ_2 , and angle, δ , characterising the dimensions of the gun and the electron energy, E .

$$E > \left(\frac{211}{\pi} \right) \left(\frac{T}{11,600} \right) \left(\frac{\tan^2 \delta}{f(\delta) \sin^2(\theta_2)} \right) \quad (4.1)$$

This inequality must be satisfied for saturation of the space. In figure 6 the equality represented by equation (4.1) is shown as the line $I/I_{\text{max}} = 1$. Other lines parallel to this line represent currents less than I_{max} . The perveance defined as I/V , is represented by the lines sloping upward to the right. Consequently regions of interest lie above the appropriate current ratio line and to the right of the microperveance line. It can be seen that with a microperveance of unity, that no space can be saturated with an anode voltage of less than 220 V, and that for 10 V, the most that can be expected is 25% saturation, with a convergence angle of 18° , and a current of about $20 \mu\text{A}$.

Although the useful range of a unipotential electron gun is usually considered to be at high energies, it can be

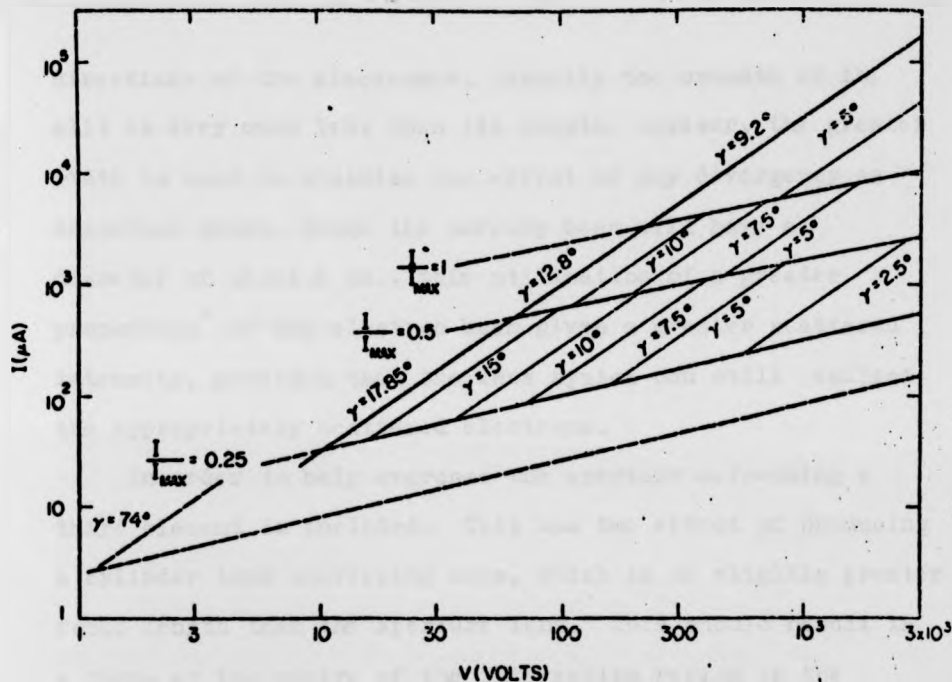


Figure 6. Graph of current versus voltage showing regions accessible to guns capable of saturating a given space with I_{max} .

usefully employed if the angular divergence is not too large. The divergence angle becomes much less critical as the size of the aperture increases.

Pierce (1940) has established the shapes of electrodes such that parallel electron flow, satisfying Poisson's equation, can exist under space charge limiting conditions, adjacent to a charge free region. There is still of course the effect of the lens (divergent) formed by the anode slit.

The design chosen was to use a rectilinear Pierce electrode system with the breadth of the slit only half of its length, Using this arrangement, the appropriate Pierce electrode design was used for both transverse

directions of the electrodes. Usually the breadth of the slit is very much less than its length, however, the greater width is used to minimise the effect of any divergency as described above. Since the mercury beam will have a diameter of about 4 cm., this utilisation of a greater proportion* of the electron beam gives a greater scattered intensity, provided that the lens system can still collect the appropriately scattered electrons.

In order to help overcome the aperture defocusing a third element is included. This has the effect of producing a cylinder type converging lens, which is of slightly greater focal length than the aperture lens. This should result in a focus at the centre of the interaction region in the absence of space charge dominated conditions. The overall design of the electron gun can be seen from Figure 5.

The gun is positioned on a tripod arrangement which permits slight variation in distance from the mercury beam centre. The wires associated with the gun are clamped between the gun and support table and pass through the aperture in the turntable through which the mercury nozzle protrudes.

The cathode used is an oxide cathode of area 5 mm x 18 mm from a mullard PL56 pentode valve. A fine tungsten mesh of 93% optical transmission is used at the exit aperture and at the front of the anode. The best operating conditions were found when the anode is operated at about 80% of the final potential.

*The large angular acceptance that is implied here is acceptable since, for an intense source of polarised electrons, it is the gross shape of that electron polarisation which is under investigation and will be used, and not very sharp structure with a resultant decrease in total intensity.

A disadvantage of any "simple" electron gun is that if it is required to alter the emission current, e.g. to check the linearity of scattered signal to primary current, then the electron beam properties may be altered. By varying any intermediate potentials the focusing properties of the beam may change, alternatively if the heater current is adjusted then the temperature of the cathode can produce variations of the contact potential between the electron beam and the cathode,

4.6 The Electron Collector.

Any background electrons present in the main scattering chamber must be reduced to a minimum. To realise a low electron background, an efficient collector of the primary beam is essential. Since the collector must be opposite the electron gun at all times, the method used is to completely surround the mercury interaction region with a cylinder, inside of which the electron gun can rotate. (see Plate 2). This cylinder forms the collector and end caps are used to partially enclose the ends.

A grid was used in front of the collector to avoid secondary electrons re-entering the scattering region. This was later removed because of problems experienced with a discharge taking place.

The end cap near the turntable has an 8 cm circular aperture cut in it allowing the mercury nozzle to protrude and the electron gun connections to pass through. The mercury boiler and collector are insulated from the turntable

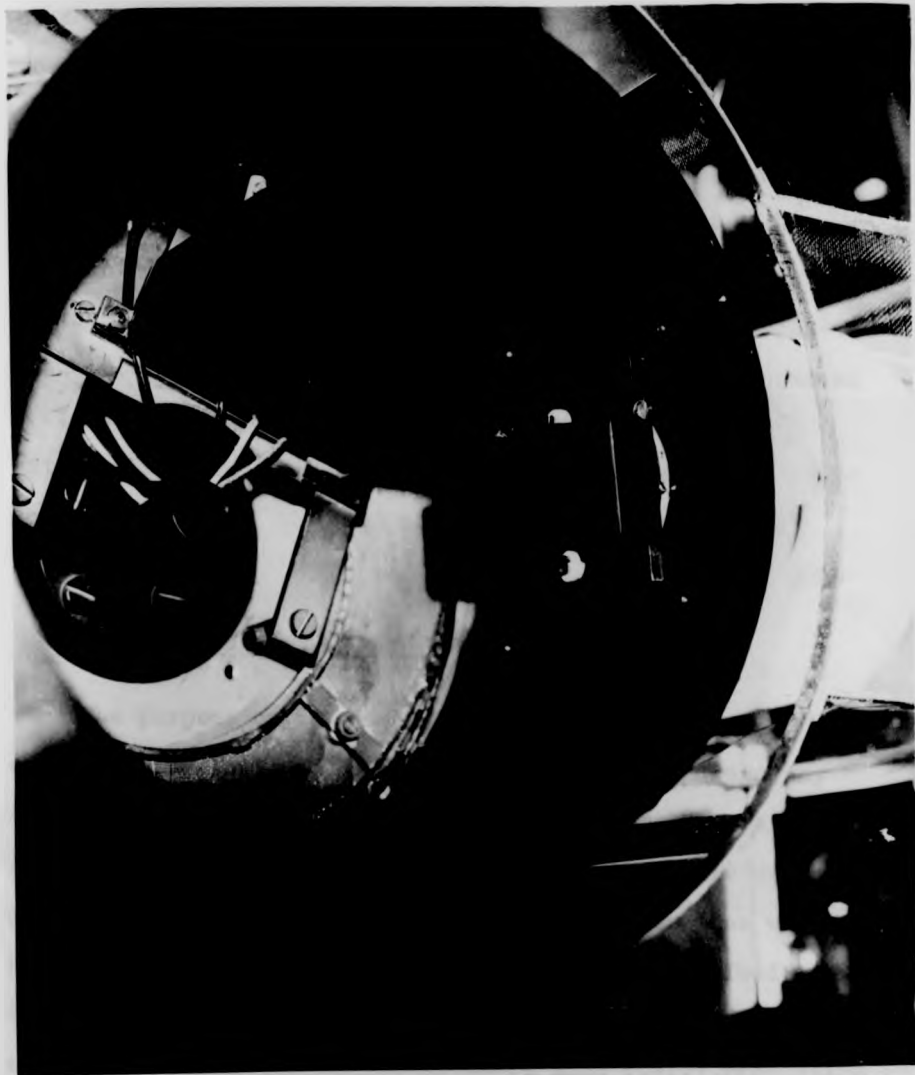


Plate 2.

View of the Electron Gun and the
Mercury Interaction Region.

so that the interaction energy can be biased with respect to earth.

The end cap at the opposite end contains an aperture shaped so as to fit the mercury condenser, and has a system of three electrically insulated grids across this aperture. The central grid is biased the same as the cathode to prevent the electrons escaping in to the main scattering chamber. The other two grids are biased such as to present a field free interaction region and a grounded screen externally. The passage of mercury vapour was almost unaffected due to the high transmission tungsten gauze used.

4.7 The Mercury Filter Lens System.

The purpose of this lens is to remove electrons suffering inelastic collisions from the mercury (and any secondary electrons finding their way into the lens system). It also images the interaction region at the centre of the scattering chamber with a magnification of less than unity. Five element filter lenses such as have been described in the literature (Wilmers, Haug & Deichsel, 1969, and Simpson and Marton, 1961) are excellent where good energy resolution and a small angular acceptance is required. Because of the lack of available space, and the fact that a fairly large angular acceptance is desirable, this type of lens is not the most suitable. Another system, which has larger acceptance angles, is a three element lens, which operates with the central element providing the cut-off. The only

way to vary the focusing for different energies with this type of lens, is by varying the relative physical dimensions of the lens elements since the potentials are all fixed (outer elements at interaction potential with the inner element near the cathode potential).

The chosen system was a four element system (see Figure 5) where the outer two are fixed at the interaction potentials the second element is near the cathode potential, and the third element is available for focusing the image on the interaction region. The first lens element and the entrance aperture to lens element no, 2 is covered with a fine tungsten gauze, whose mesh size is smaller than the spacing between those elements. This ensures that the function of the first element only provides a field free interaction region, and does not influence the electron trajectories. The exit of element no.2 and the entrance of element no.3 along with the exit of element no. 3 and the final lens element forms two field lenses, which produce a focused beam on the alkali interaction region.

The cylinder part of the collector and the lens elements are surrounded by a grounded tungsten mesh to eliminate any stray electric fields near the alkali scattering region.

4.8 The Alkali Filter Lens and Injector System.

Here, because of the much smaller interaction region (i.e. alkali beam diameter), and because a good angular and energy resolution is required, the limiting apertures

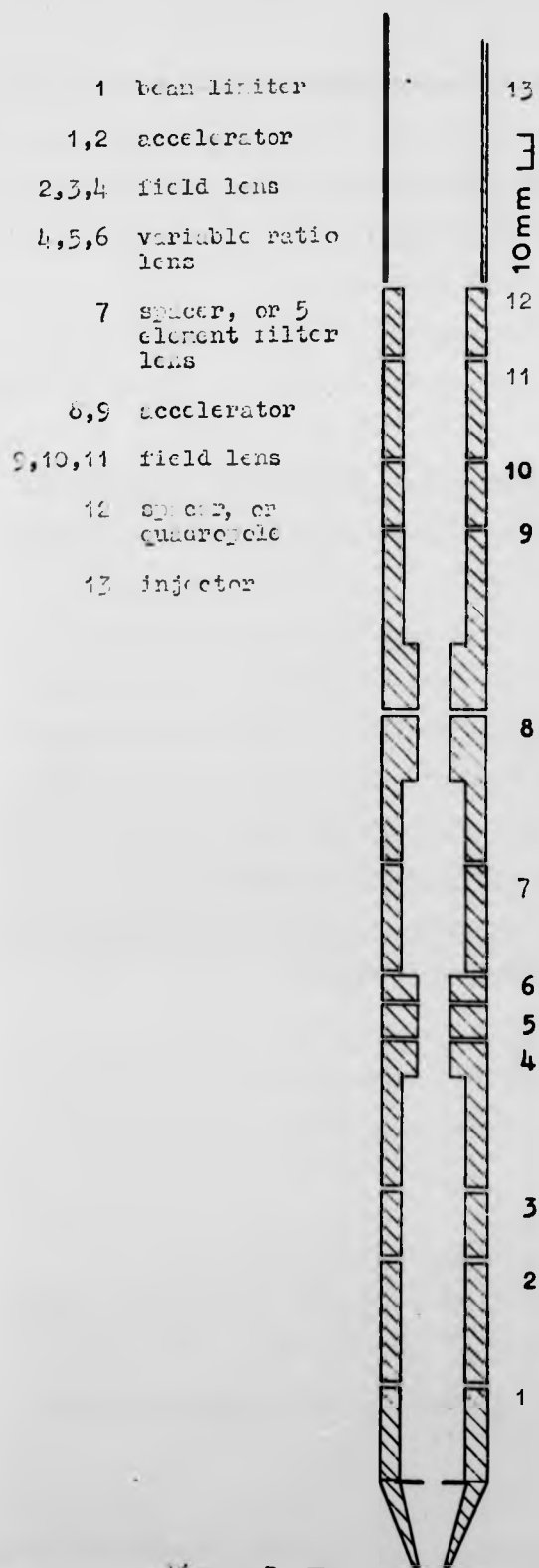


Figure 7 The alkali lens and injector system.

are very much smaller. (see Figure 7). The first element* of the lens serves so as to limit the scattering region forming an object. The electrons forming this object are then accelerated by the second element to about thirty times the scattering energy. The beam then passes through a field lens, which forms a well focused beam which can then be used to produce a parallel beam at the entrance aperture of the filter lens, by means of a variable ratio lens.

The filter lens itself (not shown in Figure 7) is of the type described by Simpson & Marton (1961), which consists of two Soa type immersion lens mounted back to back. The potential and size of the central aperture of the filter lens defines the actual energy resolution of the lens.† A parallel beam is formed on the last aperture of this lens and is accelerated and then focused by a further field lens. The beam can then be deflected using a set of quadropole deflection plates (not shown in Figure 7) before being further accelerated for injection into the Mott accelerator.

During the polarisation measurements the filter lens was replaced by a plain cylinder allowing greater intensities through to the Mott analyser since energy discrimination is not required at this stage. The deflector quadropole

*This element has a front rectangular slit with a circular aperture, of the same area as the slit, which can readily be replaced by a larger or smaller aperture if desired.

†The retarding plane aperture can be readily exchanged by one of a different diameter.

was also removed after it had been shown to be unnecessary.

Most of the lens system is enclosed in a grounded shield since background electrons were found to be penetrating the gaps between the elements, and reaching the Mott scattering chamber. The lens elements are clamped on to two long ceramic rods forming an optical bench.

An earthed cylinder of 40 mm diameter, manufactured from fine tungsten gauze, is placed between the two lens systems. This eliminates any stray electric fields which may be present and avoids any electrostatic deflection of the beam when passing between the two systems.

4.9 The Mercury Oven. (see figure 5).

Because collimators cannot be used* and it is necessary to maintain a low background pressure in the main scattering chamber, the mercury oven is placed as close as possible to the interaction region in order to obtain the greatest mercury density. This is achieved by having the mercury oven situated on the large turntable, with the nozzle protruding through the aperture in the small turntable.

Because of the rotation of the mercury source, it is essential that the mercury boiler be rotationally symmetric about the nozzle axis. It can be seen that the body has the form of a cylinder with twelve immersion type heaters arranged near the circumference, equally spaced around it. (Benson, 1970). When the system is rotated a minimum amount

* Any collimator used, if not cooled, would lead to an increase in background pressure of the main scattering chamber, and if cooled, apart from problems of clogging, would be difficult to arrange in practice due to the required rotation of the coolant supply.

of time is required before equilibrium is reached.

The temperature of the mercury is obtained from chromel-alumel thermocouples, of which there are six equally spaced around the boiler. As the boiler is rotated the thermocouple which is nearest the lowest point, i.e. the one which is adjacent to the liquid mercury level, is used for control purposes. All the thermocouples are of comparable lengths to minimise any differences between them.

Provision is made for heating to be applied to the nozzle region but it has not been found necessary. The nozzle being in a vertical plane does not clog up at all with mercury droplets due to the high angle of contact of mercury with stainless steel.

The nozzle used at first was a laval nozzle, but since the optimum mercury density was reached before supersonic conditions prevailed, the result was to decrease the beam density by effectively moving the aperture further from the interaction region. This laval nozzle was seen to give erratic beam behaviour at times, possibly caused by mercury droplets near the throat of the nozzle, but it never clogged up completely.

The nozzle being used at present was easily interchangeable, being sealed to the oven using a copper gasket and a knife edge on the oven. It had an aperture of 1.6 mm diameter.

Heating was done using molybdenum wire inside four way ceramic tubing which fitted inside the immersion tubes. The wire was wound such that the windings were bifilar in nature. An AC current of about 1.5 A was used to heat the

boiler to a temperature of about 120 - 130° C. The power input was typically 30 watts. The oven was mounted on four stainless steel rods which sat in PTFE support spacers in the large turntable, to minimise heat losses from it by conduction. The PTFE also served to act as an electrical insulator allowing the oven to be biased such as to provide a field free interaction region.

The large mass of mercury which the oven can hold (more than 8 kg) ensures that the main heat reservoir is the mercury itself and not the oven body. This assists in ensuring that equilibrium conditions are rapidly attained after rotation of the polarised electron source about the alkali beam axis. It also allows long periods of continuous running without requiring the system to be opened and the oven refilled. This is of advantage on health safety grounds apart from the longer integration times possible.

4.10 The Mercury Collector.

Although the mercury boiler has to rotate, it is very much easier if the mercury collector is stationary. The collector is a circular copper annulus, shaped so as to trap any mercury atoms incident on it, even if they undergo a few reflections. It is cooled to less than - 170°C by liquid nitrogen passing through pipes brazed on to the rear. To maintain this temperature the liquid nitrogen flows for spells of fifteen minutes in every half hour. The flow of liquid nitrogen is limited by the back pressure caused by

the exit pipe, and less than one gallon per hour is required. Because of the ability of mercury to amalgamate with copper, the complete assembly was plated with nickel by a chemical deposition method. This was particularly important with the brazing.

The collector is supported by a long ($\frac{1}{4}$ ") stainless steel rod, from the turntable support plate, and at the large flange. The vacuum seal is provided by a viton 'O' ring against a stainless steel pipe which was brazed on to the copper pipe inside the system. Heat gains are restricted because of the poor thermal conduction properties of the stainless steel.

The pressure in the main chamber with the mercury beam on is about 5×10^{-6} torr, which is about double that when the mercury oven is at room temperature. The mercury collector is kept cold continuously whenever the system was under vacuum. This avoids mercury condensing out elsewhere, producing electrical short circuits.

When the system was being opened up, compressed air was passed through the cooling pipes, to raise the collector temperature to near that of the room, to avoid water vapour condensing on it. The mercury then collected in a tray beneath the condenser.

4.11 Temperature Controller for the Mercury Boiler.

A thermocouple controlled thyristor unit is used to regulate the power for the mercury boiler heaters. The temperature setting is repeatable to within 0.05°C and is

stable to $\pm 0.10^{\circ}\text{C}$ or better. The temperature bandwidth is adjusted by means of a sensitivity control and a time constant control.

4.12 The Helmholtz Coils.

A magnetic field free region is necessary in the centre of the main scattering chamber in order not to perturb the electron beam.

The magnetic field present is primarily due to the earth's magnetic field, but is influenced by the mild steel girders and electrical trunking etc., of the building. The vacuum chambers, components inside the system and framework which are made of non-magnetic materials ensures that any perturbations from the apparatus itself are small. The field present amounts to about 400 mgauss which is reduced to 35 milligauss, or less, over the region traversed by the low energy electron beam, and to less than 1 milligauss in the centre of the main scattering chamber, by the use of a system of helmholtz coils described below. There remains an uncompensated AC field at the centre of 0.75 milligauss.

The larger the system of coils the greater is the region of cancellation, but due to the experimental arrangement severe constraints were placed on the actual sizes which could be used. The scale of the experiment, requiring the use of a three chamber vacuum system, one of which is floated at 100 kV., means that the coils are small,

giving fairly poor field elimination, or very large (i.e. dimensions comparable to that of the laboratory). The size of the assembly precludes useful orientation of the apparatus which would have allowed the elimination of one of the magnetic field components.

All coils were based on a system of a pair of square coils. (Firester, 1966). The across the laboratory coils were rectangular 790 mm x 880 mm with separation of 440 cm, and had the poorest field elimination. The along the laboratory coils were square with dimensions of 1.84 m and separation of 1 m, and provide the best field cancellation.

For the vertical component of the magnetic field, the coils have the form of a truncated square with the number of current turns on the shifted side AB(LM) being reduced to half that on the other three sides (see figure 8) To complete the current loop an auxiliary loop ABFE(LMQP) is used where EF(PQ) is placed on the ceiling (floor) to obtain maximum separation from AB(LM) and minimise its effect at the centre. The separation of sides AE and BF (LP and MQ) with reduced current and direction away from the region of interest ensures that the effect on the other components is minimal. This design was chosen after computing the field along the axis for several different coil combinations and types.

The dimensions are as shown in figure 8. Because the spacing of the coil is less than the size of the main scattering chamber, one of the shorter sides is arranged

Figure 9 The measured magnetic field in the region traversed by the low energy electron beam after cancellation.

- (a) Vertical component.
- (b) Component across the laboratory.
- (c) Component along the laboratory.

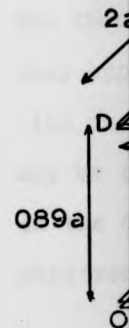
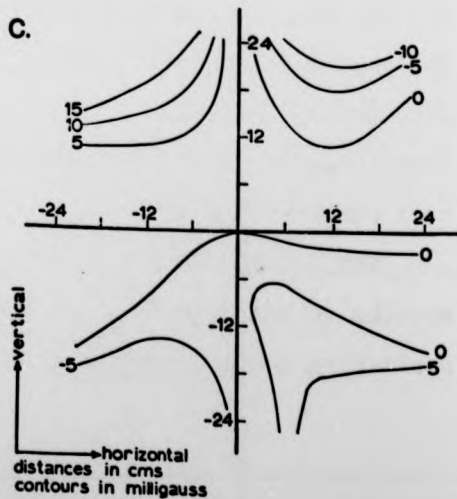
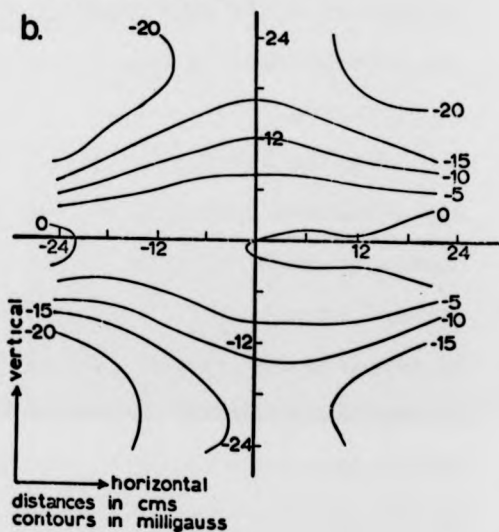
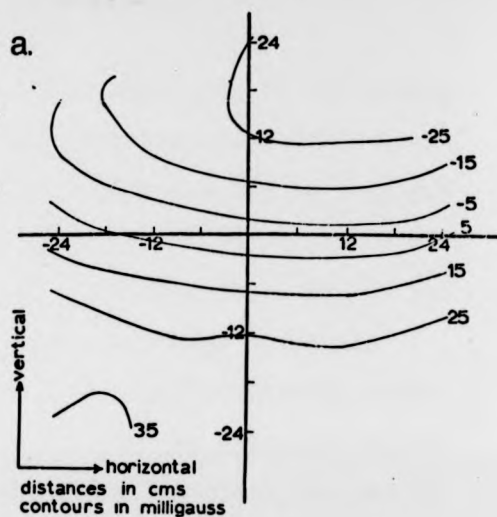


Figure 8

so that
allow the
assembly
The
in cont
The
are use

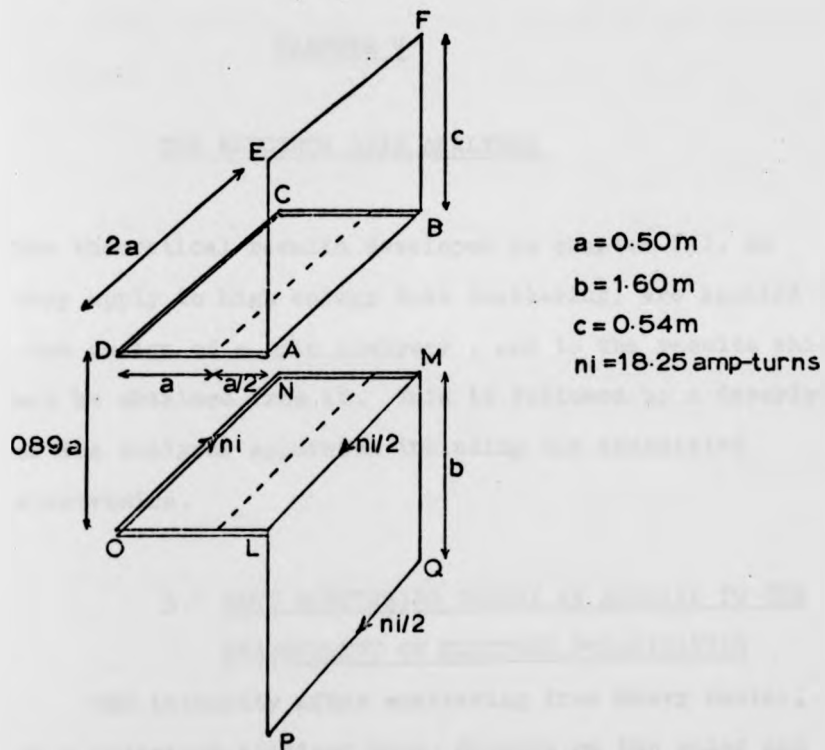


Figure 8. Helmholtz coil system for vertical component of magnetic field.

so that it can be unplugged and removed, in order to allow the large flange to be taken off for access to the assembly inside.

The measured field in the scattered plane is plotted in contour in Figure 9, for each of the three components.

Three Kepco CC 30 constant current power supplies are used to power the coil system.

CHAPTER V

THE ELECTRON SPIN ANALYSER

The theoretical results developed in chapter III, as they apply to high energy Mott scattering, are applied to the design of a spin analyser, and to the results which may be obtained from it. This is followed by a description of the analyser apparatus including the associated electronics.

5.1 MOTT SCATTERING THEORY AS APPLIED TO THE
MEASUREMENT OF ELECTRON POLARISATION

The intensity after scattering from heavy nuclei, of a polarised electron beam, depends on the polar and azimuthal angles, θ and ϕ , through equation (3 - 13), which can be written in the form

$$I(\theta, \phi) = I_0(\theta) \left[1 + P S(\theta) \cos\phi \right] \quad (5 - 1)$$

where ϕ is the angle between the normal to the scattering plane* and the direction of the initial polarisation (this is in accordance with ϕ as introduced in section 3.4(a)). P is the transverse polarisation of the incident electron beam and $s(\theta)^+$, the Sherman function, is the analysing power of the scatterer. $I_0(\theta)$ would be the intensity

* The normal to the scattering plane is defined by the direction \underline{e}_3 given by equation (3 - 10)

+ S is a function of E, Z , and θ , even although only θ is quoted here. Here consideration is only being given to the dependence of I with θ and ϕ .

scattered through angle θ in the absence of polarisation.

From equation (5 - 1), the electrons scattered such that

$$\cos\phi = \pm 1 \quad (5 - 2)$$

will exhibit the greatest sensitivity for the polarisation.

Considering $\phi = 0$ to correspond to the "up" direction and $\phi = \pi$ to correspond to the " down " direction, expressions for I_{up} , I_{down} are given by

$$I_{up} = I_0 (1 + P S) \quad (5 - 3)$$

$$I_{down} = I_0 (1 - P S)$$

so that an up- down asymmetry is given by

$$R = \frac{I_{up}}{I_{down}} = \left(\frac{1 + P S}{1 - P S} \right) \quad (5 - 4)$$

This equation, at least in principle, allows the polarisation to be determined if the Sherman function is known in advance, and the asymmetry ratio, R , can be measured. The effect however is masked because of the presence of instrumental asymmetries, caused by differences in scattering angle, solid angle of the detectors, detector sensitivity etc. If all of these asymmetries are included in a factor A , then what is actually measured is

$$R = A \left(\frac{1 + P S}{1 - P S} \right) \quad (5 - 5)$$

If the mercury scattering angle is changed from θ to $-\theta$ the polarisation changes sign also. Denoting the respective asymmetry ratios by $R(+)$ and $R(-)$, equation (5-5)

becomes

$$R(+)=A(+)\left(\frac{1+PS}{1-PS}\right)$$

$$R(-)=A(-)\left(\frac{1+(-P)S}{1-(-P)S}\right)$$

resulting in

$$\frac{R(+)}{R(-)}=A(+)\left(\frac{1+PS}{1-PS}\right)^2 \quad (5-6)$$

From this equation the polarisation of the electron beam can be determined if

$$\frac{A(+)}{A(-)}=1 \quad (5-7)$$

or, at least, is known. Equation (5 - 7) is valid if the instrumental asymmetries of the spin analyser are identical for mercury scattering angles of $+\theta$ and $-\theta$.

5.2 EXPERIMENTAL ARRANGEMENT OF THE SPIN ANALYSER

Looking again at equation (5 - 1)

$$I(\theta,E,Z)=I_0(\theta,E,Z)\left[1+PS(\theta,E,Z)\cos\phi\right]$$

Maximum sensitivity for a spin analyser requires:

- 1) $\cos\phi = 1, \phi = 0, \pi$
- 2) $S(\theta,E,Z) = \text{a maximum.}$

The first requirement can be satisfied if the normal to the plane of scattering is arranged to lie along the direction of the incident beam polarisation. This means that the scattering plane in the spin analyser is the same plane

as in the spin polariser.

For the second requirement gold was chosen since S increases with increasing Z number. Gold has been studied both experimentally and theoretically in detail and the values of $s(\theta, E)$ are well known (Lin, 1964). The dependence of S for gold upon the scattering angle, θ , and the energy, E , is shown in Figure 10.

It can be seen that increasing the energy far above 100 - 120 keV does not bring a large gain in the value for S , whilst at the same time it compounds the associated electrical breakdown problems. Also from this figure it can be seen that for 100keV, the maximum occurring at $\theta = 120^\circ$ is fairly broad, thus allowing the use of large solid angles for the detection of the scattered electrons.

For these parameters, and for an infinitely thin foil, the calculated value of the Sherman function obtained by Lin (1964), whose results overall are in good agreement with the experimental results, was used

$$S = 0.3978$$

Lin states that this result is accurate to within $\pm 1\%$ (the corrections to be applied when using foils which have a finite thickness will be discussed later).

The Sherman function at small scattering angles for an energy of 100keV is very close to zero (see Figure 10). Consequently for detectors at $\theta = 45^\circ$, an asymmetry ratio can be measured in which $A(+)/A(-)$ is the dominant factor (see equation 5.5). This provides a useful test of how good $A(+)/A(-) = 1$ really is.

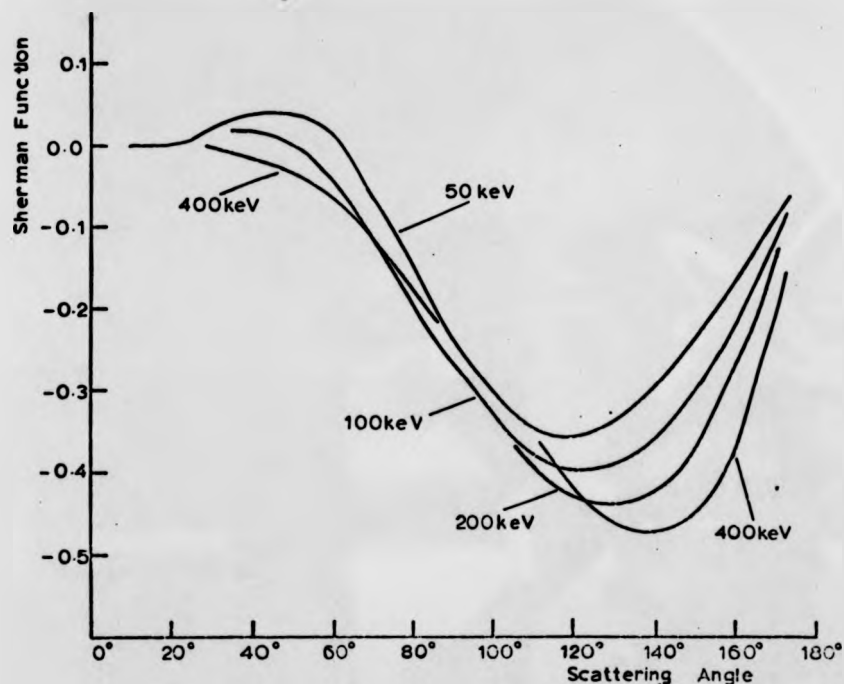


Figure 10. The Sherman function for scattering from gold as a function of energy and angle.

The arrangement which was used may be seen in Plate 3. It consists of two detectors at $\theta = 120^\circ$ and two detectors at $\theta = 45^\circ$. The details of which will now be more fully discussed.

5.3 THE MOTT SCATTERING CHAMBER.

In order to reduce the back-scattering from the walls which is proportional to Z^2 , it was manufactured from aluminium and its size was made fairly large. Aluminium also enhances the energy loss for scattered electrons, allowing them to be discriminated against from the

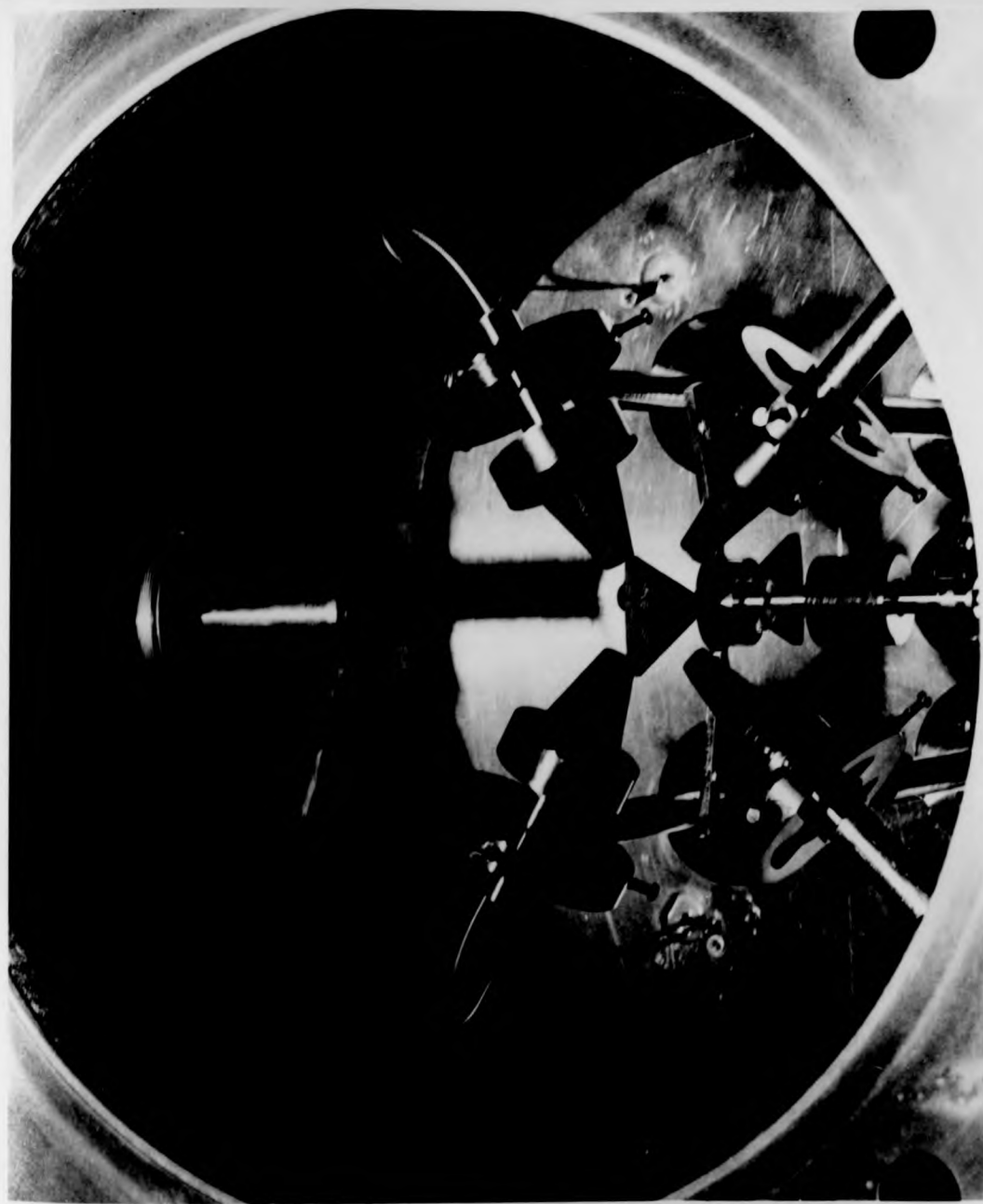


Plate 3. View inside the Mott Scattering Chamber.

elastically scattered electrons.

One of the end flanges supports the four detectors and the gold foil holder. There are two side flanges, on one of which is assembled the collimator from the accelerator lens system, and on the opposite one, a faraday cup, which is maintained slightly positive with respect to the chamber.

The scattering chamber is supported by a duraluminium assembly resting on four high voltage ceramic insulators*. This allows the complete chamber to float at 100 kV with respect to earth. The four insulators are on a further duraluminium framework which could be raised or lowered for alignment purposes. The assembly, immediately below the scattering chamber, can take two NIM bins with low voltage power supplies. All sharp edges on the upper assembly are rounded off, and on any corners where corona discharges were occurring, were covered with polythene tubing.

The mains voltage supply for the electronics is provided by a 1:1 oil filled Universal Voltronics isolating transformer capable of withstanding 130 kV. The high voltage supply is provided by a Universal

* Grateful thanks are due to the South of Scotland Electricity Board who provided the high voltage insulators used in this experiment.

Voltronics 160 kV - 5 mA oil filled generator. Since the output DC voltage of this generator is directly proportional to the input mains voltage, an Advance constant voltage transformer is used on the input. This maintains the output voltage constant to within $\pm 1\%$ for an input variation of up to $\pm 15\%$.

The ripple from the supply is quoted at 1.5% RMS at full current/voltage ratings, and so the high voltage supply is stable to within ± 3 kV. By interpolating from the calculations for the Sherman function (Lin 1964), the deviation from the quoted value is less than 0.2%. Electron intensity fluctuations do not cause trouble since all the polarisation measurements are obtained from the ratio of the number of counts in the two detectors.

For safety reasons the complete Mott scattering chamber assembly and accelerator lens is enclosed in a cage made of galvanised iron mesh, with a large perspex panel facing the electronics. Some of the electronics could be switched from the outside of the perspex panel using tufnol rods.

Because of the difficulties involved with having a vacuum pumping system "floating" at 100 kV above earth potential, the Mott scattering chamber is not pumped directly. The pumping is done by the 9" mercury diffusion pump via the main scattering chamber and the accelerator. The pressure in the Mott scattering chamber, after a few hours pumping, was roughly a factor

of ten worse than in the main scattering chamber giving a base pressure of about 10^{-5} torr.

5.4 THE ELECTRON ACCELERATOR

The electrons must be accelerated from the low voltage lens system to the required energy for the Mott scattering from gold.

The electron accelerator consists of a series of ten aluminium discs, each with a 50 mm ϕ hole in the centre, alternated with glazed ceramic discs with 100 mm ϕ holes in the centre, manufactured by Royal Worcester Industrial Ceramics (see Figure 11). To increase the leakage path the ceramic discs have a larger outside diameter than the aluminium ones, and the inside diameter is corrugated. The aluminium discs have radiused corners to eliminate discharges occurring.

Vinyl acetate was used to seal the discs together. Polyvinyl acetate powder was dissolved in a small amount of toluene to form a jelly. The jelly was then painted on the sealing surfaces, which were then baked for a few hours at 100°C to drive out the toluene. The discs were then aligned and clamped together. The complete assembly was then heated to 160°C and allowed to cool slowly over a period of several hours to 80°C , by which time the vinyl acetate had solidified, and the rate of cooling was increased.

The voltages are applied to the electrodes using a resistor chain of 10 x 10 megohm carbon resistors

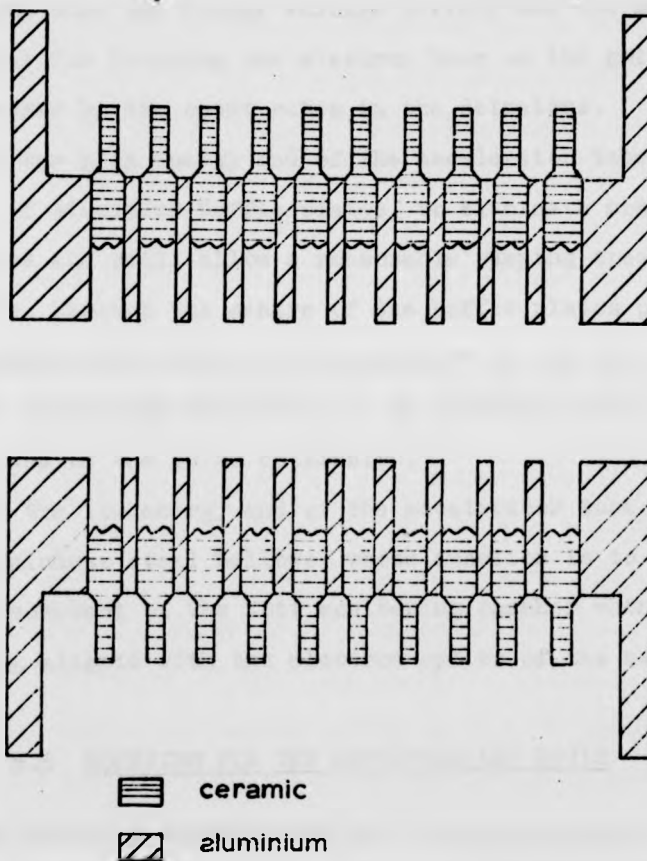


Figure 11. The high voltage accelerator assembly

between adjacent discs. The resistor chain was enclosed in $\frac{1}{2}$ " polythene tubing to prevent discharges occurring at the connections.

In principle the focusing properties could be altered by varying the number of resistors between the different discs, but in practice, it was done by using a separate 0 - 25 kV Miles Hivolt regulated power supply. This was used to maintain a voltage on the first, second, or third discs, which was continuously variable. It

was found that the linear voltage divider was the most efficient for focusing the electron beam on the gold foil, as measured by the count rates in the detectors.

At the high energy end of the accelerator tube is a series of aluminium baffle plates, to eliminate non-axial electrons and still allow a reasonable pumping speed down the tube. Through the centre of the baffle plates passes a collimator tube with a 20 mm aperture at the end. A further collimator tube with a 5 mm aperture could be attached on the end of the 20 mm collimator.

At the low energy end of the accelerator tube there is a stainless steel bellows, whose function is to allow slight movement of the Mott scattering chamber when it is being aligned with the electron optics of the main system.

5.5 MOUNTING FOR THE DETECTORS AND FOILS

The detector mounting for all four detectors are attached into the end flange, and are of stainless steel and aluminium construction. The plane of the detector can be rotated about its own mounting axis and small movements in the detector plane in any direction are possible. Supporting the end flange on a large turntable, a laser was used with a series of apertures to align the detector positions to the required angular settings with respect to the gold foil (centre of the scattering chamber). The settings obtained are as given below:

$$\theta_{+120} = 119.6^\circ$$

$$\theta_{-120} = 120.2^\circ$$

$$\theta_{+45} = 45.8^\circ$$

$$\theta_{-45} = 44.6^\circ$$

The detectors themselves were located inside an aluminium collimating arrangement which limits the acceptance angle to $\pm 15^\circ$ for the 120° scattering detectors and $\pm 10^\circ$ for the 45° scattering detectors.

Different foils were placed in a four vane shaped arrangement, made of aluminium, which could be rotated into position whilst under vacuum, by a direct rotary feedthrough calibrated in degrees.

5.6 THE GOLD FOIL.

The 'standard' foils used were gold foils of $200 \mu\text{g}/\text{cm} \pm 10\%$ thickness as supplied by the Yissum Research Development Company. The foils were mounted on an aluminium annulus 22 mm diameter before mounting in one of the vanes of the foil holder. Although the 'standard' foils were sufficiently thick to be self supporting all the foils used for the analysing power calibration of the mott scatterer and for polarisation measurements were backed with formvar. This backing was necessary for the thinner foils used in the calibration, and made even the thicker foils less susceptible to breakage. The pulse height distribution for electrons from unbacked and backed 'standard' foils showed no difference and there was no significant change in the scattered intensity.

Foils of other thicknesses were made by vacuum evaporating gold on to the backing of formvar which had previously been mounted on to an aluminium annulus.

5.7 THE DETECTORS.

The detectors used were of the silicon surface barrier and the lithium drifted silicon types, supplied by Nuclear Enterprises Ltd. Experience showed that since these detectors were being operated in a vacuum system which could be contaminated with mercury vapour, some protection was required for the front surface of these detectors. This surface, a very thin gold layer, was liable to form an amalgam with the mercury vapour, altering the properties of the gold-silicon junction. All the detectors used had their gold surface coated with formvar (Hils & McGregor, 1973, also see appendix 4). This coating is sufficiently thin so as not to seriously degrade the resolution of the detectors for 100 keV electrons. In Table 4 can be seen the noise performance of one of the surface barrier detectors (detector NSB 1017 - 300 - $\frac{1}{2}$, using a NE 5287A pre-amplifier) before and after coating with formvar. Although initially the noise level was higher, after one hour it was at its original level.

The details of the detectors are given below.

	$\pm 120^\circ$ detectors	$\pm 45^\circ$ detectors
type	Si surface barrier	Li Drifted silicon
sensitive area	300 mm ²	100 mm ²
depletion depth	100, 500 μ m	500 μ m
resolution (quoted) keV FWHM	27, 60	24, 28
operating bias voltage	6	200

It was found that the coated surface barrier detectors were not able to withstand the full bias voltage without occasional breakdowns occurring. The operating bias voltage is very much reduced from the maximum recommended, but is always kept great enough to ensure full collection of the charges produced in the detector.

TABLE 4.

Values of total RMS noise from a 5287A preamplifier and the NSB 1017 surface barrier detector, before and after coating the detector with Formvar.

bias voltage	RMS NOISE (mV)		
	before coating with formvar	immediately after coating with formvar	one hour after coating with formvar
0	370	392	369
5	149	174	145
10	111	125	108
15	95	107	93
20	87	98	86
30	79	90	78
40	75	86	75
50	73	84	73

5.8 THE DETECTOR ELECTRONICS.

As can be seen from Figure 12 the electronics can be considered in three stages:

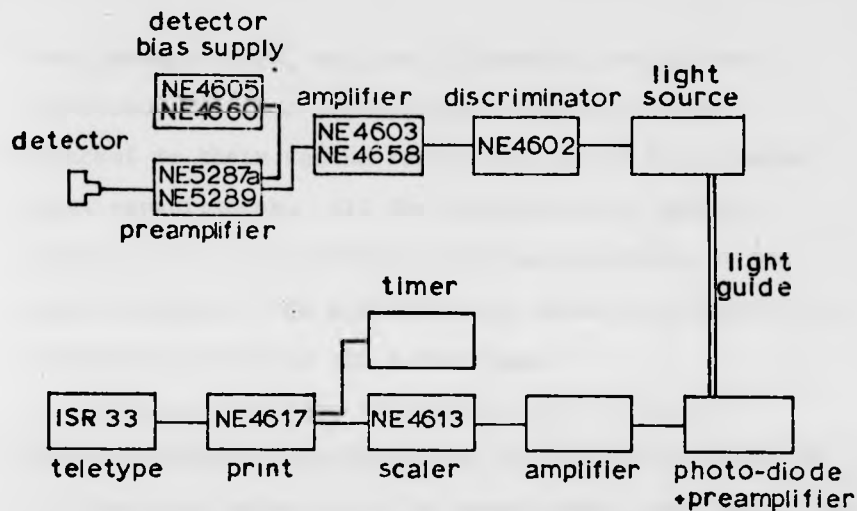


Figure 12. Block diagram of the detection electronics.

(a) from the detector to the analyser 'floating' at 100 kV

(b) optical telemetry - that part bringing the signal pulse from 100 kV to ground potential

(c) the scalers and teletype at ground potential.

The second stage could be omitted altogether if all of the detection electronics could be operated at the same potential. However, it is much more convenient if the scalers are operated at ground potential, if for instance, gating is required.

5.8(a) DETECTION AND AMPLIFICATION

There is a separate channel for each of the detectors and at the high voltage end, with the exception of the

four preamplifiers, all the electronics are in two NIM bins. The four preamplifiers were all placed adjacent to their vacuum feedthrough so as to minimise input capacitances. All the electronics at ground potential were in a NIM bin with the exception of the photo-diodes and the preamplifiers which were mounted on the perspex panel of the safety cage.

When an energetic electron enters the surface barrier detector sensitive area it produces a number of electron hole pairs as it is slowed down. By biasing the detector these charges are collected, and applied to the NE5287A preamplifier. This preamplifier produces an output pulse the height of which depends only on the energy of the incident particle (for a 100 keV electron a 25 mV output pulse). The main capacitance degrading the performance of the preamplifier is the detector capacitance. This combined with the noise of the detector results in moderate resolution (~ 25 keV fwhm). The output pulse has a fast risetime dependent on detector capacitance, with a 50μ sec decay.

TABLE 5.

Amplifier Settings for Optimum Pulse Shaping

Amplifier	Gain	T C (μ s)
NE 4603	512	0.8 (S.D.) 1.6 (D.D.) 0.8 (INT)
NE 4658	2800	0.4

The preamplifier output pulse is then fed to a NE 4603 amplifier, which provides pulse shaping allowing optimisation of the shaped output pulses.

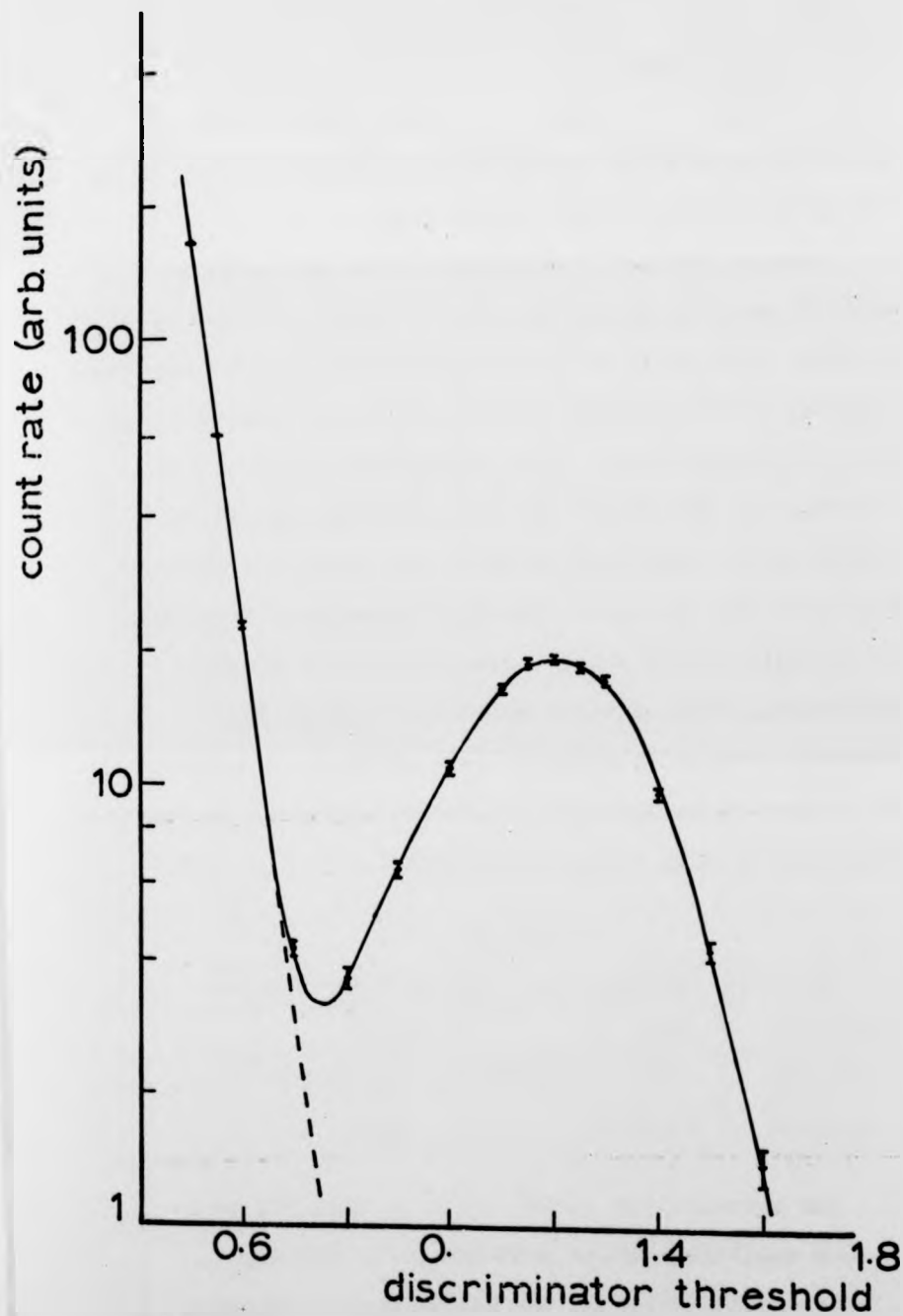


Figure 13. A pulse spectrum for 100 keV electrons scattered from gold.

The sett
 obtained
 cancella
 stage of
 The doub
 output p
 energy o
 discrimi
 scattere
 is used.
 output p

The
 similar
 noise le
 pre-ampl
 output p
 the dete
 detector
 pulse sh
 analyse
 The
 measuri
 electro
 monitor
 two cha
 thresho
 energy

The setting at which the best energy resolution was obtained is given in Table 5. 50 μ s pole zero cancellation takes place after the first differentiation stage of this amplifier eliminating any undershoot. The double differentiated output is used giving an output pulse whose amplitude is proportional to the energy of the initiating electron. In order to discriminate against noise pulses and inelastically scattered electrons, a NE 4602 single channel analyser is used. When triggered the analyser produces a positive output pulse of 5 V amplitude and 100 ns duration.

The circuitry for the 45° detectors is very similar but because of less detector capacitance, the noise level was considerably lower allowing a NE 5289 pre-amplifier to be used, which produced an inverted output pulse of 1 mV for a 100 keV electron incident in the detector. The main amplifier used with these detectors is a NE 4658 amplifier. It has more limited pulse shaping than the NE 4603 but greater gain. The analysers are the same as for the other detectors.

The settings for the analysers were obtained by measuring a pulse height distribution for 100 keV electrons scattered from gold. Two channels were monitored for constancy of current, while the other two channels had their ΔE set at 0.2 V and their lower threshold values incremented in steps of 0.4 V over the energy range. Such a spectrum can be seen in figure 13.

1.8
shold
electrons

The lower threshold value for the analyser was set to the value corresponding to the peak energy minus half of the FWHM and the upper value was set 5 V greater.

It can be seen that the electronic noise is completely discriminated against. This was also confirmed by switching off the 100 kV accelerating supply and the count rate in all channels was observed to be zero.

5.8.(b) OPTICAL TELEMETRY.

The analyser pulses are used to modulate a fast light emitting diode. The light is transmitted to a fast photo-diode at ground potential, by means of a 6 mm \varnothing x 600 mm long light guide. The light modulations are reconverted to pulses, and after amplification and suitable shaping, drive the scalars directly.

The Light Source. A Hewlett Packard gallium arsenic electroluminescent diode type HP 5082-4120 is used. The wavelength radiated by this diode is strongly peaked at 9000 Å with a FWHM of 330 Å and is emitted into a cone of a half angle of 35°. The rise time of a pulse is about 100 ns. The light output is 2 μ W/ma which is linear with forward current applied to the diode.

The Photodiode. A Hewlett Packard silicon planar PIN photodiode type HP 5082-4207 was used. The frequency response extends from DC to 1GHz whilst the quantum

detection efficiency is constant over six orders of magnitude of intensity. The efficiency is $0.4 \mu\text{A}/\text{uW}$.

The circuits used for driving the light source and the photo-diode preamplifier were those from Hewlett Packard application note 909 (with a few minor modifications).

The Driving Circuit (see Figure 14). The light emitting diode was placed in the collector circuit of a conducting transistor (collector current of roughly 20 mA). When the analyser pulse is applied to the base of the transistor it serves to modulate the collector current and thus the emitted light. The rise time of the light emitting diode is limited by the minority carrier lifetime which is partly compensated for with the 100 pF capacitors in base and emitter circuits. These have the effect of rapidly injecting or removing from the light emitting junction any charge necessary to change from one stable state to another.

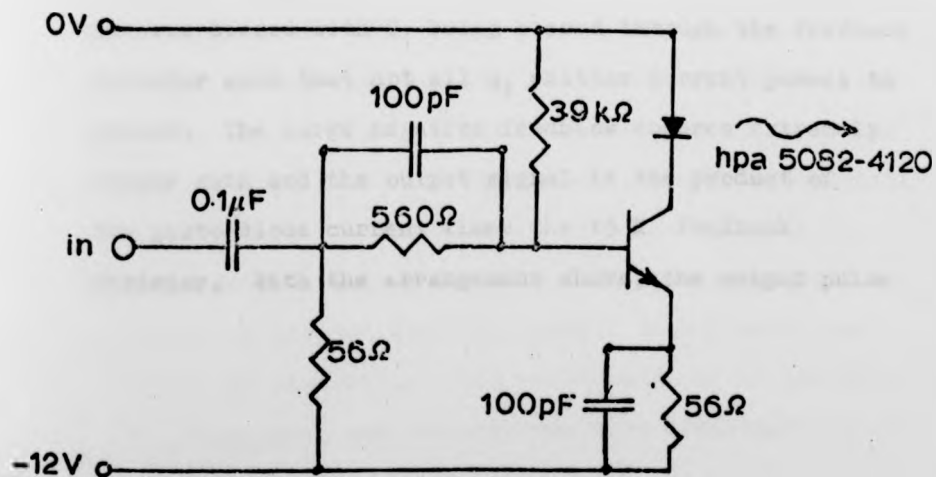


Figure 14. Light emitting diode circuit.

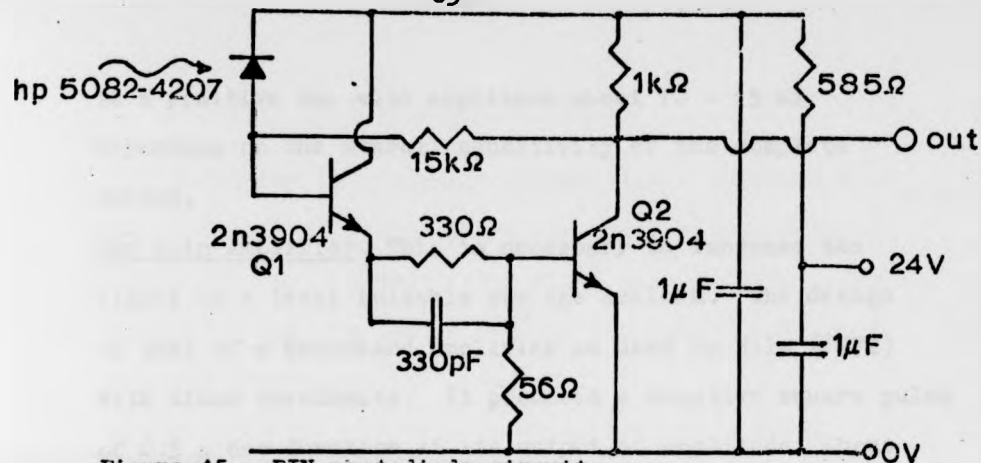


Figure 15. PIN photodiode circuit.

The Photo-Diode Preamplifier Circuit (see figure 15)

In order that the overall response of the photo-coupling circuit be determined by the light-source, the pre-amplifier must present a low resistance and low capacitance load to the photo-diode. Using 2N3904 transistors this is achieved, Q₁ is used as an emitter follower with its emitter connected to the base of Q₂. There is no feedback multiplication of the base-collector capacitance since its collector is grounded. The 15 k resistor provides negative feedback at base of Q₁ from the collector of Q₂. The photo-diode is reverse biased with Q₁ being biased through the feedback resistor such that not all Q₁ emitter current passes to ground. The large negative feedback ensures extremely stable gain and the output signal is the product of the photo-diode current times the 15 k feedback resistor. With the arrangement above, the output pulse

is a positive one with amplitude about 10 - 15 mV depending on the overall sensitivity of the complete system.

The Main Amplifier. This is necessary to increase the signal to a level suitable for the scalers. The design is that of a broadband amplifier as used by Hils (1972) with minor amendments. It produces a negative square pulse of 0.5 μ sec duration at its output of amplitude about 1 - 2 V. Saturation occurs at about 15 mV giving a 2 V output.

This output was then shaped further by use of a transistor switch which required a signal greater than about 0.5 V to operate it. This also allowed discrimination of any (noise) pulses from the preamplifiers which were below about 3 mV. This output pulse was a positive pulse of 5 V with a 0.5 μ sec width and was then directly connected to the scaler.

Telemetry Efficiency. To check the efficiency of the photo-electrical system, pulses from a pulse generator (NE 4608) were applied to a preamplifier and then as normal to an amplifier. The output pulses from the amplifier were fed to two separate single channel analysers. The positive output from the analyser was used to drive the light emitting diode and the pulses counted in the usual way. The positive output from the other analyser was used to drive a scaler directly. Both scalers could be started and stopped simultaneously. Each channel was checked out separately, from count rates of 10 per sec. to 10^5 per sec. and the readings were identical for all frequencies.

5.8(c) DATA ACQUISITION SYSTEM.

There are four scalers and one timer arranged such that they all start, stop and are reset simultaneously. The timer can be preset for a fixed time interval, or any of the scalers can be set for a preset total count, at which moment all are gated off. They are then interrogated in turn by a print control unit which prints out the total counts in each channel on a ISR33 teletype. When all five units have been interrogated, the units are reset and the cycle recommences. The results are also punched out on paper tape for analysis by computer.

CHAPTER VI

CALIBRATION METHODS

Before the Mott analyser can be used, it is necessary for it to be calibrated. This requires knowledge of the effect which multiple and plural scattering and other background effects have on the scattering asymmetries. This entailed an extrapolation procedure for foils of different thicknesses.

At the mercury scattering the correspondence between the angular setting of the electron beam and the resistance of the potentiometer is determined. The interaction energy at this stage is also evaluated by investigating the potential at which resonance effects occur.

Approximate values for the mercury beam density in the interaction region are also calculated here.

6.1 OPTIMUM THICKNESS FOR GOLD FOIL.

As the foil increases in thickness, initially the count rate increases about linearly but eventually decreases due to plural scattering. An optimum must exist beyond which the uncertainty of the resultant polarisation measurements increases. Van Klinken (1966) found the variation in $\sigma(\delta)/\delta$ for several foil thicknesses and for several electron energies, where δ is the asymmetry function (see equation 5.4) and $\sigma(\delta)$ is the standard deviation in δ . For electron energies

of 107 keV, he used a foil thickness of $225 \mu\text{g}/\text{cm}^2$

6.2. THE GOLD FOIL THICKNESS.

The thickness of the foils could be estimated by holding them in front of a light source and comparing their relative light transmissions as observed by eye.* A more quantitative method was to compare the transmission, or more correctly the scattering of an electron beam incident on the foils

The method used was to mount four gold foils in the Mott scattering chamber in the normal way. The number of electrons scattered into the detectors in a period of 10 seconds was noted and a new foil was rotated into position and the operation repeated until each foil had been in position.† The number of electrons counted in both 120° detectors were summed and likewise for the 45° detectors. This ensured that any polarisation effects were removed. The thickness was determined relative to a 'standard' foil, which was always included, by comparing the number of electrons scattered by each foil, through θ , in each cycle. These quantities were then averaged over all the cycles performed.

This method for determining relative thicknesses which assumes a linear relationship between N and t is

* Any obvious faults such as pinholes or non-uniform thickness could be seen and those foils were rejected at this stage.

† The cycle was then repeated several times (up to ten) resulting in intensity fluctuations being restricted to those occurring within one cycle which normally lasted about one minute.

only valid for very thin foils otherwise multiple scattering can effect the results obtained. Using 45° scattering as well as 120° scattering is useful as a check on this effect since the 45° value should be more sensitive to multiple scattering. However, although a discrepancy (13% for the thinnest foils) did exist it could not be explained by plural scattering. An average of the two values so obtained was used.

This operation was done using both a polarised electron beam, produced by scattering from a mercury beam, and with an unpolarised beam.

It was also repeated with the discriminator settings set much lower than the elastic scattering limit in order that inelastically scattered electrons would also be included in the measurements.

The same method was used for electrons incident on the gold foils with energies of 100 keV and 120 keV.

In each of the above checks the values were in very good agreement with each other.

6.3 DETERMINATION OF THE SHERMAN FUNCTION.

Although the values of the Sherman function have been derived theoretically and are in good agreement with experimentally derived values, these values are of no use as they stand. They apply for the case of single scattering with no background effects. In practice, multiple scattering which depends critically on the scattering geometry occurs. Multiple scattering can

(1920-1921)

...

...

...

$$1.0 \pm 0.1$$

$$1.0 \pm 0.1$$

$$1.0 \pm 0.1$$

...



...

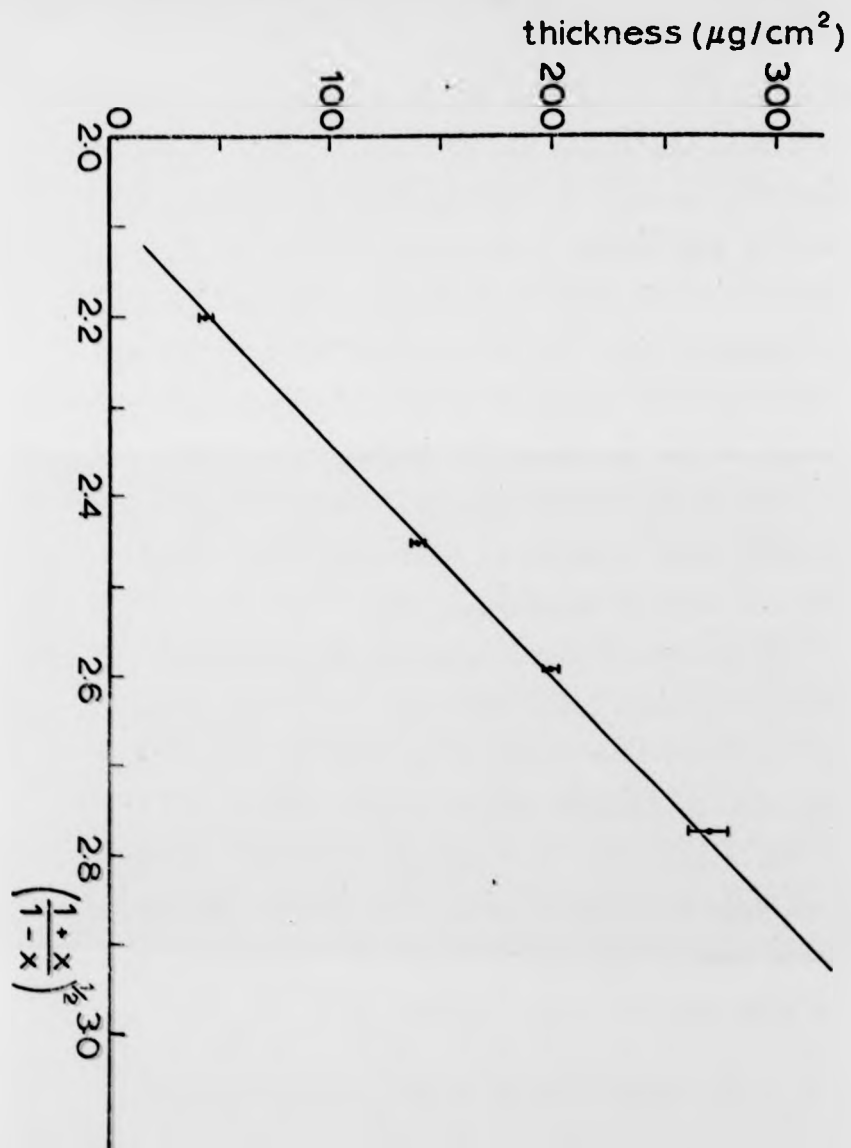


Figure 16. Graph of scattering asymmetry against gold foil thickness.

be elim

If thin

and a p

the bes

Po

produce

the mer

had bee

electro

determi

number

equatio

been ev

St

values

of the

disreg

straig

This b

where

which

T

as the

The pr

of the

90° fo

be eliminated by an extrapolation to zero foil thickness. If thin foils are used a linear extrapolation exists and a plot of $(PS)^{-\frac{1}{2}}$ against the foil thickness gives the best linearity.

Polarised electrons of unknown polarisation were produced by scattering the primary electron beam from the mercury beam in a region where a maximum asymmetry had been observed (95° scattering angle for 13 eV electrons). The asymmetry value, and hence $(PS)^{-\frac{1}{2}}$ was determined in the usual way, from the ratio in the number of counts in the 120° detectors as given by equation (5.3) for each of four foils whose thickness had been evaluated previously.

Since the statistical errors in the asymmetry values were considerably less than the averaging errors of the thickness of the foils, the former were disregarded in a least squares fit for the best straight line (see figure 16).

This best fit straight line satisfied

$$t = a + b (PS)^{-\frac{1}{2}}$$

where $a = 4.08 \pm 0.13$

$$b = 1.96 \pm 0.06$$

which gives $(PS_0)^{-\frac{1}{2}} = 2.09 \pm 0.09$

$$\text{This results in } S = (-0.259 \pm 0.022)$$

as the Sherman function for the 'standard' foil.

The process was repeated for another polarisation state of the incident electron beam, the scattering angle being 90° for 11 eV electrons. The value predicted for the

$\mu\text{g/cm}^2$)

300
-

y against

Sherman function for the 'standard' foil was -

$$S = -0.239 \pm 0.030$$

These two values were averaged giving

$$S = 0.25 \pm 0.02$$

as the value for the Sherman function of the 'standard' foil. The same 'standard' foil was used in all the polarisation runs and at no time did it show any sign of damage due to irradiation.

It is worthwhile noting that the uncertainty in the 'standard' foil thickness of $\pm 10\%$ does not enter into the above determination of $S(t)$ which is concerned with an extrapolation of relative thicknesses only.

6.4 DETERMINATION OF ANGULAR SETTINGS.

The angular position of the electron gun on the small turntable is referred to the straight through position, and is measured by means of the resistance between a fixed point and a sliding contact on a potentiometer wire. (see section 4.4).

The potentiometer wire was taken from a ten turn, Model A, Beckman Helipot. The resistance of the helipot was 100 kilohms with a linear tolerance of $\pm 0.25\%$. The total resistance, when cold, of the part of the potentiometer used was 36.48 ± 0.02 kilohms. Using the calibration marks in its PTFE mounting at 60° intervals, any lack of linearity was checked for, and a calibration value, ρ , was obtained in reduced units

of resistance, $R(\text{meas.})/R(\text{total})$.

$$\rho = 300.75 \pm 2\% \text{ Deg/unit.}$$

Reduced units of resistance are necessary because when in situ the potentiometer wire experiences radiation heating from the mercury boiler. The total resistance, R_T , was then measured as well as the resistance to the sliding contact, R_B , and the angle with respect to either end of the wire could then be determined.

Although the method above provides a scale calibration, it does not relate to the angle which the electron gun makes with the lens system. Using the sum of the counts in the 45° detectors and scanning the electron gun about the straight through position, the zero degree position was obtained from the line of symmetry when the count rate was plotted against resistance R_B .

Another method used was to look for the symmetry between minimum in the scattered intensity at both positive and negative scattering angles. This was done for the minima appearing around 80° angle of scattering for the incident energies of 13.1 eV and 15.1 eV. Good agreement was found between both these methods.

The effect of any non-linearity in the resistance values caused by uneven heating of the potentiometer wire is considered to be small since the resistance wire itself is wound on a 3 mm diameter copper wire. The total change in resistance corresponds to an increase of 1.3%.

From the errors in the methods above, the final

calibration in the angular position of the electron gun is expected to be accurate to within $\pm 2.5^\circ$ and the reproducibility is accurate to $\pm 0.2^\circ$.

6.5 THE MERCURY BEAM DENSITY.

The rate of effusion from the oven into a vacuum can be obtained from kinetic theory and is governed by

$$dQ = \frac{n \bar{v} A_s}{4 \pi} \cos \theta d\omega$$

where dQ is the number of molecules emerging per second into solid angle $d\omega$ at an angle of θ with respect to the normal of the aperture of area A_s . n is the number of particles per unit volume and \bar{v} is the mean molecular velocity inside the source.

It is more convenient to consider a relation for the beam density which will be obtained some distance from the source. Substituting for n , \bar{v} and d and considering a point along the axis the intensity is given by

$$I = 1.118 \times 10^{22} \left(\frac{p A_s A_d}{L^2 \sqrt{MT}} \right) \quad (6.1)$$

where M is the atomic weight, T is the absolute temperature of the source, p is the pressure in the source (in torr) and I is the number of molecules per second passing through an area $A_d \text{ cm}^2$ at a distance of $L \text{ cm}$ from the source.

The beam density (in atoms/cm³) at this point is given by

$$\rho = 6.5 \times 10^{17} \frac{A_s p}{L^2 T} \quad (6.2)$$

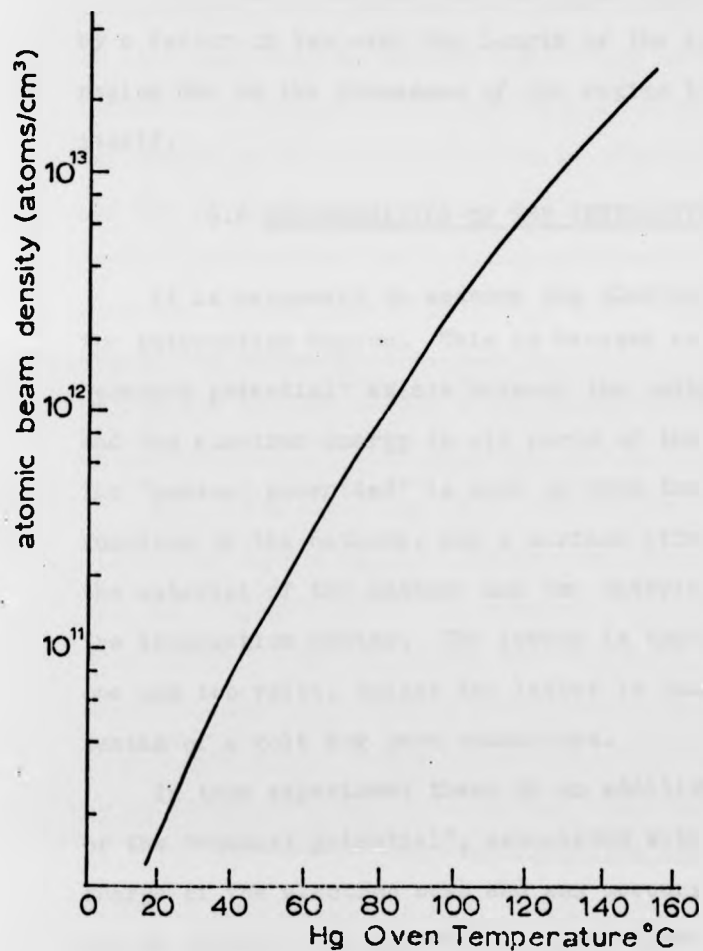


Figure 17. Mercury beam density in the interaction region as a function of oven temperature.

Using the values for A_g and I given below along with values for p and T from tables, the mercury beam density was obtained for the temperature range used (see figure 17) At the operating temperature the temperature was typically between 10^{-4} - 10^{-3} torr.

$$A_g = 0.025 \text{ cm}^2$$

$$L = 2 \text{ cm}$$

It is worth noting that the beam density can vary by a factor of two over the length of the interaction region due to the closeness of the region to the nozzle itself.

6.6 DETERMINATION OF THE INTERACTION ENERGY

It is necessary to measure the electron energy in the interaction region. This is because no unique "contact potential" exists between the cathode potential and the electron energy in all parts of the system. The "contact potential" is made up from the work function of the cathode, and a surface effect between the material of the cathode and the material surrounding the interaction system. The former is typically between one and two volts, whilst the latter is only a few tenths of a volt for pure conductors.

In this experiment there is an additional component of the "contact potential", associated with the space charge of the electron beam and any mercury ions which may be present. In appendix II this effect is formulated.

The determination of the "contact potential" is made by observing the resonance structure in elastically scattered electrons from mercury and helium.

6.6(a) USING THE RESONANCE STRUCTURE IN MERCURY.

There has been a number of resonances observed in elastic scattering from mercury. Kuyatt, Simpson and

Mielczarek (1965) observed resonances in the transmission of electrons through mercury vapour and Düweke, Kirchner, Reichert and Staudt (1973) have reported on the angular dependence of differential cross-section measurements for two of those resonances. A study was made to investigate whether these resonances could be observed with the present apparatus. This will depend on whether any of the resonance structure is sufficiently broad enough for the effect not to be masked by the electron energy spread in the interaction region.

The cathode voltage could be scanned over a restricted energy range. The mercury oven temperature was set to about 120° C and several scattering angles were studied. The electrons were detected in the same manner as for polarisation measurements by scattering from a gold foil. Since polarisation effects were not being considered and intensity was important, the thickest foil ($270 \mu\text{g}/\text{cm}$) was used, and the counts from all four detectors were added together and displayed on a ratemeter (NE 4607). The output from this ratemeter was plotted on an X - T chart recorder. A recording of scattered intensity against cathode potential could be obtained. The focusing of the lens elements was carried out by optimising the count rate at the mid-voltage value of the scanning range.

Although some structure did appear in the scattered intensity traces, any assignment of a particular resonance was generally not possible due to the breadth of the structures. The traces which were reproducible had a

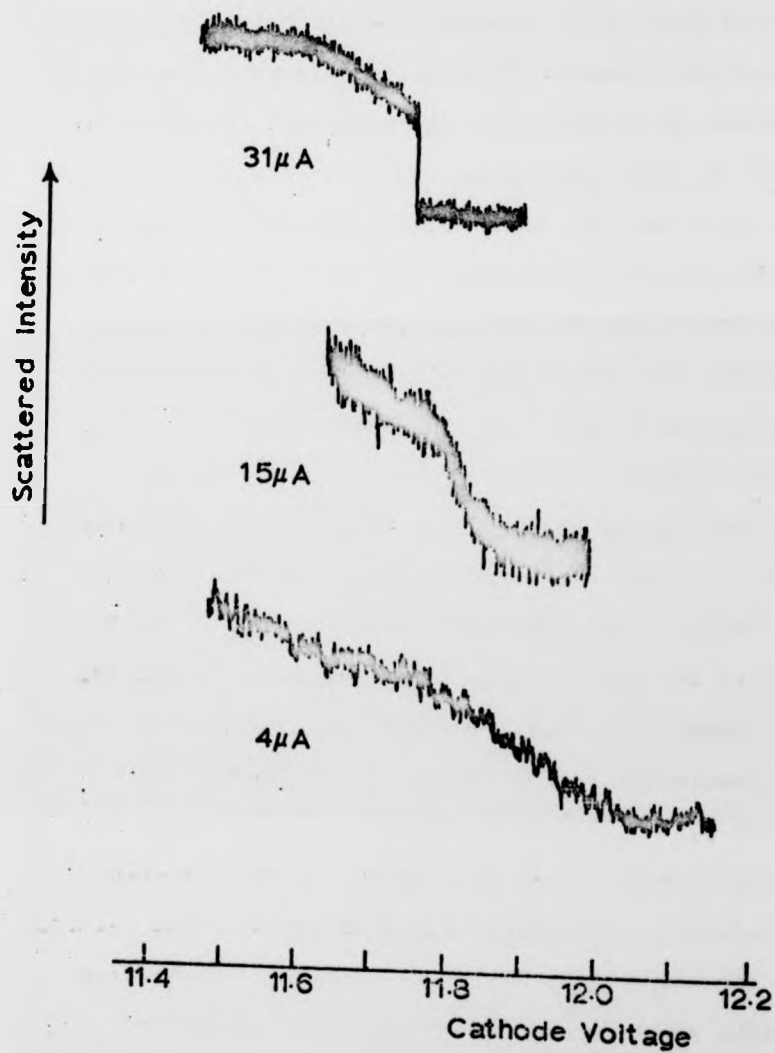


Figure 18. Scattered intensity as a function of primary current near the mercury ionisation threshold.

very dis
angles of
much less
in the s
of

The
was gover
ratemete
was used
electron
step dec
change f
figure f
of about
This di
ionisat
potenti

In
intensi
to 13 v
in heli
ascribe
Contact
been as
and the
into ac

*The res
from th
(privat

very distinctive feature, especially at scattering angles of less than 60° where the other structures were much less pronounced. This was an abrupt discontinuity in the scattered intensity at an applied cathode potential of

$$V(k) = 11.7 \pm 0.1 \text{ volts}$$

The abruptness of this discontinuity on the trace was governed entirely by the time constant of the ratemeter, even when the smallest time constant of 0.1 sec. was used. The abruptness was affected by the primary electron current. As the current was lowered the step decreased in height until a rapid but continuous change in the scattered electrons was measured (see figure 18). There was also a slight shift in position of about 0.1 volts towards higher cathode potentials. This discontinuity occurred near the threshold of ionisation for mercury (10.4 volts interaction potential).

In figure 19 there is a trace of the scattered intensity as the cathode voltage is scanned from 5 volts to 13 volts. Subsequent to investigating a resonance in helium (next section) some resonances have been ascribed* and are shown on a corrected energy scale. Contact potentials of 1.5, 1.6, and 0.9 volts have been assumed for the first two, the following four, and the last two resonances respectively. This takes into account the space charge depression increasing with

*The resonance energies have been increased by 0.6 volts from the results of Kuyatt, Simpson and Meliczarek (1965) (private communication with Burrow and with Ottley).

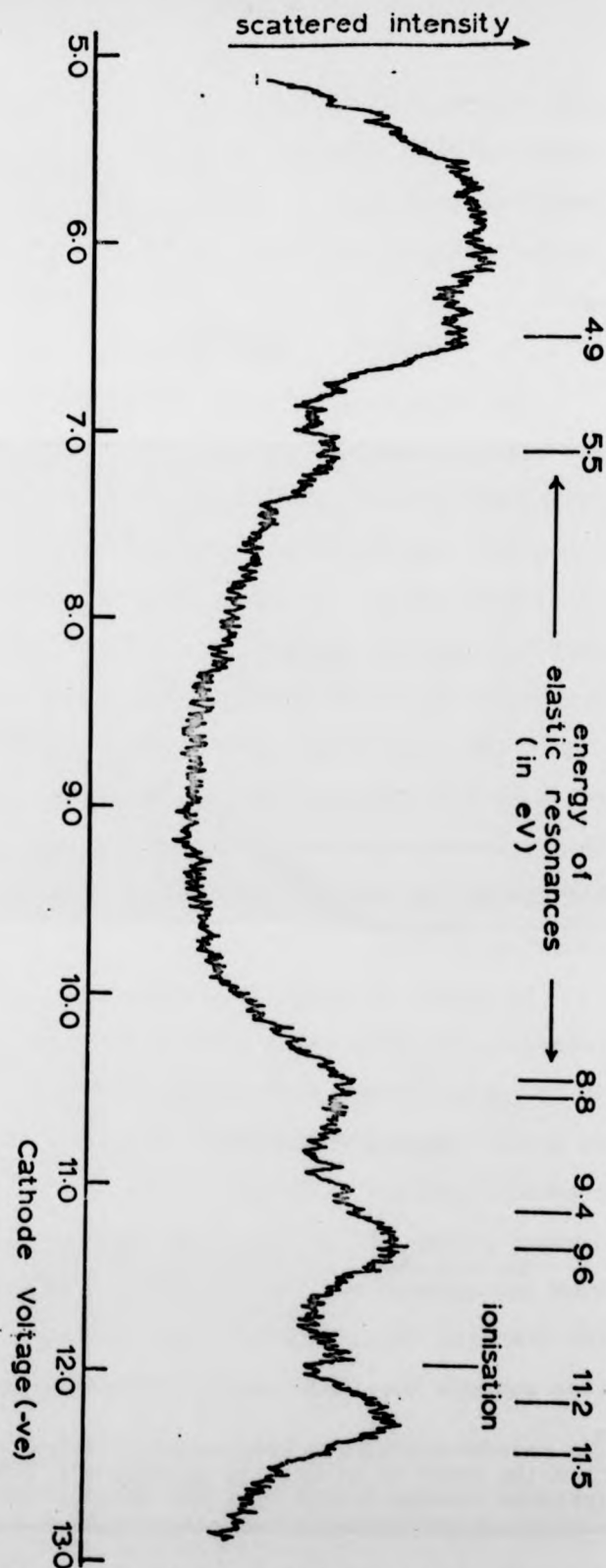


Figure 19. Resonance structure in the electron intensity

increasing

An effect

is inferred

ionisation

space char

for elect

Be

details

also bec

greater

A method

10.4 eV

space ch

6

Usi

into the

helium t

describ

elastic

Mielcz

correspo

ion stat

appears

Therefor

expecte

pumped

increasing current, until cancellation by ions occurs. An effective contact potential of

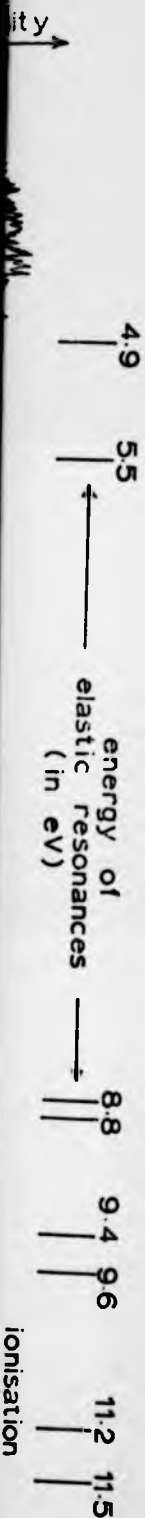
$$\phi_{\text{eff}} = 1.5 \pm 0.5 \text{ volts}$$

is inferred, for interaction energies below the ionisation level in mercury. This value includes a space charge depression estimated to be about 0.4 volts for electron currents of typically 30-40 μA at 10 volts.

Because of the difficulty of getting quantitative details from the resonances in mercury scattering, and also because this method was not available for energies greater than about 10 eV it was not followed further. A method was still required for energies greater than 10.4 eV since the presence of ions will influence the space charge depression due to the electrons.

6.6(b) USING THE 19.3eV RESONANCE IN HELIUM.

Using a dosaging valve, helium gas was leaked into the system providing a background pressure of helium throughout the system. Using a similar method described in section 6.6(a) the 19.3 eV resonance in elastic scattering from helium (Kuyatt, Simpson and Mielczerak, 1965) was looked for. This resonance corresponds to the virtual formation of a negative ion state with the configuration $(1s2s^2)^2S_{\frac{1}{2}}$, and appears as a large increase in transmitted current. Therefore a decrease in the scattered signal is to be expected. Helium has the advantage of being easily pumped allowing fairly high pressures to be used and



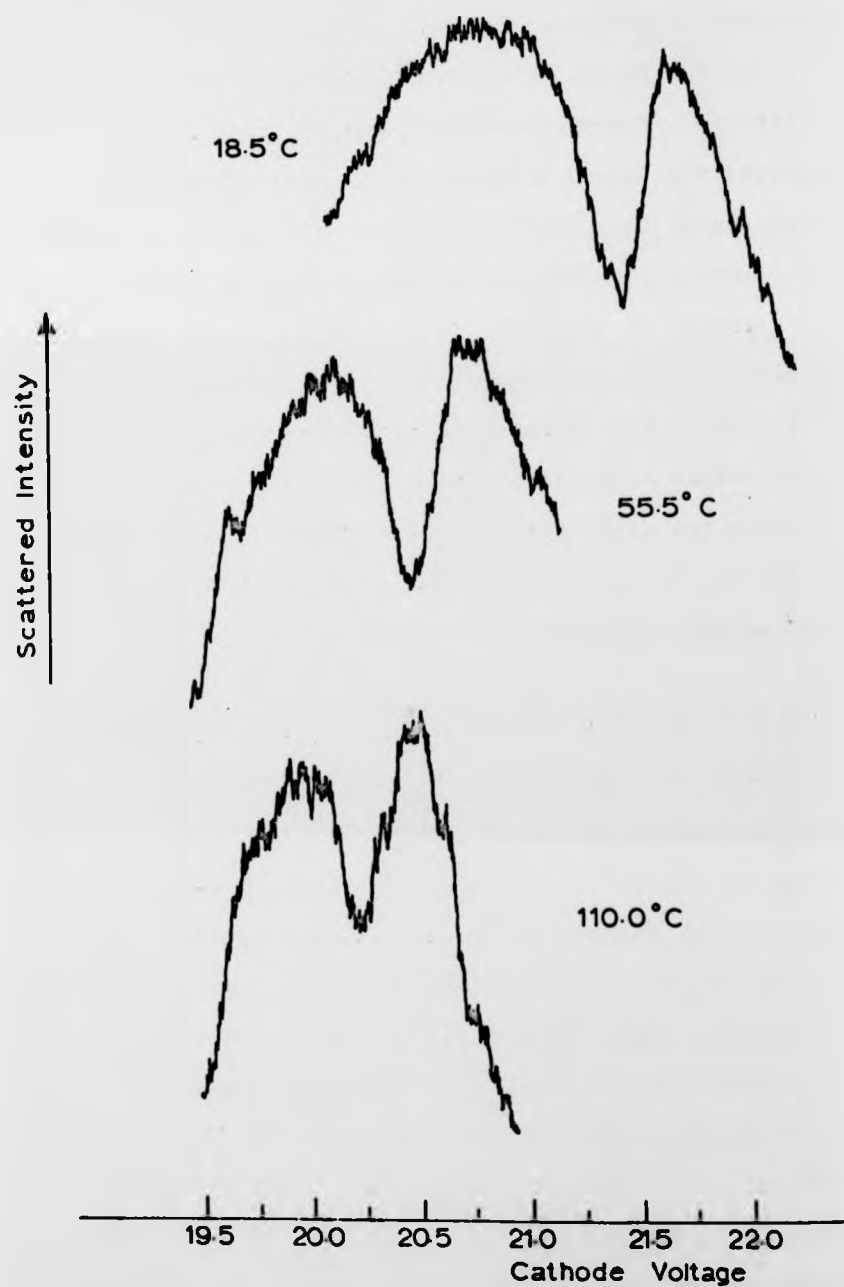


Figure 20. Variation with mercury density (oven temperature) of resonance structure in the electron intensity elastically scattered from helium at 90° .

also being
was found
then the
system, a
pressure
of about

The
scatteri
curves w
producing
angle wa

The
until we
temperat

The over
normal
so obtai

of the
to the
cathode

then pl

interac

the boi

By

thus al

charge,

includi

also being inert does not contaminate the system, It was found that if the pressure was less than 10^{-4} torr He then the resonance signal was lost in the noise of the system, and if more than about 2×10^{-3} torr He then pressure fluctuations occurred. A background pressure of about 1×10^{-3} torr He was used for all measurements.

The change in the shape of the resonance with scattering angle was investigated and a set of dispersion curves was obtained with the 90° scattering angle producing a reasonably symmetric depression. This angle was used subsequently.

The cathode potential was scanned from 19.5 volts until well clear of the helium resonance and the temperature of mercury boiler was noted for each scan. The oven was slowly heated up from 18°C to above the normal operating temperature. A few of the resonances so obtained can be seen in Figure 20. The centre of the resonance was taken as the point corresponding to the mid-point of the full width half minimum. The cathode potential at which the resonance occurred was then plotted against the mercury density in the interaction region as determined from equation 6.1 and the boiler temperature (see figure 21).

By extrapolating to zero mercury density, and thus also zero ion cancellation of the electron space charge, the value of the total contact potential including the electron space charge (ϕ^{te}) was obtained.

22.0

age

Oven
ature in the
scattered

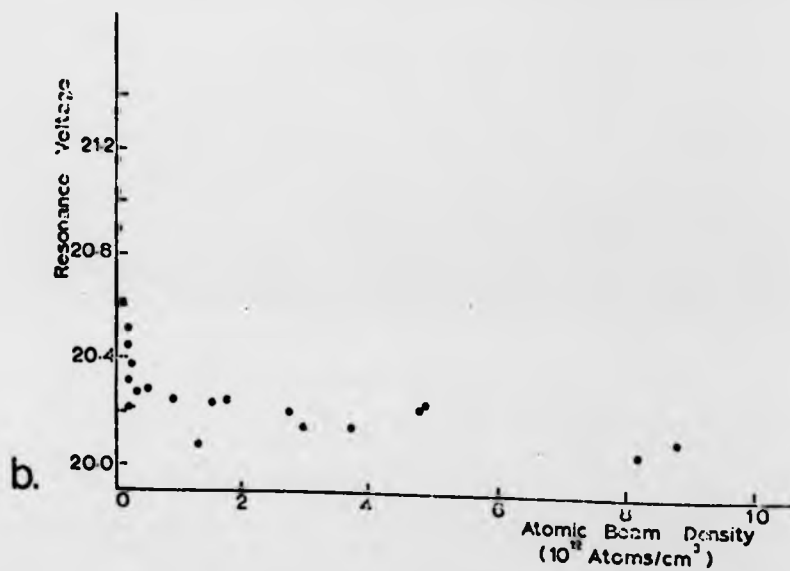
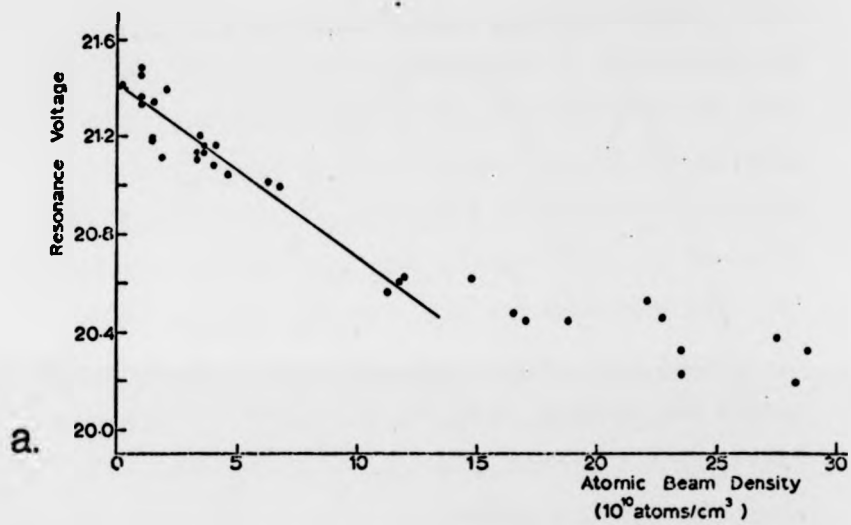


Figure 21. Position of the 19.5 eV resonance structure in helium as the mercury beam density is varied.

A l
figure 21
 12×10^{10}
and total

From figu
in the pr
nearly lo
potential
the ion
temperat

The ion
until th
repel th
region w
From
can be e
interact
potentia

6.

The
region
rate.

A least squares fit was made for all points of figure 21a, which were for a mercury density of up to 12×10^{10} atoms/cm³. Values for the resonance potential and total 'contact potential' were obtained.

$$V_R^e = 21.4 \pm 0.1 \text{ volts}$$

$$\phi^{te} = 21.1 \pm 0.1 \text{ volts}$$

From figure 21b the cathode voltage at resonance in the presence of the ion space charge can be seen to nearly level out giving values of the resonance potential and the "contact potential" including the ion space charge (ϕ^{ti}) at the normal operating temperature to be

$$V_R^i = 20.2 \pm 0.1 \text{ volts}$$

$$\phi^{ti} = 0.9 \pm 0.1 \text{ volts}$$

The ion space charge can become appreciable because until they establish a large enough electric field to repel themselves they move slowly out of the interaction region with the thermal velocities of the atoms.

From the value of ϕ^{ti} an effective "contact potential" can be established which is applicable to all interaction energies, greater than the ionisation potential, when a mercury beam is present in the system.

$$\phi^{eff} = 0.9 \pm 0.1 \text{ volts}$$

6.6(c) EQUILIBRIUM BETWEEN IONS AND ELECTRONS.

The number of mercury ions present in the interaction region is governed by the production rate and the loss rate. There are two main processes which take part in

25 30
Beam Density
(atoms/cm³)

10
Density
(cm⁻³)

Resonance
of mercury

the loss rate. Initially the escape rate is governed by the thermal velocity of the ions (confirmed by the straight line extrapolation to zero mercury density, above).

Once the total ion charge is greater than the electron charge, the space charge effect changes from a potential depression to a potential enhancement. The positive space charge effect begins to cause the escape rate to increase by mutual repulsion of the ions.

These effects are outlined in appendix 2. A result in qualitative agreement with those measured is obtained for the voltage depression (or enhancement) as a function of the atom beam density.

6.6(d) EXPERIMENTAL DETERMINATION OF POTENTIAL DEPRESSION.

Further justification is required before it can be stated with conviction that these voltage shifts detailed above, arise from the influence of space charge from the electrons and ions which are present, and not from for instance a mercury / helium mixture having a different contact potential from helium alone. This justification can be obtained if it can be shown that the equations in appendix 2 are satisfied when only helium is present.

With the mercury boiler cold, the anode potential was used to alter the primary current, and a series of scans was performed to measure the variation on the cathode voltage, corresponding to the 19.3 eV resonance

in Helium, with the incident current. As before the angle of scattering was 90° . Any change in the focusing of the electron beam due to the method of adjusting the current cannot affect the voltage at which the resonance takes place.

In table 6 can be seen the measured values of the the primary current and the cathode voltage at resonance. Also listed in this table is the space charge depression as calculated from equation (A2.3). To obtain the value to be used for the $\ln R/R_0$ term, reference is made to figure 21 and an estimate for the value V_p at which the ion space charge effect takes over from ion drift effect is obtained. This value was used to obtain the space charge depression (i.e. condition where space charge effects cancel each other out) for use with one of the primary current values for obtaining the $\ln R/R_0$ term. Because at different currents the dimensions of an electron beam under space charge conditions vary, corrections must be applied to compensate for this. Use is made of the Universal space charge curve (Pierce, 1954, p. 202) by considering a constant position along the axis and evaluating the change in beam radius. This correction was carried out for each of the current values. This procedure was repeated for slightly different conditions when the mercury boiler was a few degrees hotter.

In the last column is tabulated ($V_R - \Delta\phi$). For each of the primary currents it can be seen that there is good agreement between each of them confirming that the assumptions regarding the nature of the potential shift are reasonable.

TABLE 6.

Resonance voltage for different primary currents
after allowing for a space charge depression.

Primary Current	Cathode Voltage at Resonance	Correction for primary Beam Dimensions		Space Charge Depression	
i (μ A)	V_R (volts)	$\ln 1/R$	$\ln R/R_0$	$\Delta \phi$	$V_R - \Delta \phi$
104	21.06	0.00	1.14	0.81	20.25
79	20.94	0.15	1.29	0.70	20.24
49	20.80	0.46	1.60	0.54	20.26
25	20.74	0.79	1.93	0.33	20.41
110	21.33	0.00	1.44	1.08	20.25
52	21.02	0.46	1.90	0.67	20.35
34	20.73	0.65	2.09	0.49	20.24
33	20.74	0.69	2.13	0.48	20.26
16	20.49	0.99	2.43	0.27	20.22
14	20.47	1.05	2.49	0.24	20.23
6	20.30	1.35	2.79	0.11	20.19

CHAPTER VII

THE MEASURED ASYMMETRIES.

In this chapter attention is paid to the asymmetries actually measured, and to how they relate to the actual electron beam polarisation. Consideration is given to the importance in avoiding instrumental asymmetries and to the methods for detecting them if they exist. The influence of electromagnetic fields on the polarisation vector is also discussed.

7.1 INSTRUMENTAL ASYMMETRIES.

The main difficulty in polarisation measurements by means of a Mott scattering arrangement is that caused by instrumental asymmetries. These effects can greatly exceed the small variations in intensity arising from genuine polarisation effects. Such effects can be caused by effects which are constant in time, but others can be of a more randomly varying nature.

The time independent, or at worse slowly varying, effects such as solid angle subtended by the detectors, angular misalignment of the detectors, background effects can be included in the factor A of equation (5 - 4). These asymmetries will cancel in the evaluation of the polarisation value.

However, the time varying effects are more troublesome and more detailed consideration will be given to them. They will most probably be caused by the beam shifting its position of incidence and/or

its angle of incidence on the gold foil. In this experiment this is possible if the primary electron gun does not rotate symmetrically about the mercury beam causing the lens system to be viewing a variable scattering volume. This point is considered in Appendix 3.

Another cause could be a background effect which varies in a random fashion. Such an effect is present in the field emission (Malter effect) background from the accelerator system. This effect varies from day to day and decreases as the background mercury pressure in the main scattering chamber rises. The last element of the alkali filter lens system which was manufactured from aluminium was copper plated to reduce the field emission from it. The remaining field emission electrons were counted by regularly blocking the filter lens during polarisation runs. This count was then subtracted from the signal counts.

Any large fluctuations in the counting rates which would not appear on all the detectors simultaneously will also cause asymmetries. These fluctuations could be due to electrical interference caused by ground loops picking up spurious pulses. To overcome the ground loop problem it is necessary to be careful when earthing the preamplifiers, both the ones at high voltage and the ones at the pulse telemetry receiving end. Other dubious earths exist at the signal feed-throughs into the Mott Chamber. In order that such effects might be allowed for, integration times were kept fairly short,

ten to fifty seconds, dependent on count rates, and repeated several times at each setting.

To investigate spurious asymmetries a method in which polarisation effects are insensitive is required. It is necessary to look at the variables present in the scattering process, viz, E, θ and Z , and consider them further in the way in which the scattering process is altered as they are changed. Theory predicts that S decreases at low E , small θ , low Z and because of multiple scattering as t increases. If by adjusting at least one of these parameters it is possible to have a test for unwanted asymmetries, any corrections necessary can be applied to the data.

7.1(a) USING LOW ELECTRON ENERGY.

This was the method used by early investigators who assumed that the asymmetry function decreases strongly with energy. This ignored the fact that such instrumental asymmetries as they are seeking to investigate may also be energy dependent. In any case this point would be true to the extent that as the energy decreases, multiple scattering in the foil. unless the foil was replaced by a thinner one, will increase, changing the sensitivity of the device. However, at very low energies the polarisation effects can again become large as is seen by experiments on mercury from a few eV to a few keV.

7.1(b) BY VARYING SCATTERING ANGLE.

As can be seen in figure 10 the Sherman function is nearly zero for $\theta < 50^\circ$, so it is mainly the instrumental asymmetries which are present here. This method has an advantage that it can be carried out simultaneously with the polarisation measurement and that the counting rates are increased at smaller angles. This last effect makes it very sensitive to any changes in angle of incidence on the foil.

7.1(c) USING A LOW-Z SCATTERER.

The asymmetry for a low Z material like aluminium ($Z = 13$) at 100 keV at a scattering angle of 120° is about 7% of that for gold (Sherman, 1956, Lin, 1964) at the same energy and angle. If the gold foil is replaced by an aluminium foil, the measured asymmetry due to polarisation will be reduced to less than 7% of the original asymmetry. The differential scattering cross section for 100 keV electrons at 120° scattering is reduced by a factor of 1000 for aluminium compared to gold, so for comparable scattered intensity a considerably thicker foil must be used. However, because the differential cross section for aluminium has more pronounced angular dependence than that of gold, the plural and multiple scattering effects are more pronounced and therefore the angular distribution of the scattered electrons will be different.

7.1(d) USING A THICK SCATTERER.

For extremely thick foils, multiple scattering is the dominant effect, and the resultant asymmetry due to the polarisation can be reduced to less than 10% that of an infinitely thin foil. Because of the greater differential cross section, it is best to use a thick foil of high Z material to increase the scattered intensity, for instance, tungsten foil.

The most useful method of checking on spurious asymmetries is that of varying the scattering angle. This method requires an additional pair of detectors and associated electronics but allows simultaneous measurement, whereas using different foils entails a separate measurement when conditions are not necessarily exactly the same, and is also time consuming.

Two additional detectors were used at $\pm 45^\circ$ scattering angles, where the Sherman function is small. The asymmetry ratio for these detectors was calculated in a similar way to that of the 120° detectors. This ratio is used as a monitor to provide details of which values include an instrumental asymmetry.

A check was carried out on the fact that an asymmetry due to polarisation was indeed caused by electron polarisation, by using the method of low Z scatterer. The primary scattering conditions from which an asymmetry had been produced for gold foil as the scatterer, were used with an aluminium foil of 2 mg/cm^2 thickness, and an asymmetry looked for.

The asymmetry detected was only about 10% of that produced by the gold foil. This is what would be expected if this asymmetry was produced by a polarisation effect, whereas if it had originated from instrumental effects the asymmetry should remain largely unaltered. Any check on the polarisation detected using other foils was not carried out since the Sherman function is (for most other materials readily obtainable in the form of foils) considerably reduced. This would require increased integration times with considerable repetition.

7.2 EFFECT ON THE SPIN OF AN ELECTRON OF A HOMOGENEOUS FIELD.

Consideration must be given to how, if at all, the electron polarisation produced by scattering from mercury atoms is altered in its passage to the alkali scattering region, and on to the Mott spin analyser.

In a homogeneous electric field, only the field component transverse to the electron motion will produce a change in the electron spin direction, with respect to the momentum direction (Bargmann, Michel & Telegdi, 1959, and Meister, 1962). In the present apparatus the only transverse electric field present is the focusing effect of the lens elements. This effect is cancelled out when the electron beam is focused at a point further down the system.

In a homogeneous magnetic field, the magnetic moment associated with the electron spin experiences a torque.

This leads to the electron spin precessing around the magnetic field with the Larmor frequency of a free electron.

$$\omega_L = eB/m = 1.78 \times 10^{10} \text{ sec}^{-1} (\text{Wb/m}^2)^{-1}$$

The spin direction will rotate through an angle given by

$$\phi = \omega_L T$$

where T is the time of flight. From the knowledge of the energy of the electron and the magnetic field (approximately) along the electron trajectory this angle is estimated to be

$$\phi < 4 \times 10^{-2} \text{ rad.}$$

This means that the two detectors in the Mott chamber are at angles of $(\pi/2 \pm 0.04)$ radians with respect to the spin direction.

The polarisation can be resolved into two components, one lying in the plane of scattering ($P \sin \phi$), and one normal to the plane of scattering ($P \cos \phi$). It is only the latter component which will give rise to an asymmetry in the electron count rate between the two 120° detectors (see section 3.4)

$$\frac{\Delta P}{P} = 1 - \cos \phi \approx 10^{-3}$$

The correction between the measured polarisation values and the actual polarisation values is considerably smaller than the errors associated with the polarisation measurement and will be neglected.

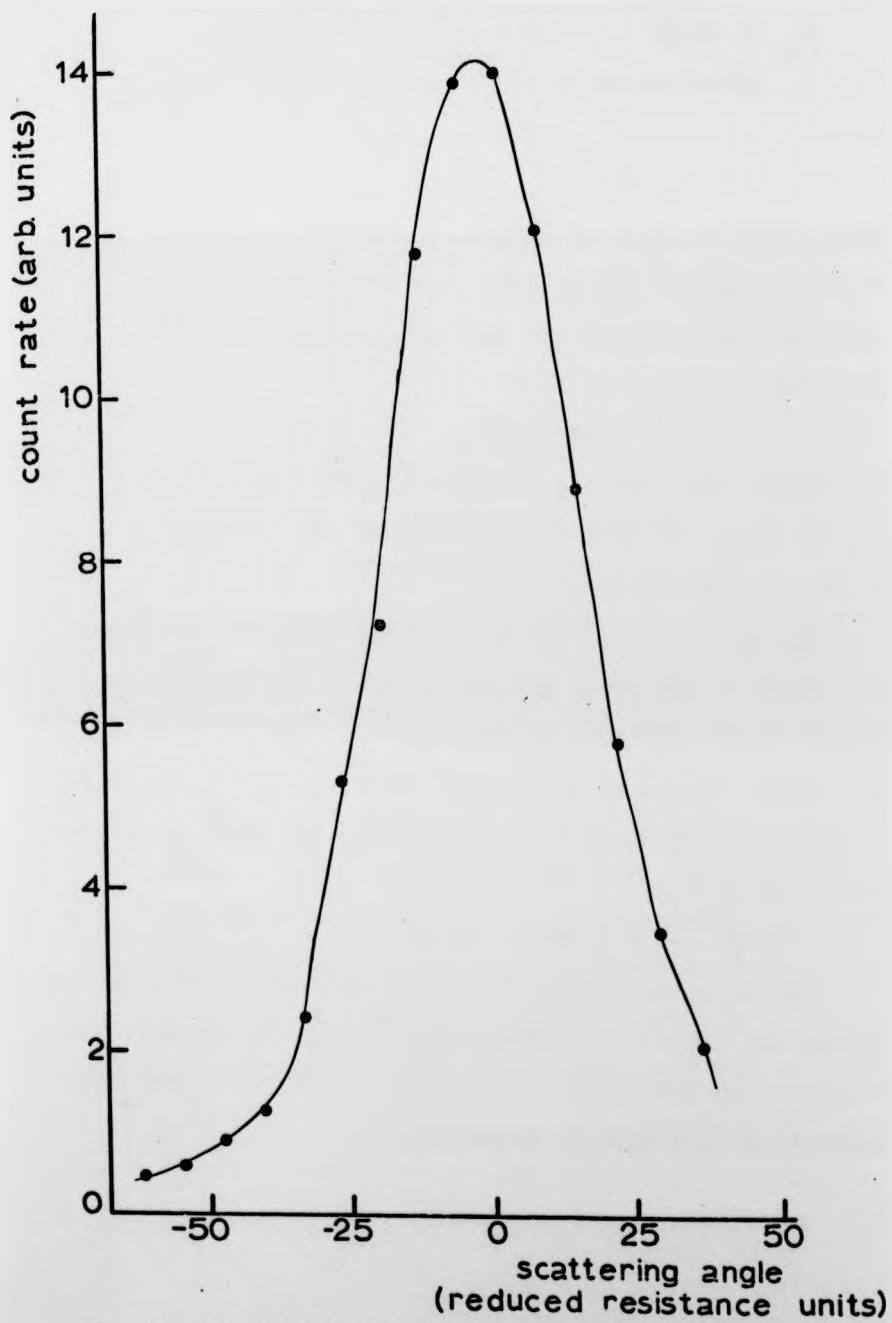


Figure 22. An electron beam profile.

In o
the filte
electron
In order
primary o
electron
in the Me
was plot
electron
electron
the width
lens sys
over man

The
is its c
used to
straight
gun and
and the
detector
an integ

7.3 MERCURY FILTER LENS PERFORMANCE.

In order to ascertain the angular acceptance of the filter lens at the mercury scattering stage the electron gun was swept over the straight through position. In order that the detectors were not saturated, the primary current was reduced to about 10^{-8} A. The electron signal was detected using the 45° detectors in the Mott chamber, and the sum of both the scalers was plotted as a function of angular setting of the electron gun. In Figure 22 can be seen a typical electron beam profile obtained by this method. From the width at half maximum the angular acceptance of the lens system was obtained. An average value, taken over many different conditions, is given by

$$\Delta\theta = \pm 6^{\circ}$$

The most important quantity of a filter lens is its cut-off performance. The source of electrons used to measure this, was the electron gun near to the straight through position. With the potentials on the gun and lens elements as below, the $V(F2)$ was altered and the number of electrons transmitted to the 45° detectors in the mott scattering chamber counted with an integration time of 10 secs. (see Figure 23).

$$\begin{array}{ll} V(k) = - 8.0 & V(F1) = V(F4) = 0 \\ V(A) = - 1.0 & V(F3) = + 1.0 \end{array}$$

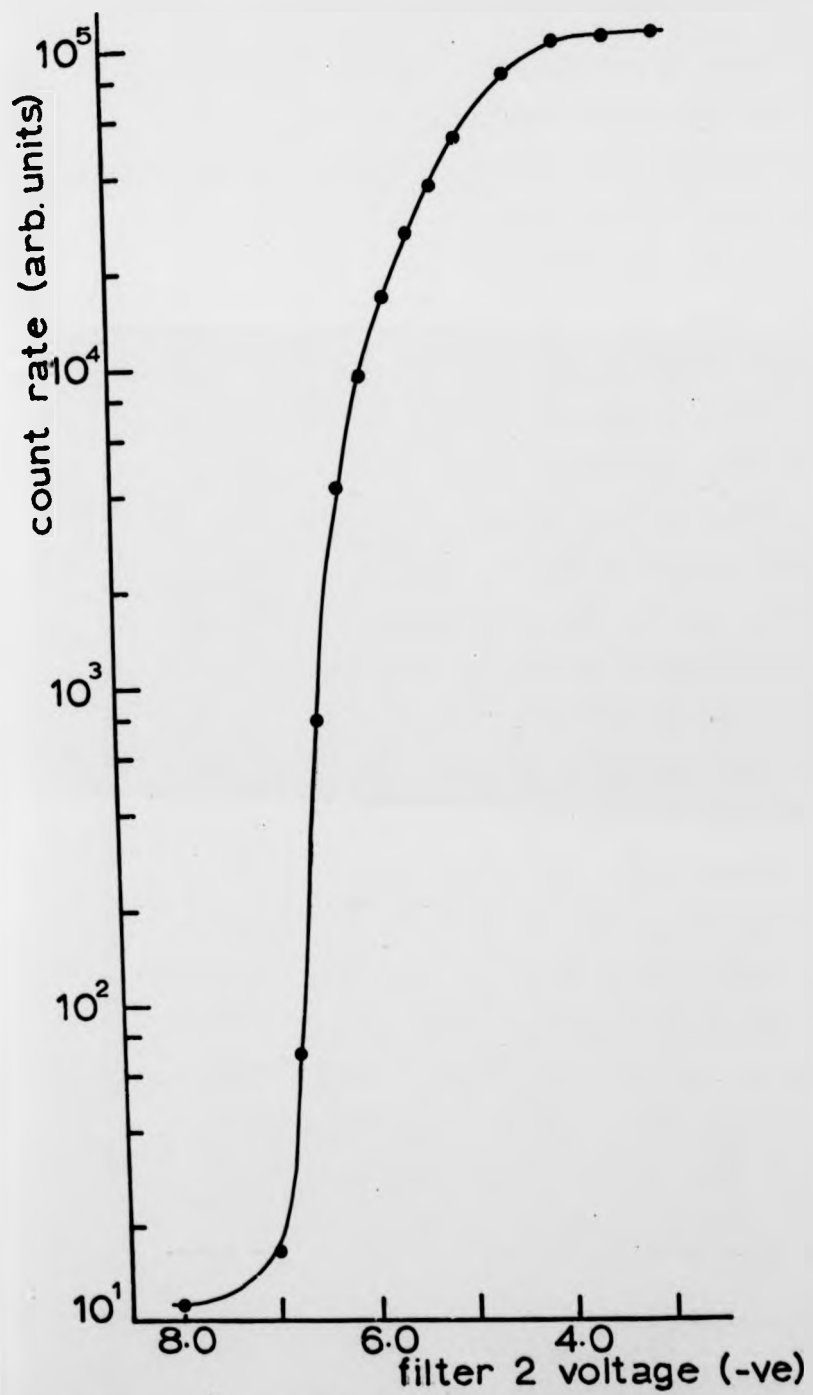


Figure 23. The mercury filter lens performance.

A use
the ΔE_{10}^{90}

In fact it
count rate
maximum r
could have
is suitab
first exc
the trans
positive
inelastic
with the

Opt
scatteri
of filter
el
fi

7.

Sim
and the
are to
of the
is as n

A useful measure of the cut-off effectiveness is the ΔE_{10}^{90} value. The value so obtained is

$$\Delta E_{10}^{90} = 2.1 \text{ volts.}$$

In fact it could be even less than this, since the count rate at full transmission was exceeding the maximum rate for the electronics, so pile-up of pulses could have been occurring. In any case this cut off is suitable for a mercury system since mercury has its first excitation level at 4.9 eV. In order to maximize the transmission the F2 lens was always kept 5 V more positive than the cathode. This prevented any inelastically scattered electrons being transmitted since with the contact potential

$$E_{\text{ex}} + \phi_{\text{cp}} > 5.0$$

Optimum focusing for transmission into the Mott scattering chamber was obtained by suitable adjustment of filter element F3. Typical potentials applied were

$$\text{electron gun } V(k) = - 16.0 \quad V(A) = - 3.0$$

$$\text{filter lens } V(F2) = - 11.0 \quad V(F3) = - 3.0$$

$$V(F1) = V(F4) = 0$$

7.4 PERFORMANCE OF ELECTRON COLLECTOR.

Since both the scattering from the mercury beam, and the subsequent scattering from the alkali beam, are to be carried out in the same vacuum chamber, it is of the utmost importance that the electron collector is as nearly "black" as possible. Those electrons

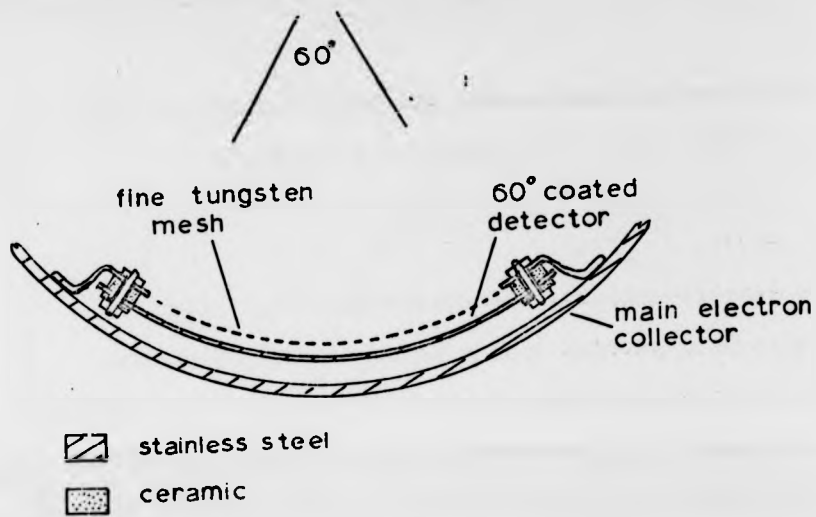


Figure 24. The 60° segment collector

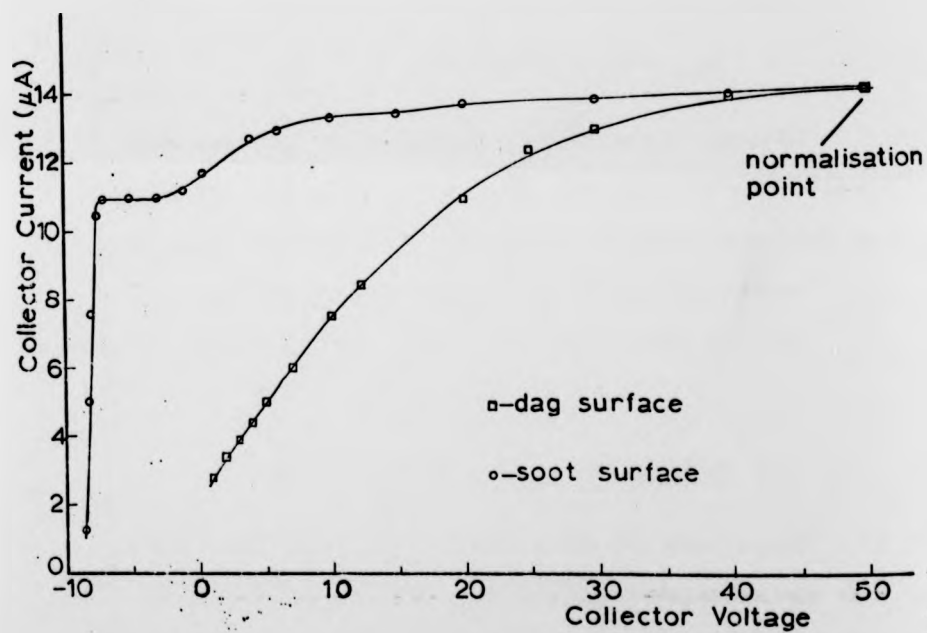


Figure 25. Efficiency of a sooted surface compared with a DAG surfaces as an electron collector. Sooted surface collectors current normalised to that of DAG surface. Cathode voltage of -9.25 volts.

which are
from the
may ultim
accelerat
reject th
surface p
unwanted
obtained
that clea
surface.


Usin
coated wi
collector
then coat
Coal gas
the smok
a jet wa
Again th
voltage
measured
coated s
The
independ
to incre
10 volts
zero vol
electron
acceler

which are not immediately collected can bounce many times from the lens components and the vacuum tank walls, and may ultimately find their way to the entrance of the accelerator tube. At that stage it is impossible to reject those background electrons. Several different surface preparations were tried in order to reduce those unwanted electrons. From the large amount of background obtained without any surface treatment, it was obvious that clean stainless steel is not a suitable collecting surface.

Using the 60° segment collector (see Figure 24) coated with DAG, the collector current as a function of collector voltage was measured. The segment collector was then coated with soot using the following method: Coal gas was bubbled slowly through some benzene, and the smokey flame produced on burning the mixture from a jet was directed on to the surface to be coated. Again the collected current as a function of collector voltage for constant primary beam conditions was measured. In Figure 25 can be seen the results of DAG coated stainless steel and of soot coated stainless steel.

The soot coated collector current appears to be independent of the applied voltage up to -0.5 volts and to increase slowly as the voltage was increased from 10 volts up to 50 volts. The effect of going through zero volts on the collector is not unexpected. The electrons see a retarding field collector becoming an accelerating collector.

n electron
ector



normalisation
point

40 50
Voltage

compared with a
coated surface
DAG surface.

Since the gauze has an 85% optical transmission, up to 15% of the incident current will be incident on the tungsten gauze. Any secondary electrons produced at the gauze will have almost zero energy, and will not be capable of reaching the collector in a retarding field condition. However it is possible for them to reach the collector when an accelerating field is applied, leading to an increase in the collected current. On the DAG coated surface, at 50 volts the amount of the primary current collected was approximately seven times that collected at 0 volts, whereas with the soot coated surface this value was only 20% greater.

As a result of these measurements the cylindrical electron collector was coated with soot. Soot had the advantage of a uniform layer being easily deposited on awkward shapes. In order to reduce the effect of any reflections, the stainless steel elements of the mercury filter lens were coated internally with soot. In addition, it appeared that sooted surfaces had a further advantage that mercury droplets were less likely to adhere to them than to unsooted surfaces. The first few elements of the alkali filter lens were likewise treated internally and externally. Any other surfaces which were likely to receive electron bombardment were also coated with soot.

7.5 LINEARITY OF COUNT RATE WITH BEAM DENSITIES.

The scattered intensity in a collision process should be linearly proportional to the incident flux of either

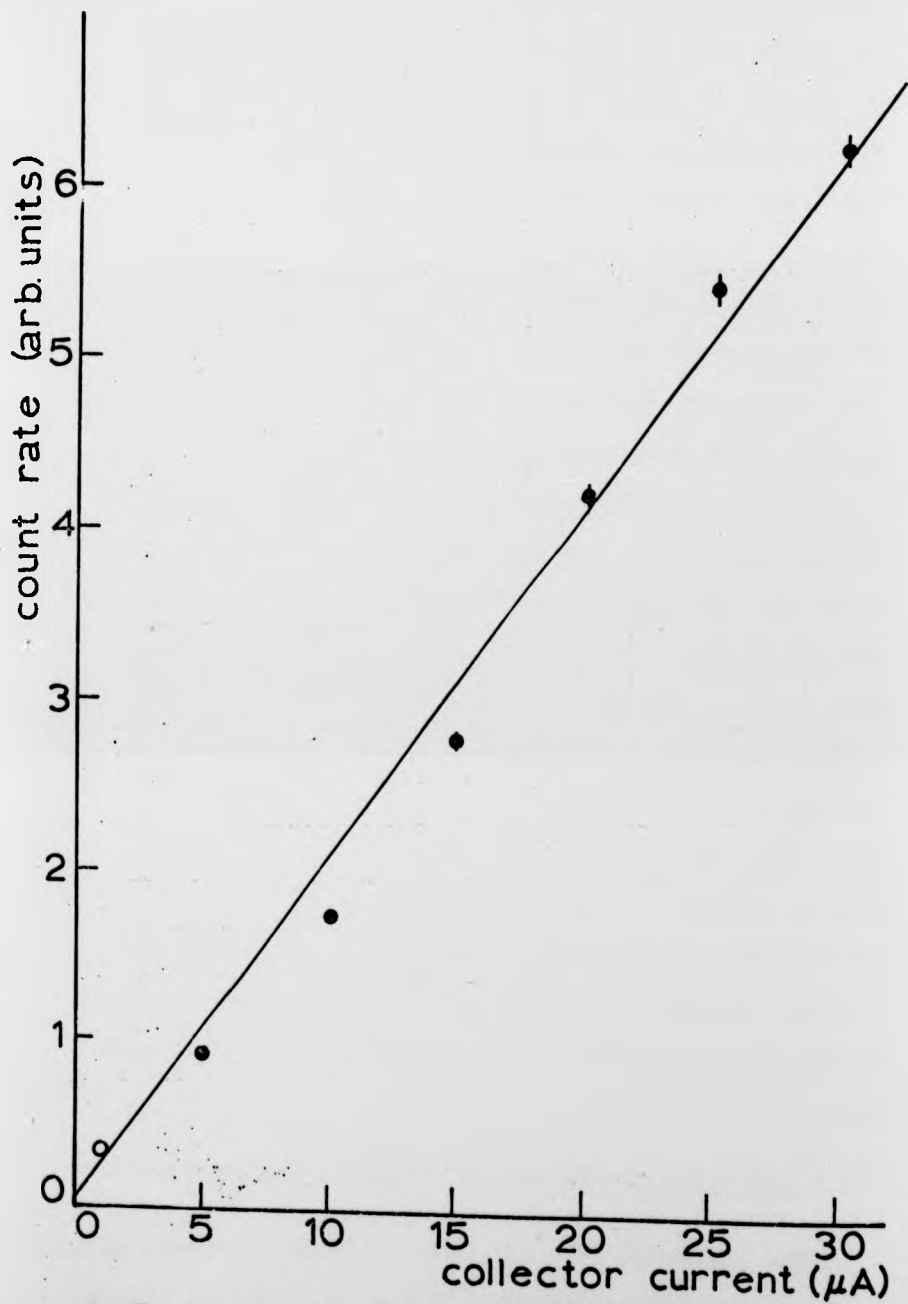


Figure 26. Linearity of Signal with Primary Electron Current.

of the two
scattering
with the
measured
from that
region.

The
after sca
function
Measureme
present a
the mercu
scattered
Typical
be seen
linear w

To
only be
100 seco
results
as a fun
there is
it may b
In the f
no appre
electron
 10^{12} -

This

of the two beams*. That this is true for the mercury scattering process, must be checked since any non-linearity with the primary beams could result in the polarisation, measured at the Mott scattering chamber, differing from that actually present at the alkali interaction region.

The number of electrons reaching the detectors after scattering from the gold foil was measured as a function of the primary electron beam current. Measurements were taken both with the mercury beam present and the scattered signal looked at, and without the mercury beam by looking at background electrons scattered from inside the cylindrical collector. Typical results can be seen in Figure 26, where it can be seen that the count rate on a detector was indeed linear with the primary electron current.

To check the linearity with the atomic beam could only be done by counting continuously, in intervals of 100 seconds, as the boiler was slowly warmed up. The results can be seen in Figure 27, where the count rate as a function of mercury beam density is plotted, when there is a scattering angle of 90° . From this figure it may be noted that there are three separate regions. In the first region at low mercury densities there is no appreciable signal detected and only background electrons and noise is seen. In the region of $10^{12} - 10^{13}$ atoms/cm³, a linear relationship exists

* This should also hold at any part of the lens system.

30
ent (μ A)

ry Electron

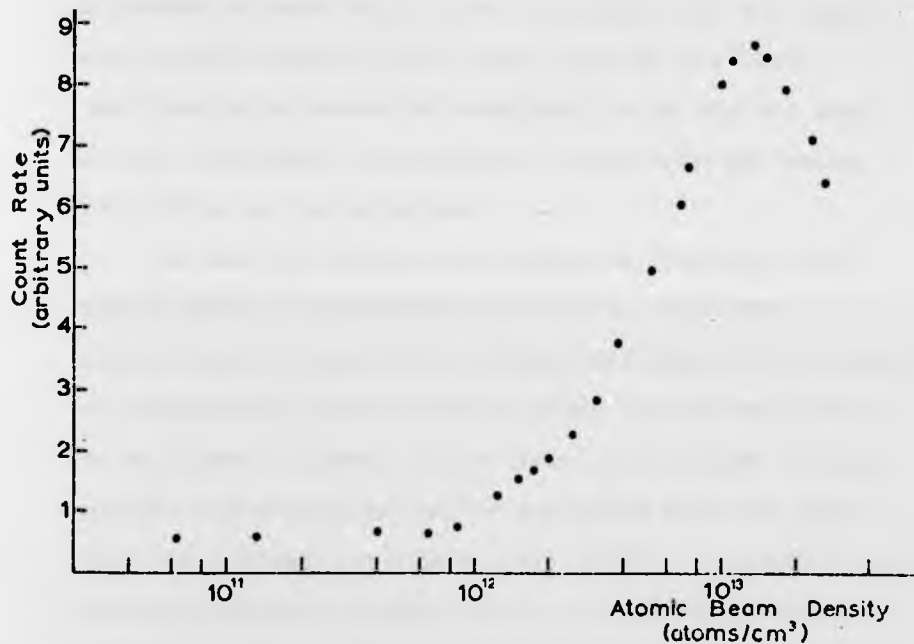


Figure 27. Variation in Signal with Beam Density.

between the mercury pressure and the number of counts detected. In the third region at higher mercury densities, the count rate flattens and eventually falls. Here the electrons undergo appreciable plural scattering.

Several ways were tried to extend the linear part of the curve. The methods described earlier for the reduction of electrons scattered from the collector, escaping out of the ends of the collector, and attempts at the elimination or reduction of the field emission from the electrodes at potentials near to earth potential, all have as their aim an increase in linearity at the lower end. It is worthwhile noting that none of these effects can be eliminated by the use of higher discriminator

settings at the pulse analysis stage. This is because all such electrons only differ in energy from the signal electrons by normally much less than 100 eV. Once they have experienced the acceleration to 100 keV their energy difference is negligible compared to the energy resolution of the detectors.

In order to increase the range of linearity into region three, it would be necessary to limit the interaction region, which although defined by the primary electron beam, is not defined by the mercury beam which is much more diffuse. Since there is a diffuse mercury source, scattering out of the scattered beam can occur from the interaction region until inside the electron optics, where the mercury density will be considerably reduced. To reduce this supplementary scattering region it would be necessary to use a collimating system for the mercury beam. In the present experimental arrangement space and pressure requirements made this unattractive, so little can be done at the upper end of linearity, More serious however, than the decrease in signal in this region, is the parallel effect of depolarisation caused by plural scattering. This point is discussed in the following section.

Another possible reason for the levelling in region three could be if the mercury density in the beam were not to be directly proportional with the pressure inside the oven, i.e. when effusive flow no longer exists and equation 6-2, used for the determination of the atomic density, is not valid. This occurs whenever the oven nozzle radius is of a larger size than the mean free path

of the molecules. At 127°C the pressure in the oven is about 1 torr and the mean free path is about 0.5mm. As the temperature and pressure increase further this effect will become increasingly more important.

Up till now it has been tacitly assumed that the reduction in the count rate in region three has been caused by scattering out in the interaction region. However, with the background pressure in the scattering chamber having risen to about $5-7 \times 10^{-6}$ torr, it is necessary to ensure that it is not caused by scattering out in the long travel between the interaction region and the detectors, part of which is at very low energy, where the electron scattering is most significant.

By allowing the mercury condenser to warm up it is possible to obtain a pressure in the complete system of up to 2×10^{-4} torr, which is many times greater than that produced when the mercury oven and the condenser are running, but becoming comparable with the mercury densities obtained in the interaction region.

With the electron gun directed straight through the lens system, the count rates in the detectors were monitored as a function of the background mercury pressure. This was done both as the condenser warmed up, and cooled down again. It was found that for partial pressures of mercury in the system of greater than 4×10^{-5} torr, a small decrease in the count rate was observed. However, at the pressures typically present under normal running conditions there was no significant attenuation.

From these results the earlier assumption that any attenuation in the scattered beam takes place in

the vicinity of the interaction region appears to be justified.

7.6 PLURAL SCATTERING DEPOLARISATION.

As noted in the previous section some effects, such as plural scattering cause a depolarisation of the scattered electron beam, which is more important than a small reduction in intensity. One such effect related to the mercury density was investigated. As the mercury density increases, the probability that electrons are scattered many times through fairly small angles (multiple scattering) increases as also does the probability of electrons being scattered more than once through fairly large angles (plural scattering). Both of these effects, or a combination of them, will mean that any electron scattered into an angle θ , could be obtained by a double scattering through angles ϕ and $(\theta - \phi)$, or multiple scatterings through angle δ with $\theta = n\delta$, in addition to the single scattering through θ . Consequently the resultant polarisation is some combination of $P(\theta)$, $P(\phi, \theta - \phi)$ and $P(n\delta)$. The relative intensities of each polarisation state being proportional to the respective cross-sections.

Because of the rapid variation in cross-section with angle the result is to fill up the minima at the expense of the maxima, with a corresponding reduction in the polarisation.

To investigate this, the polarisation distribution was measured for several different mercury beam

densities corresponding to oven temperatures of 93.5°C, 115°C, 133°C, & 150°C, for electrons with energies of 6.5 eV and 14.1 eV. The results for 14.1 eV can be seen in Figures 28 & 29.

With these asymmetry ratios* it is also worthwhile looking at the scattered intensities which have not been normalised in any way, apart from knowledge that their primary currents were similar in each case.

The dependence of 'X' on the mercury beam density can be seen to show extreme 'X' values for an oven temperature of 115°C. A striking effect is that at much higher densities, corresponding to 150°C, the peak near a 60° scattering angle has been reduced to almost unity from 1.23 whereas at a 100° scattering angle the 'X' value has only been altered slightly.

If a comparison is now made between the scattered intensity measured at these angles, it can be seen that in going from densities corresponding to 115°C to those corresponding to 150°C that a local maximum at 105° disappears leaving only a hint of its existence. The effective cross-section at this angle being considerably reduced. Near to a 60° scattering angle, although there is no structure observed, the cross-section is considerably increased.

These effects can be qualitatively thought of as scattering into the minima away from the maxima. That the 100° minimum in 'X' is less affected than the 60° peak in 'X' is due to the much more rapid change of 'X' at the 60° peak coupled with the very much larger

* Zero polarisation exists when $X = 1$

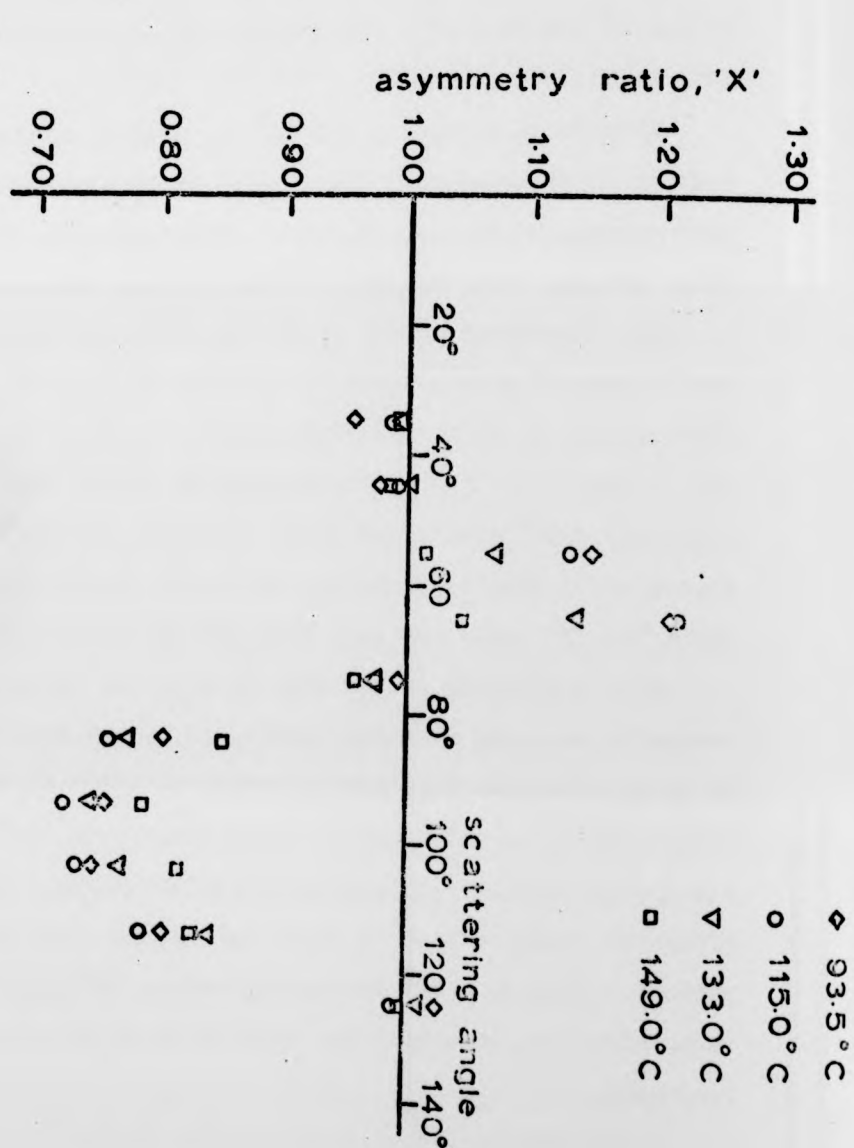
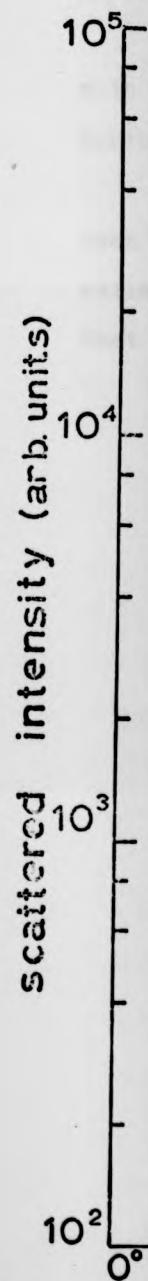


Figure 28. The variation in the asymmetry ratio with the mercury beam density (oven temperature) for 14.1 eV electrons.



Figure

ratio, 'X'

1.20
1.30

◇ 93.5°C
○ 115.0°C
▽ 133.0°C
□ 149.0°C

symmetry ratio
density (oven
electrons.

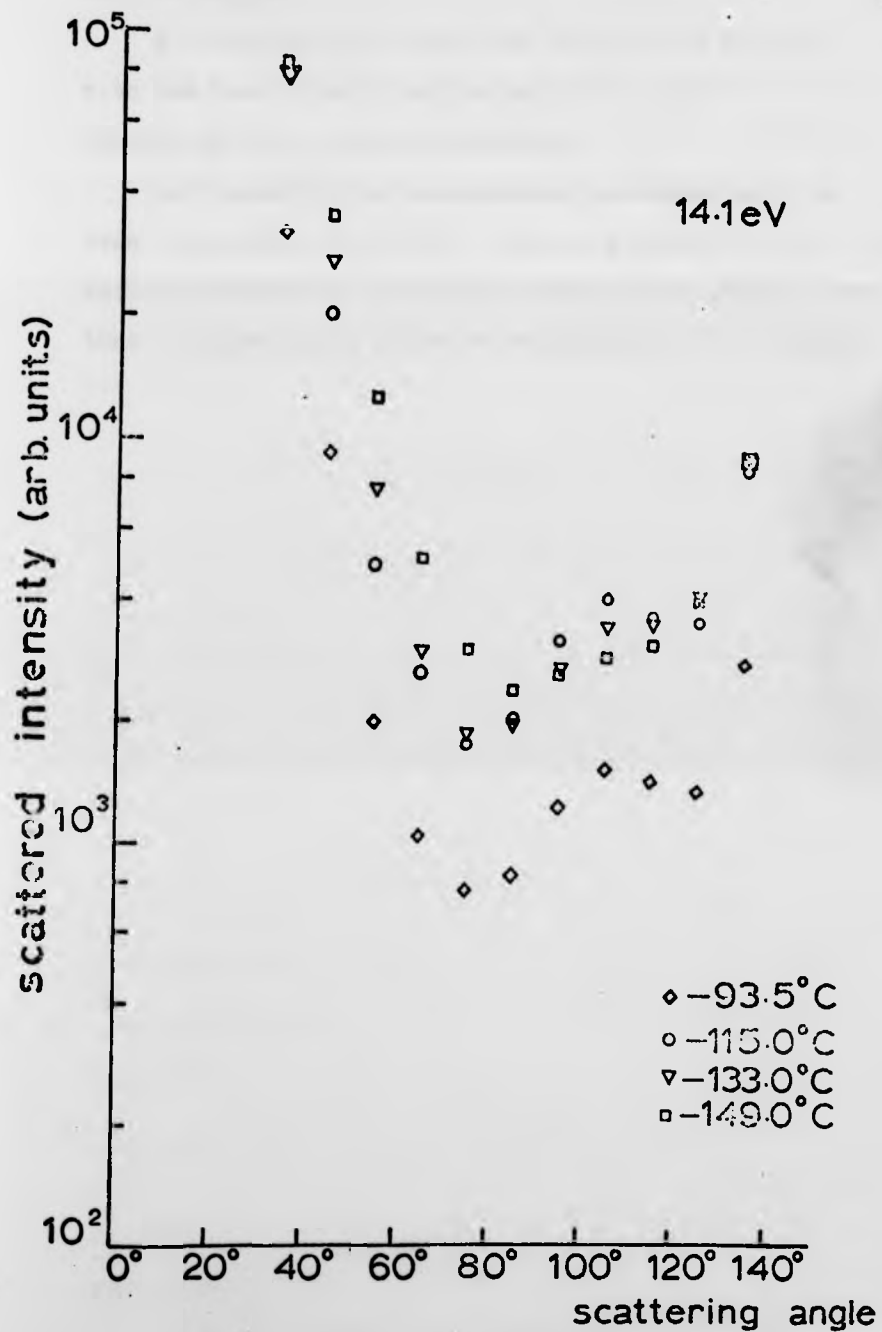


Figure 29. The variation in the scattered intensity with the mercury beam density (oven temperature) for 14.1 eV electrons.

cross-section in the vicinity of that peak towards smaller angles.

A corresponding result was obtained at 6.5 eV with the beam density corresponding to 114°C exhibiting the greatest asymmetry.

All polarisation measurements were made with an oven temperature of 114°C . With this value it is estimated that for all energies and angles studied here, that no significant pressure depolarisation is present.

CHAPTER VIII.

RESULTS OF POLARISATION MEASUREMENTS.

The errors in the measured quantities are fully discussed before the polarisation values and scattered intensities which were obtained are presented. A comparison is made of the values for the polarisation at different scattering energies, and the optimum conditions for operating as a polarised electron source are stated.

8.1 THE ERROR IN ELECTRON POLARISATION MEASUREMENTS.

In the following, the standard error associated with a quantity A is denoted by δA . Suffixes i and j are used to denote detectors up or down (i = 1 or 2 respectively) and positive or negative angular settings (j = 1 or 2 respectively). The quantities are defined below.

number of scattered electrons in channel ij	=	S_{ij}
up-down ratio	R_j	= S_{1j} / S_{2j}
asymmetry ratio	X	= $(R_1 / R_2)^{1/2}$
polarisation	P	= $\frac{1}{S} \left(\frac{X-1}{X+1} \right)$

The errors in these quantities are given by

$$(\delta R_j)^2 = R_j^2 \sum_i \left(\frac{\delta S_{ij}}{S_{ij}} \right)^2 ; \quad (\delta X)^2 = \frac{X^2}{4} \sum_j \left(\frac{\delta R_j}{R_j} \right)^2$$

$$(\delta P)^2 = \frac{4}{S^2} \frac{(\delta X)^2}{(X+1)^4} + \left(\frac{X-1}{S^2 (X+1)} \right)^2 (\delta S)^2$$

If only the statistical error in P associated with X is considered meanwhile

$$\delta P_{st} = \frac{X}{|S|(X+1)^2} \left[\sum_{ij} \left(\frac{\delta S_{ij}}{S_{ij}} \right)^2 \right]^{\frac{1}{2}} \quad (8.3)$$

Usually N_{ij} is the quantity which is measured and this includes a background component B_{ij} . This component, B_{ij} , is measured by blocking the filter lens. The measuring time for the scattered signal is t times longer than for the background, so

$$S_{ij} = N_{ij} - t B_{ij}$$

If Poisson statistics applies for the count rates

$$\text{this results in } (\delta S_{ij})^2 = N_{ij} + t^2 B_{ij}$$

If the limiting case of $B_{ij} \ll S_{ij}$ then equation (8.3) becomes

$$\delta P_{st} = \frac{1 - (PS)^2}{4|S|} \left[\sum_{ij} \frac{1}{N_{ij}} \right]^{\frac{1}{2}}$$

When the above limiting case is not applicable then equation (8.3) is given by

$$\delta P_{st} = \frac{1 - (PS)^2}{4S} \left[\sum_{ij} \frac{N_{ij} + t^2 B_{ij}}{(N_{ij} - t B_{ij})^2} \right]^{\frac{1}{2}}$$

Considering the error in P associated with the accuracy of the knowledge of the Sherman function,

$$\delta P_s = P \left(\frac{\delta S}{S} \right)$$

When P is small this systematic error, δP_s , will normally be smaller than δP_{st} but will become increasingly more significant as the polarisation increases in magnitude.

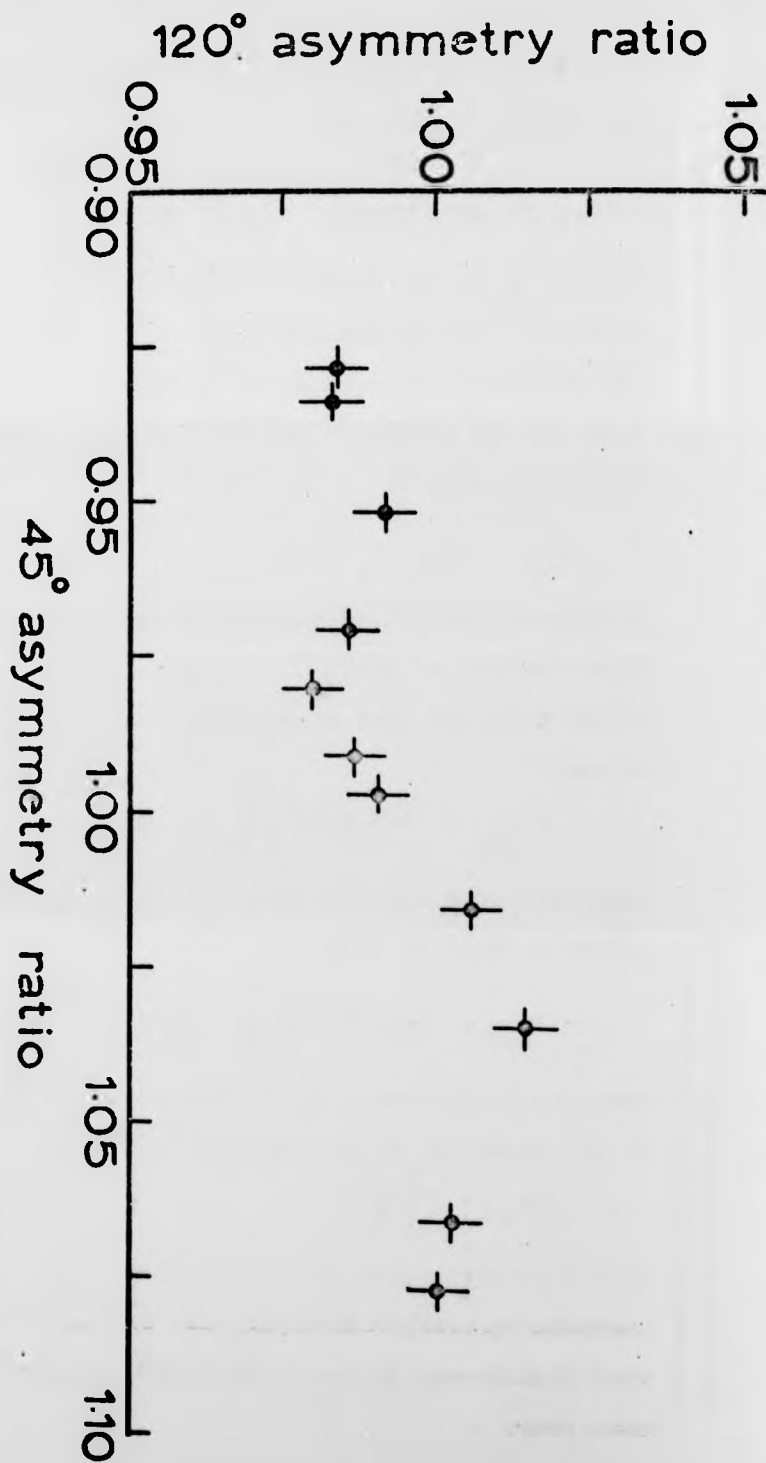


Figure 30. Relationships between 45° asymmetry and 120° asymmetry.

the M
which
walls
scatt
are c
as de

beam
such
monit
energ
confi
place
Using
accel
which
120°
an al
of th
The o
and c

polar
cause
asymm
the 4
beam
relat

There are two types of instrumental asymmetries in the Mott spin analyser. The first is a static asymmetry which relates to the amount of back scattering from the walls, the relative efficiency of the detectors and the scattering angle viewed by the detectors. These factors are constant in time and are allowed for in the S value as determined experimentally.

The other type of asymmetry is that associated with beam shifts on the gold foil. As outlined in section 7.1 such instrumental asymmetries present can be detected by monitoring the asymmetry ratio for 45° scattering of high energy electrons from gold. An attempt was made to confirm this prediction by using an aluminium foil in place of the gold foil in the Mott scattering chamber. Using the deflector system at the high energy end of the accelerator tube, a series of measurements were made from which the corresponding asymmetry ratios of the 45° and 120° scatterings were determined (see figure 30). Using an aluminium foil reduced any effects due to polarisation of the incident beam to about 10% of the effect with gold. The observed shifts are independent of the polarisation and caused by the beam shift alone.

The large aperture arrangement used in the polarisation measurements, was used, and is probably the cause of no definite correspondence between the two asymmetry ratios being obtained. It was confirmed that the 45° detectors are more sensitive to shifts in the beam position. Because of the uncertainty in this relationship, instead of applying a correction factor

etry ratio

1.05

en 45° asymmetry

to the polarisation values, the quoted error of these values includes a term from this instrumental asymmetry when it is present.

A 4% deviation from unity for the 45° asymmetry ratio is considered to produce an error in the 120° asymmetry of 1%. Over the range of asymmetries measured this corresponds to a possible error of 2% about the polarisation value. A proportional error δP_1 , is estimated whenever the 45° asymmetry ratio deviated by more than 1% and less than 6% from unity. Polarisation values where the deviation exceeds 6% were discarded. This only occasionally occurred at the extremes of the angular range.

Instrumental errors detected as above, appeared to fluctuate from one run to another, sometimes being almost negligible over a complete run, and on other occasions changing between each point. The cause of these fluctuations is unknown, but may be due to drifts in the lens voltages including the accelerator lens.

Another source of possible error in the measurements is the accuracy of the angular settings. In particular the asymmetry ratio is dependent on quantities obtained at settings of $+\theta$ and of $-\theta$. If $+\theta$ and $-\theta$ do not correspond to the same scattering angle then an error will result. This was checked by inspecting the symmetry for the scattered intensity at positive and negative angular settings. For energies below 20 eV the two angular distributions are symmetric to less than 5° . For energies greater than 20 eV the discrepancy could be greater than

10° between the two distributions. These discrepancies are thought to be caused by a misalignment of the electron gun. The variation with energy is caused by the "quality" of the electron beam improving with increasing energy. A well defined beam is more susceptible to misalignment than is a diffuse beam.

Using the 6.5 eV and the 14.1 eV results, angular shifts were introduced in the calculations. The effect can be seen in tables 7 and 8 where shifts of 0° and $\pm 10^\circ$ are included. It can be seen that the peak polarisation is almost unaffected even by large shifts of 10° . Where the polarisation values change rapidly, large changes are experienced.

It is estimated that for energies less than 20 eV polarisation values are correct to within $\pm 2\%$ about the polarisation values. For the energies greater than 20 eV the polarisation values are estimated to be correct to within $\pm 2\%$ about the values, if the angular scale is reduced by about 4%. In all cases, the errors at the broad maxima of polarisation values are estimated to be smaller than those ascribed to the statistical and instrumental errors.

scattering angle	polarisation (%)		
	angular shifts		
	-10°	0°	$+10^\circ$
75°	-17.3	-21.0	-25.9
85°	-23.7	-28.6	-27.3
95°	-28.7	-27.4	-18.5
105°	-17.9	- 9.0	3.0

Table 7. The effect of an angular shift of $0^\circ, \pm 10^\circ$ between positive and negative angles for an electron energy of 6.5 eV,

scattering angle	polarisation values		
	angular shifts		
	-10°	0°	+10°
55°	-12.9	-30.1	-29.0
65°	-41.1	-40.0	- 8.3
75°	-26.4	55.4	25.1
85°	37.4	56.9	55.5
95°	68.5	67.2	67.0
105°	64.3	64.1	53.5

Table 8 The effect of an angular shift of 0°, ± 10° between positive and negative angular settings for an electron energy of 14.1 eV.

8.2 DIFFERENTIAL CROSS-SECTION AND SCATTERED INTENSITY

The differential cross-section is related to the scattered intensity through the relation

$$N(\theta) = \left(\frac{1}{e} \right) n_a l_{\text{eff}} \sigma(\theta) d\omega \quad (8.1)$$

where $N(\theta)$ is the number of electrons/sec scattered through an angle θ into solid angle $d\omega$. $\left(\frac{1}{e} \right)$ is the incident number of electrons/sec. n_a is the target atom density and l_{eff} is the scattering length visible by the lens system.

Relative cross-sections are often measured since this removes the necessity for absolute values to be determined for equation (8.1). In these instances, the electron current is usually extremely stable, n_a can usually be monitored for constancy and l_{eff} and $d\omega$ can be accurately defined or are known to be constants. In

the present apparatus the only quantity which is known to be constant is d , the solid angle of acceptance of the lens system.

Although the electron current was measured continuously by the cylindrical collector, variations of up to 10% were detected in going from one extreme to the other. This could partly be due to different collection efficiencies as the beam hits different areas of the collector surface. If the electron gun was left stationary, the current was stable to within a few percent for periods longer than a complete polarisation run. The currents as measured for both a positive and the corresponding negative scattering angles were equal to within $\pm 3\%$. The true electron gun current is considered to be constant to within $\pm 3\%$ over a single run.

The atomic beam conditions depend on the source aperture and oven conditions. The mercury oven temperature is kept constant to $\pm 0.10^\circ$ ensuring that the mercury pressure inside the oven is constant to $\pm 2\%$. No fluctuations in count rate were noticed which could be attributed to clogging of the nozzle. The atomic beam conditions are estimated to vary by less than $\pm 2\%$ with time. The actual beam density does vary considerably with distance in the interaction region, due to the proximity to the source and the absence of collimating apertures.

Since the mercury beam is diffuse, an effective scattering length must be considered. This will vary with the scattering angle. It can be shown that approximately

$$l_{\text{eff}} \propto \frac{\sin \theta}{\sin(\theta - \epsilon) \sin(\theta + \epsilon)} \quad (8.2)$$

where θ is the electron scattering angle and ϵ is the acceptance angle of the lens system.

The misalignment causing the discrepancy in scattered intensity between positive scattering angles and negative scattering angles will also affect l_{eff} . By comparing the two distributions, this effect is estimated to amount to about $\pm 10\%$ for all energies. It is estimated, that to allow for these angular shifts, the angular scale used must be reduced (increased for $-\theta$ results) by about 4% for energies greater than 20 eV. For energies below 20 eV the angular shifts are sufficiently small that no correction need be applied.

8.3 RESULTS.

The results for the electron polarisation and the scattered intensity for electron energies in the range from 6.5 eV to 44.1 eV can be seen in figures 31 - 42.

The scattered intensities shown in figures 31 - 42 are the raw count rates obtained by summing the counts in the 45° detectors. They have not been adjusted for the factor l_{eff} in equation (8.2).

In figure 42 the differential cross-section at 45 eV obtained by Deichsel, Reichert & Steidl (1966) has been multiplied by the factor given by equation (8.2) for l_{eff} , and compared with the present results at 44.1 eV. This factor has not been applied for their 7 eV results plotted in figure 31 since at this energy the electron beam is considerably less well defined, and the factor l_{eff} used above is no longer valid.

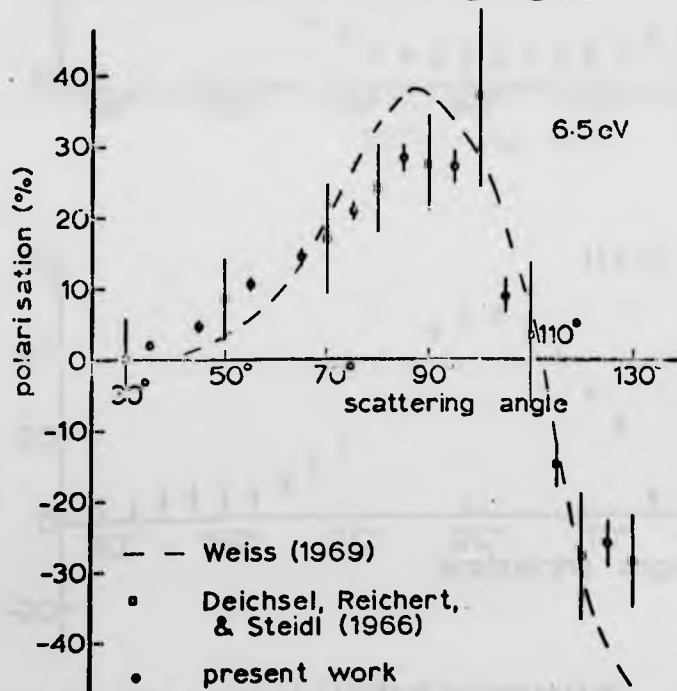
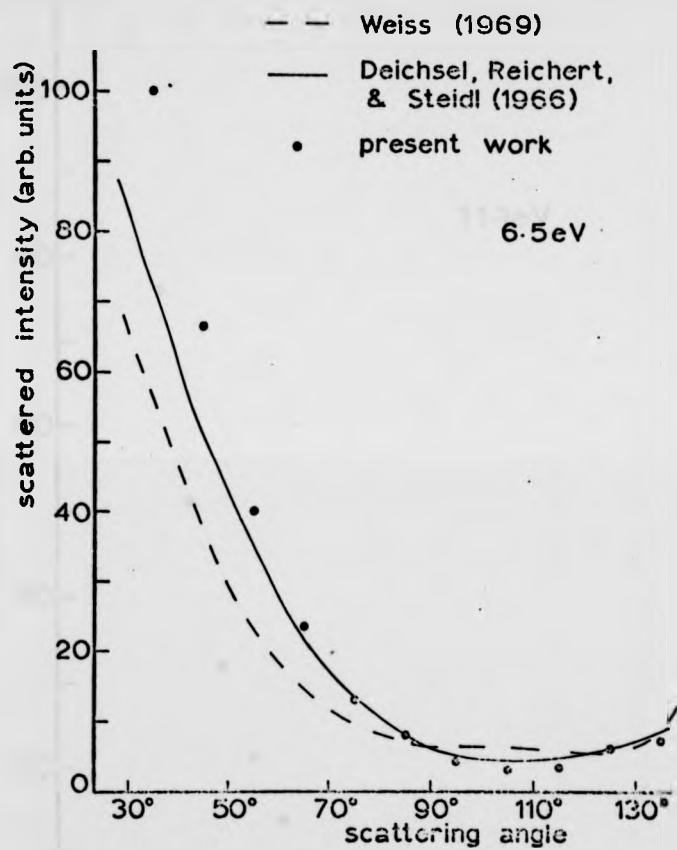


Figure 31. The measured electron polarisation and the scattered intensity for 6.5 eV electrons.

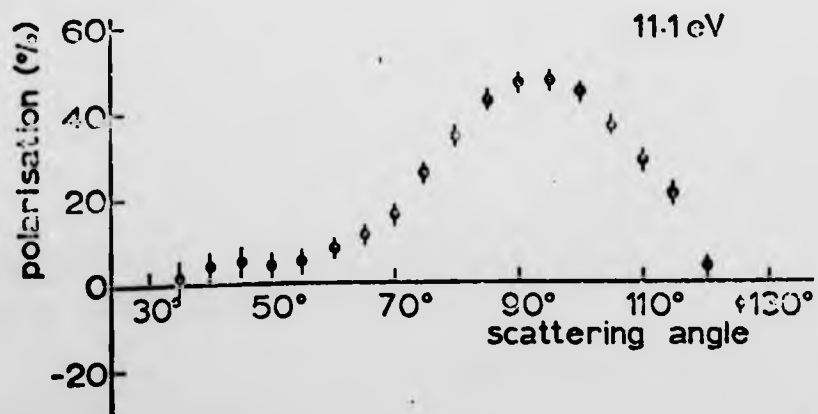
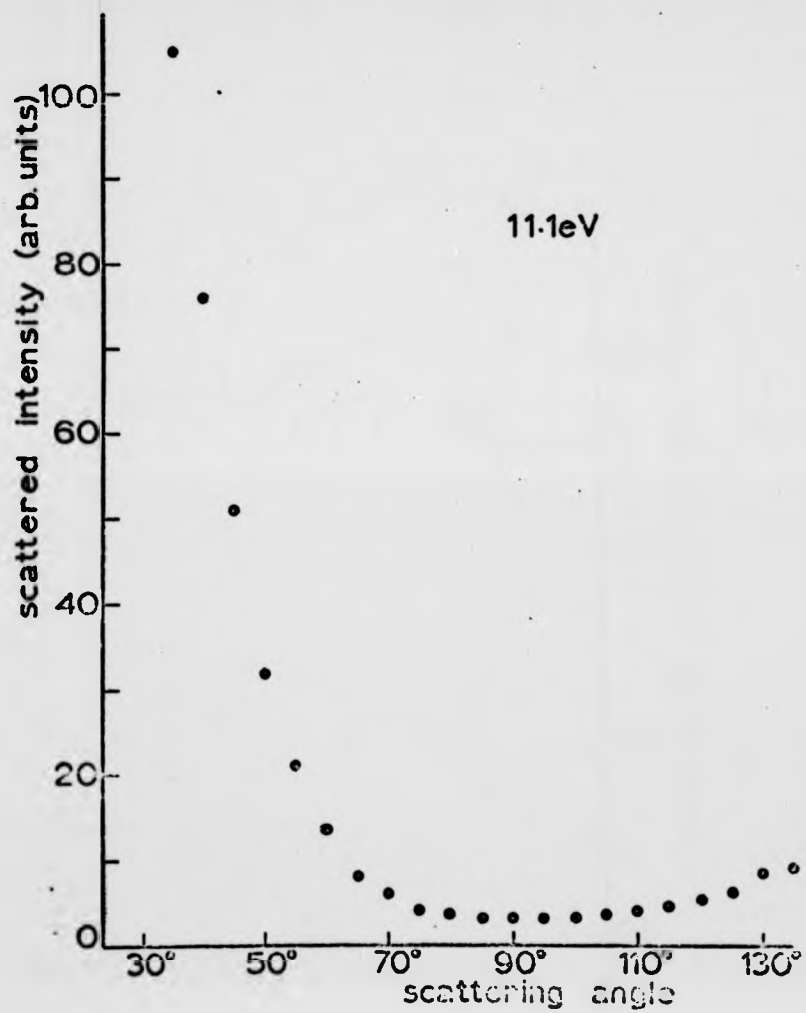


Figure 32. The measured electron polarisation and the scattered intensity for 11.1 eV electrons.

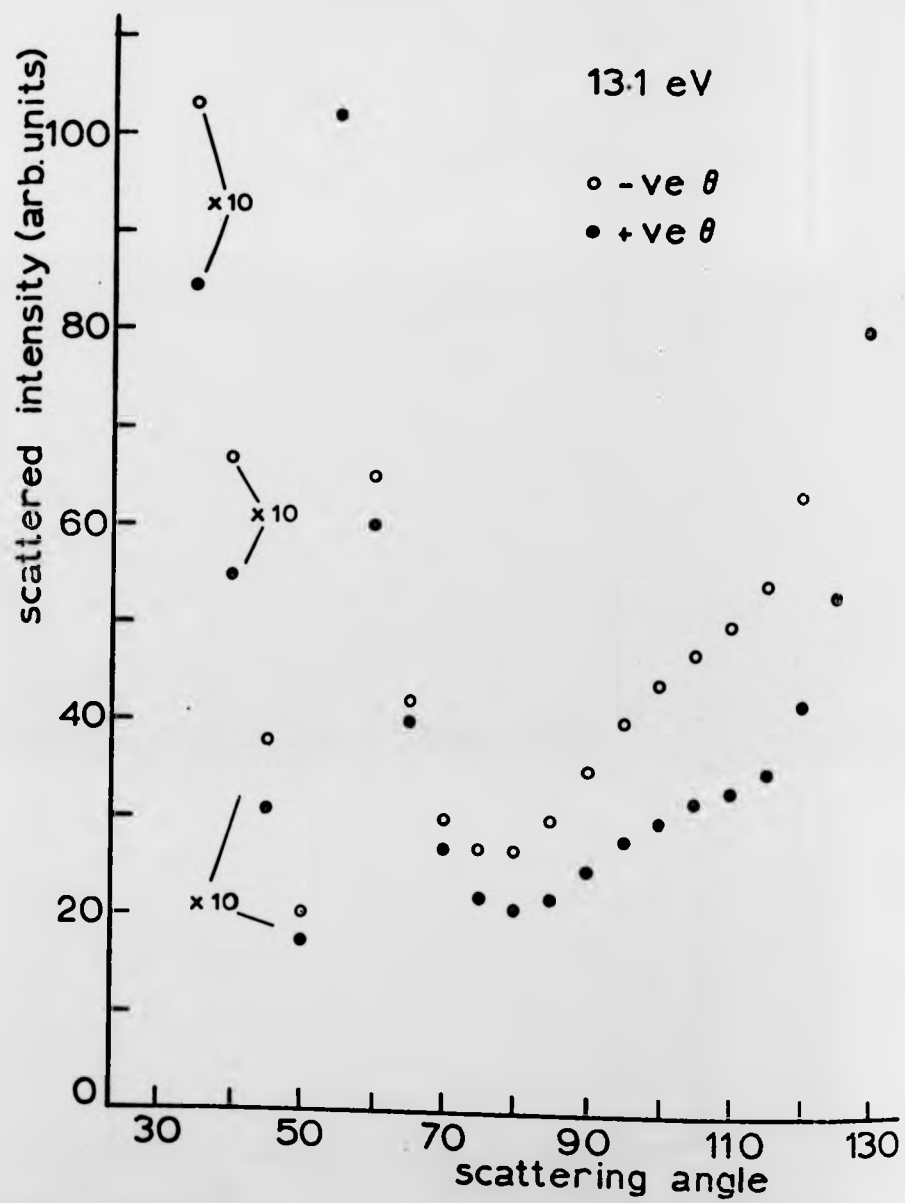
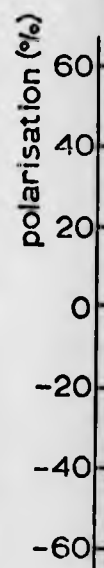


Figure 33(a).



Figure

Figure

13.1 eV

○ -ve θ
● +ve θ

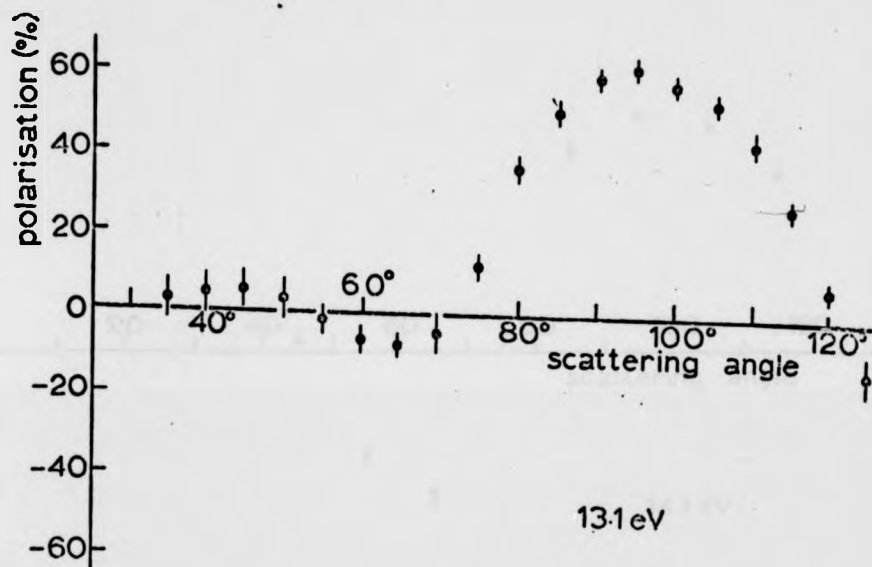


Figure 33(b).

Figure 33. The scattered electron intensity (a), and the measured electron polarisation (b), for 13.1 eV electrons.

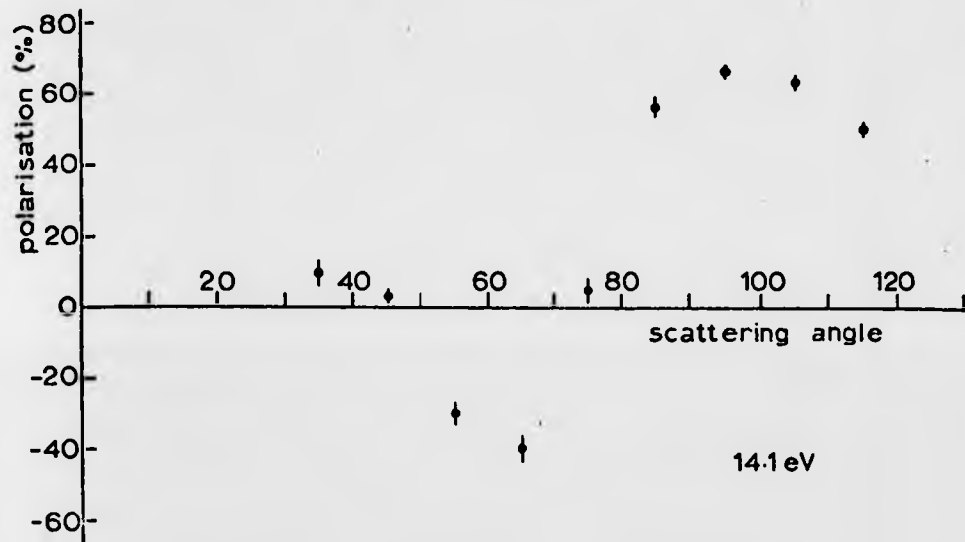


Figure 34. The measured electron polarisation for 14.1 eV electrons (see figure 29 for the scattered intensity).

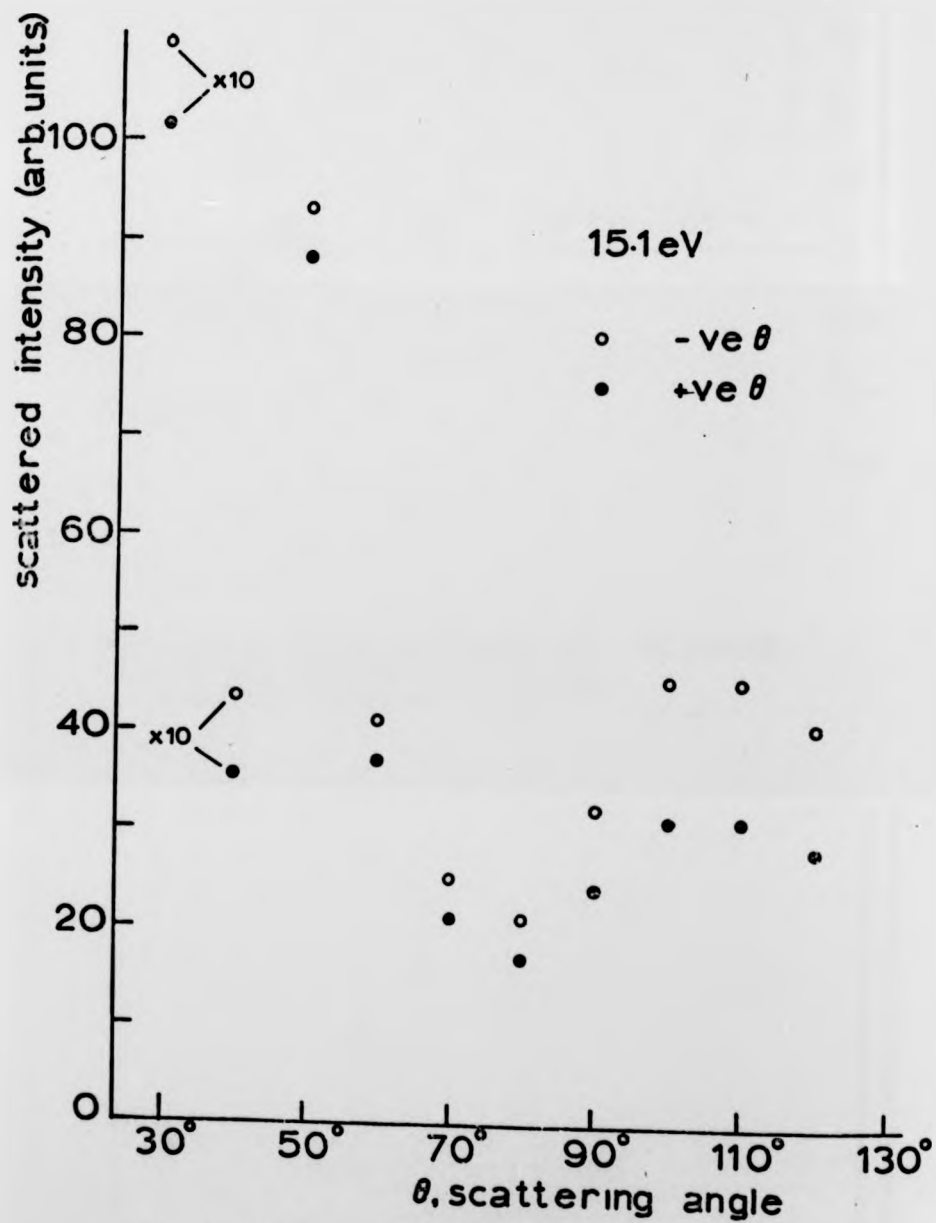
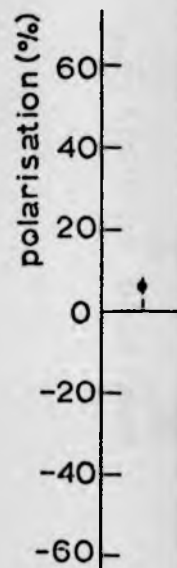


Figure 35(a).



Figure

Figure

15.1 eV

-ve θ

+ve θ



110° 130°
scattering angle

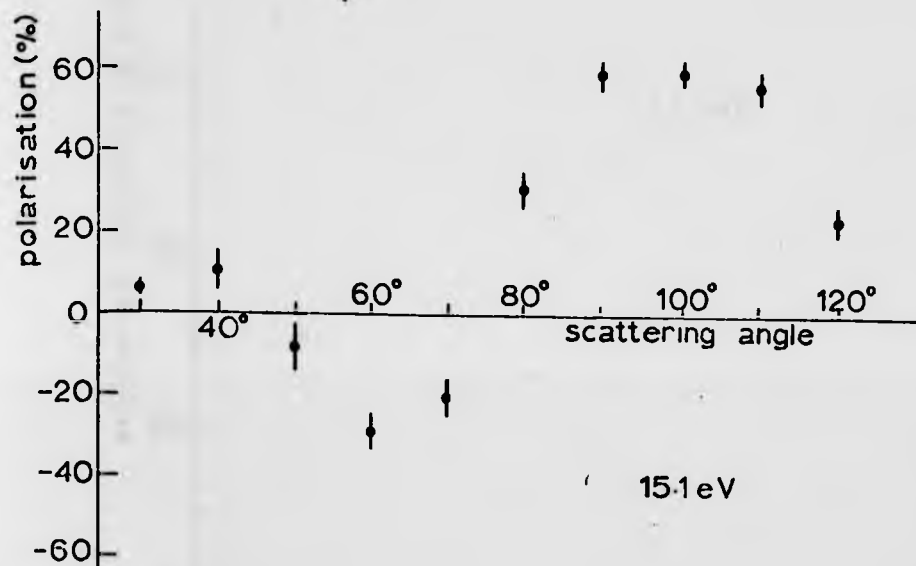


Figure 35(b).

Figure 35. The scattered electron intensity (a), and the measured electron polarisation (b), for 15.1 eV electrons.

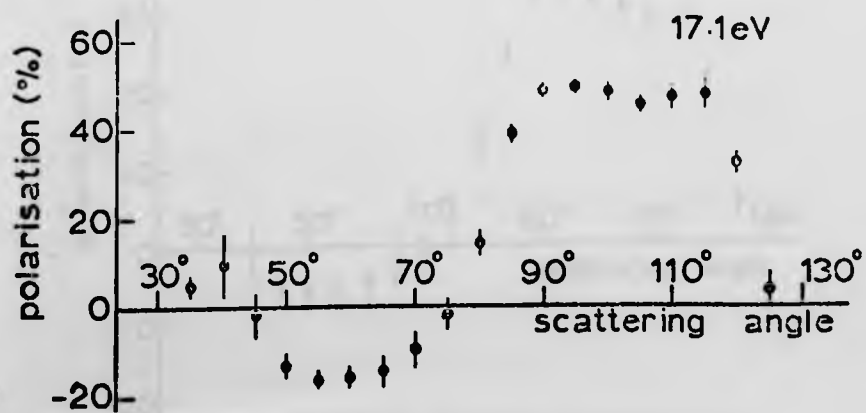
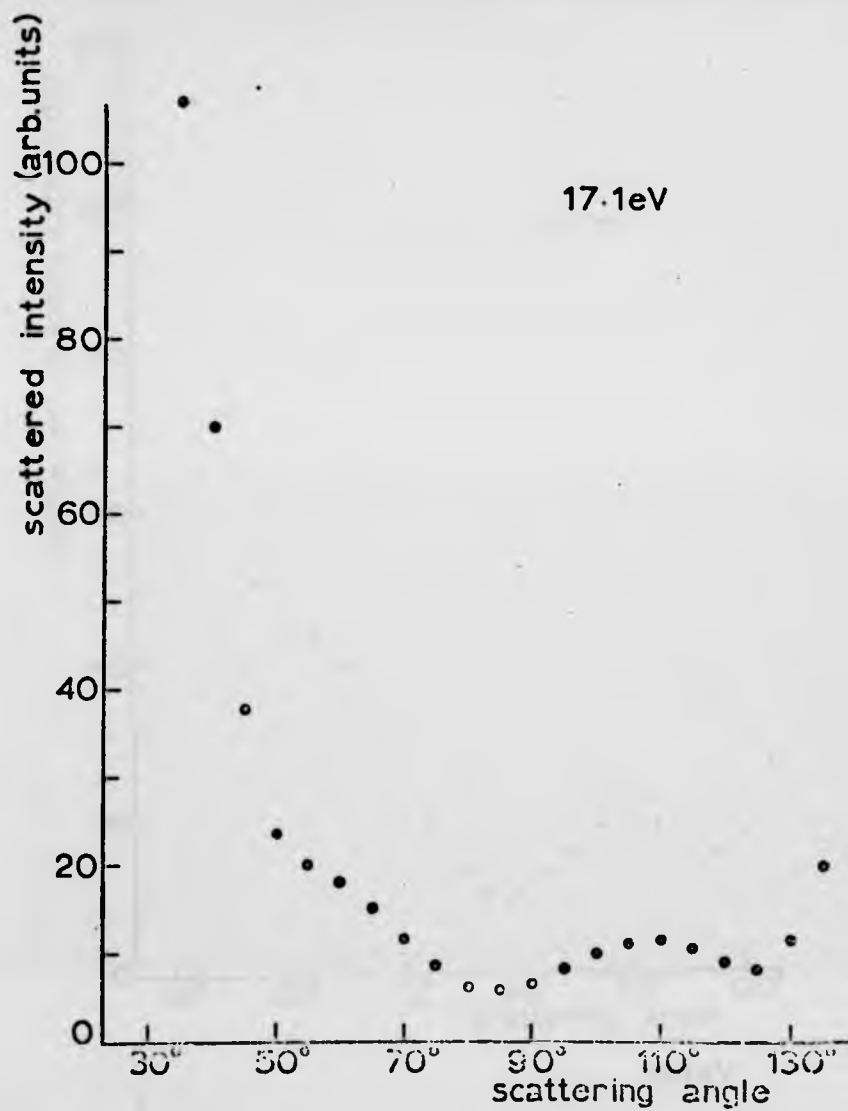


Figure 36. The measured electron polarisation and the scattered intensity for 17.1 eV electrons.

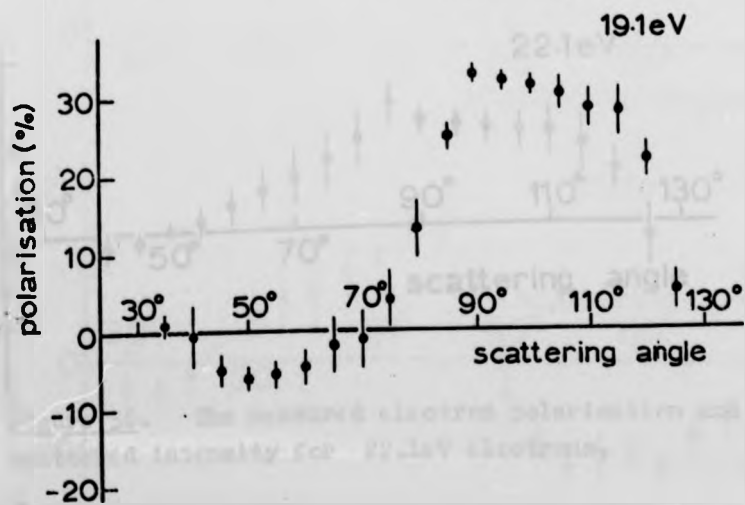
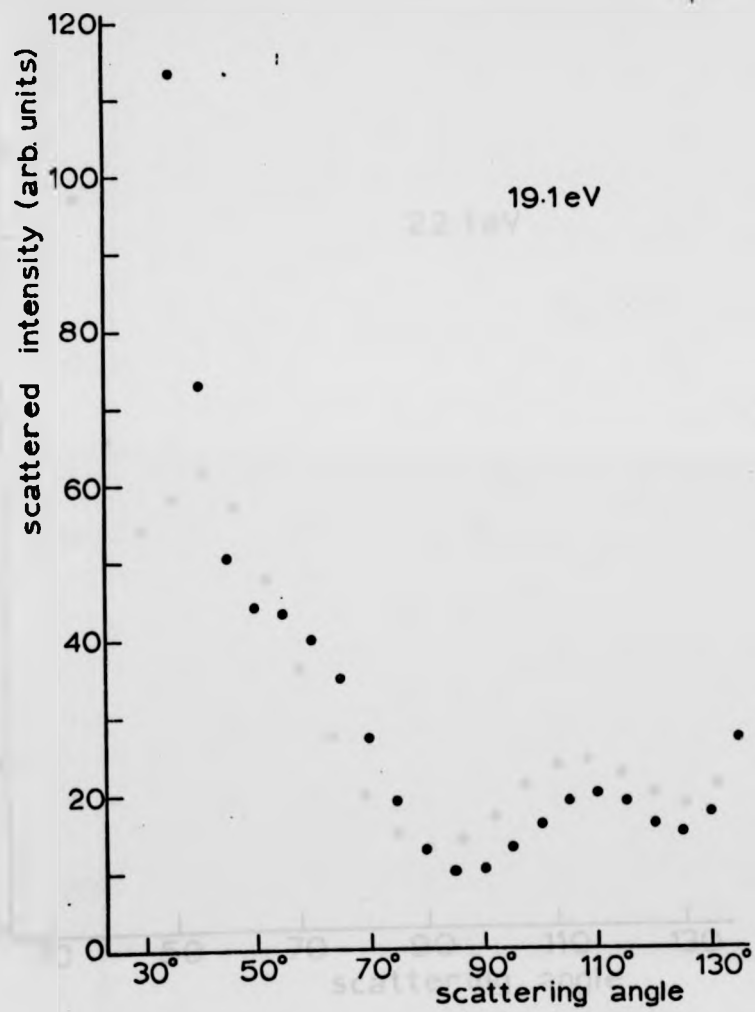


Figure 37. The measured electron polarisation and the scattered intensity for 19,1 eV electrons.

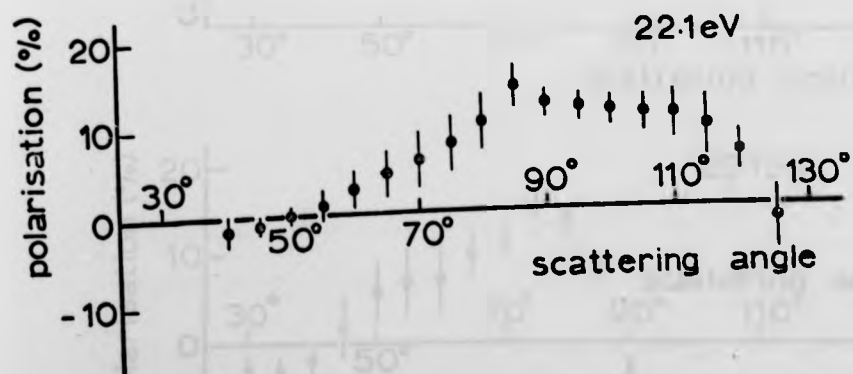
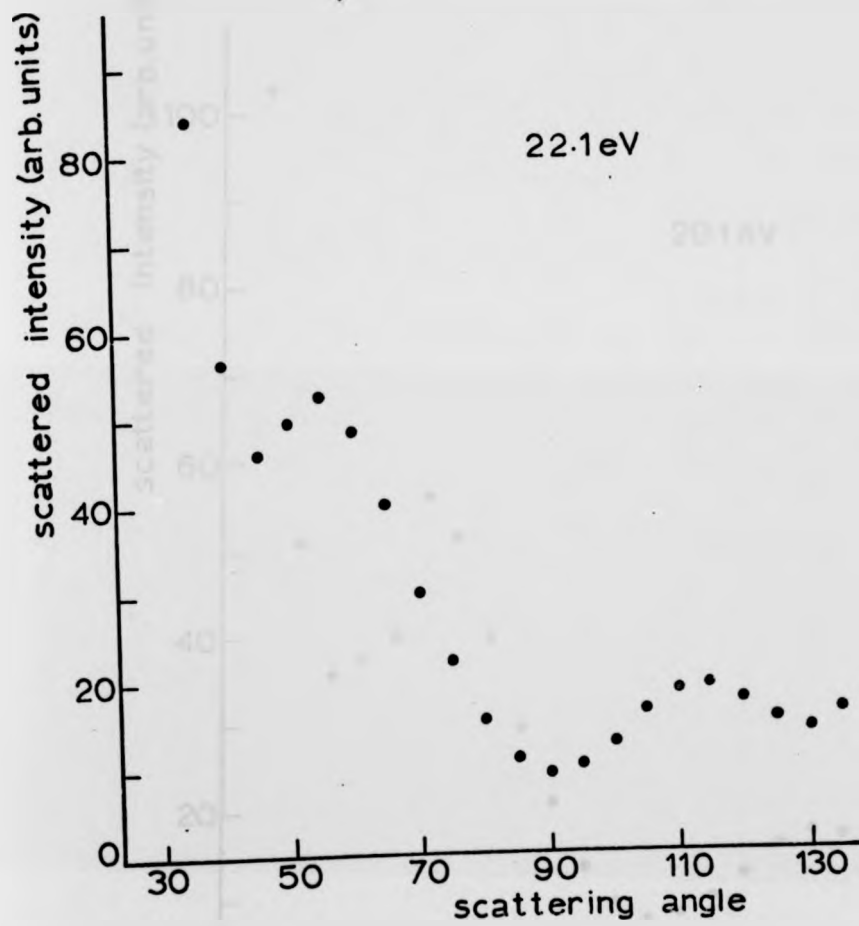


Figure 38. The measured electron polarisation and the scattered intensity for 22.1eV electrons.

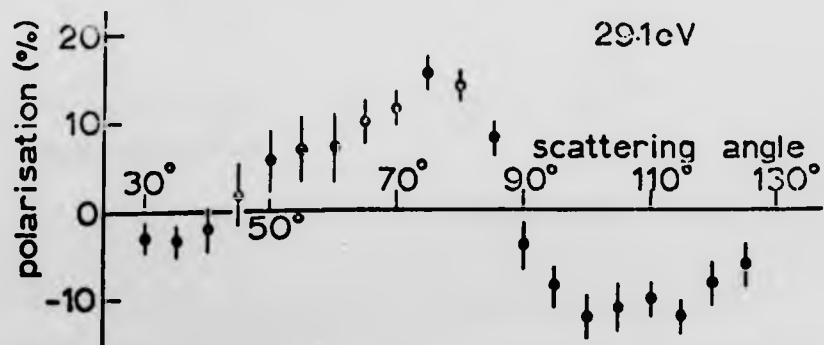
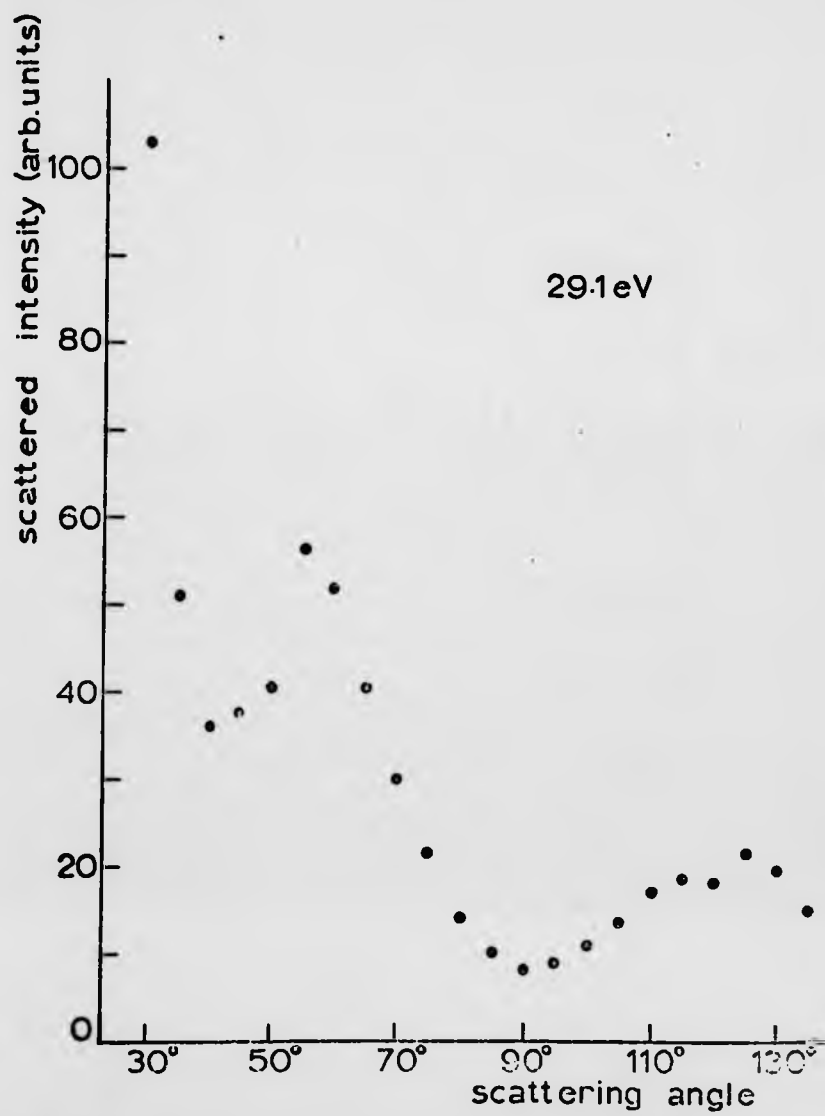


Figure 39. The measured electron polarisation and the scattered intensity for 29.1 eV electrons.

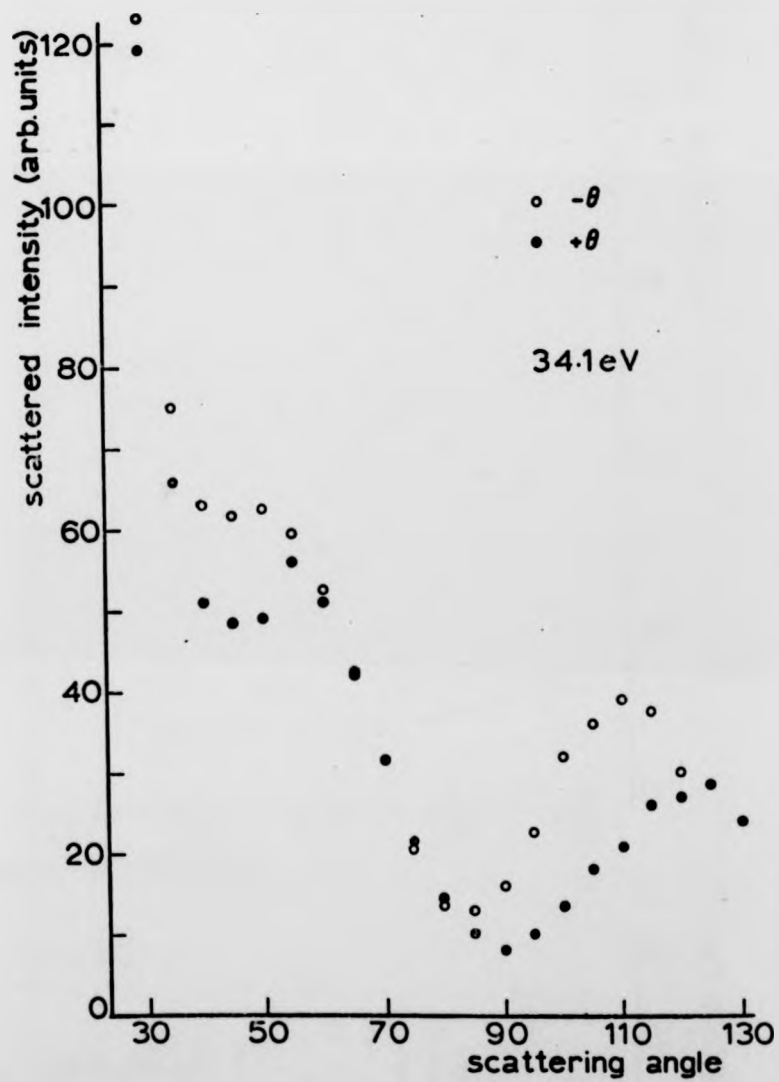
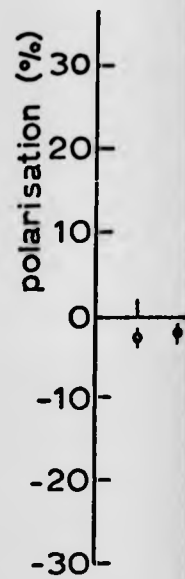


Figure 4.0(a).



Figure

Figure

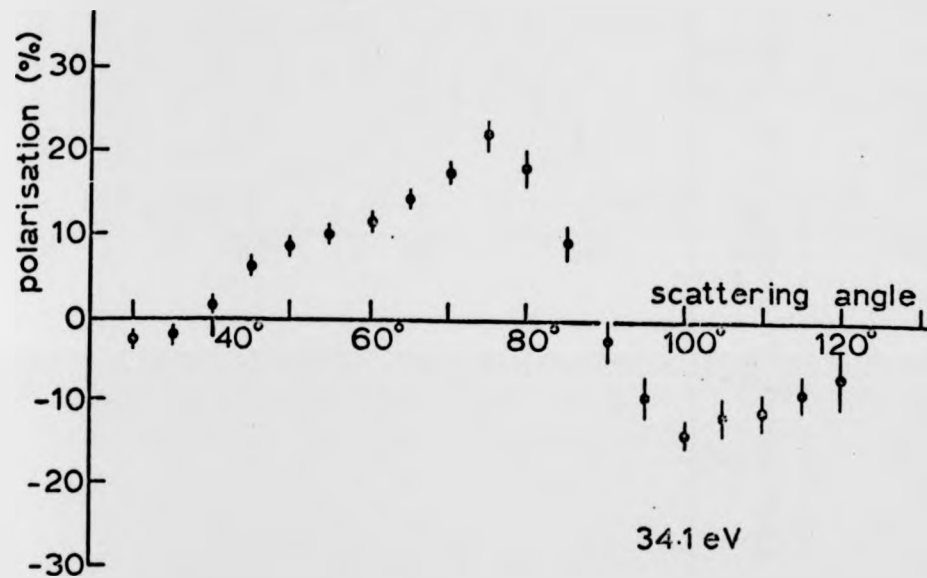


Figure 40(a).

Figure 40. The scattered electron intensity (a), and the measured electron polarisation (b), for 34.1 eV electrons.



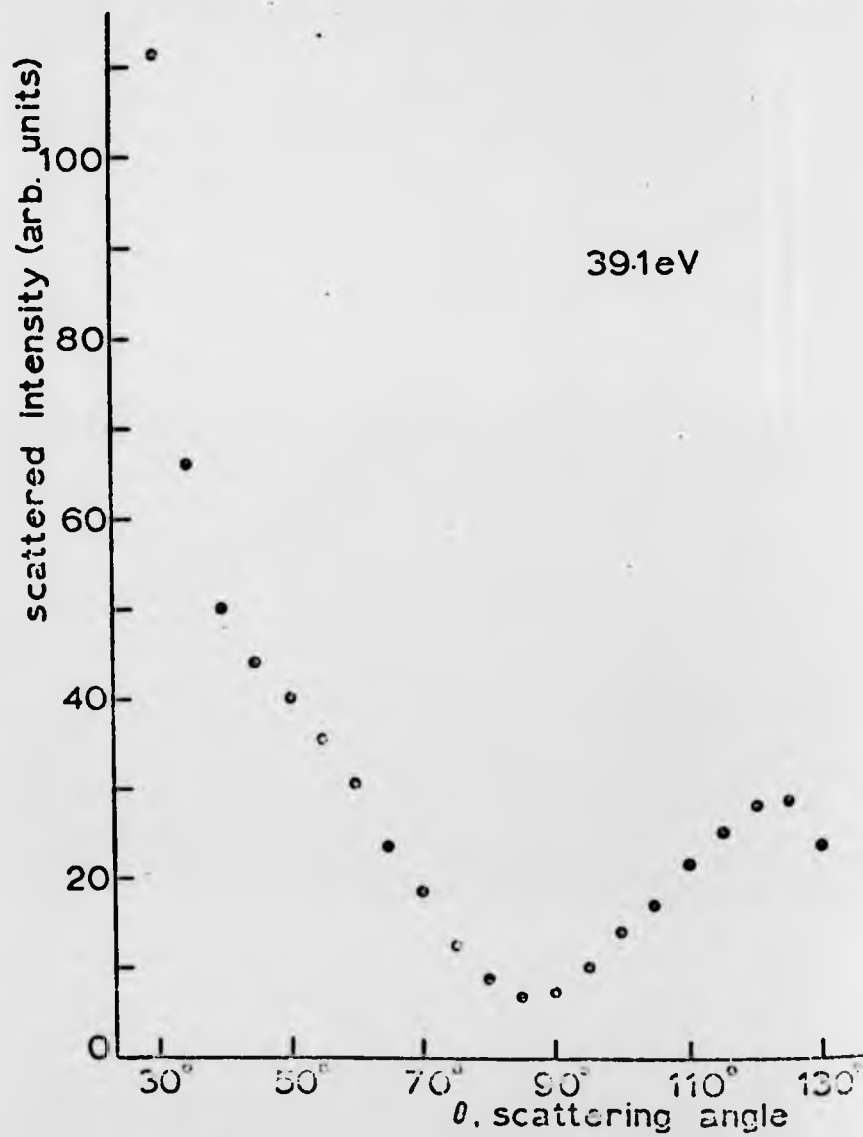


Figure 41(a).

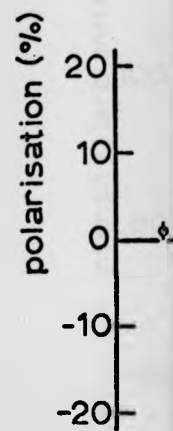


Figure 41(b).

Figure 41(c).

39.1eV

scattering angle

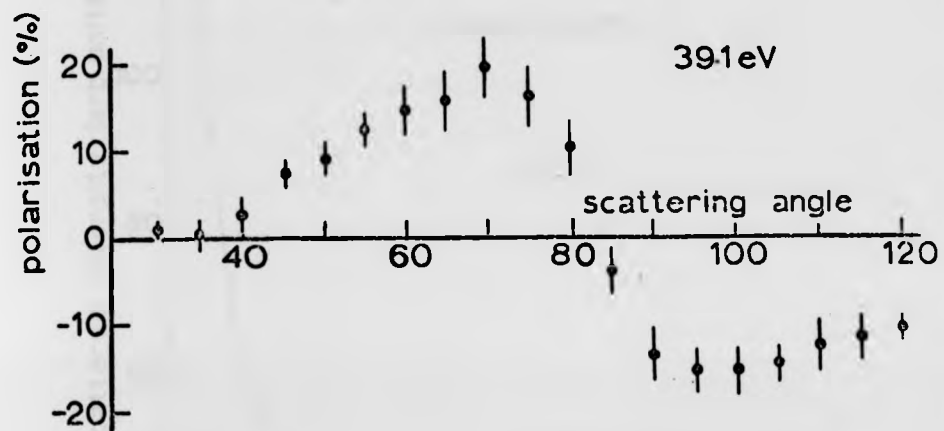


Figure 41(b).

Figure 41. The scattered electron intensity (a), and the measured electron polarisation (b), for 39.1eV electrons

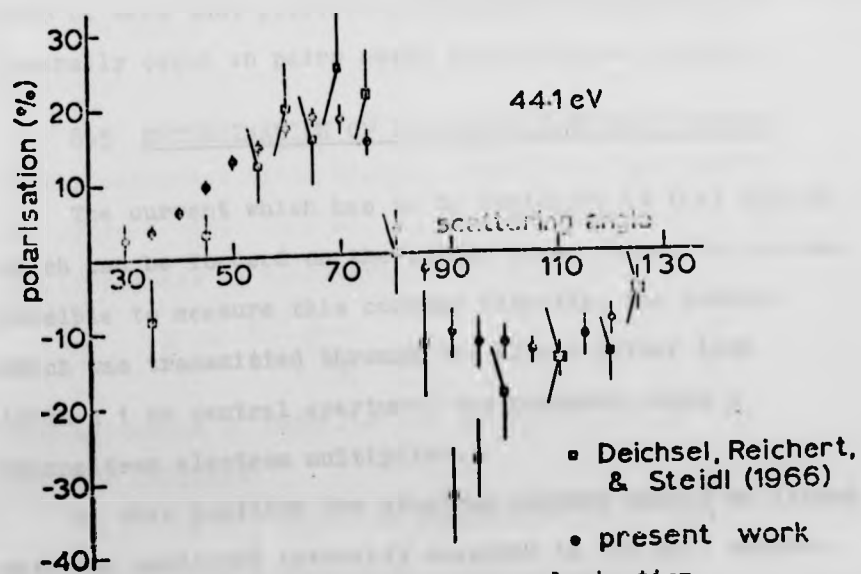
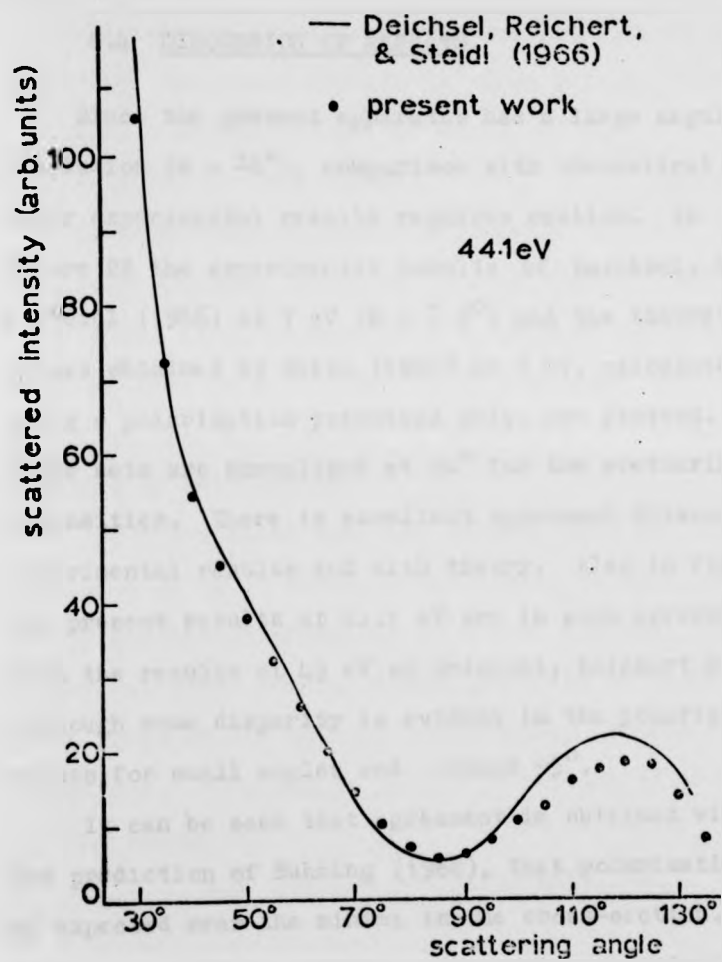


Figure 42. The measured electron polarisation and the scattered intensity for 44.1 eV electrons.

8.4 DISCUSSION OF RESULTS.

Since the present apparatus has a large angular resolution ($\theta = \pm 6^\circ$), comparison with theoretical and other experimental results requires caution. In Figure 28 the experimental results of Deichsel, Reichert & Steidl (1966) at 7 eV ($\theta = \pm 2^\circ$) and the theoretical values obtained by Weiss (1969) at 7 eV, calculated using a polarisation potential only, are plotted. The three sets are normalised at 90° for the scattering intensities. There is excellent agreement between the experimental results and with theory. Also in figure 39 the present results at 44.1 eV are in good agreement with the results at 45 eV of Deichsel, Reichert & Steidl although some disparity is evident in the polarisation values for small angles and around 95° .

It can be seen that agreement is obtained with the prediction of Buhring (1968), that polarisation is to be expected near the minima in the cross-section. It can also be seen that positive and negative polarisations generally occur in pairs about cross-section minima.

8.5 DETERMINATION OF POLARISED ELECTRON CURRENT.

The current which has to be evaluated is that current which can be focused on the alkali beam. Since it was not possible to measure this current directly, the current which was transmitted through the alkali filter lens (with a 1 mm central aperture) was measured using a channeltron electron multiplier.

At this position the electron current should be linear with the scattered intensity measured in the Mott chamber.

The relationship given below was derived from 10 eV electrons, scattered through 85° from mercury, using a primary electron current of about 10^{-8} A.

Primary electron current	10^{-5} A
Corresponding channeltron current	10^{-12} A
Corresponding intensity in Mott chamber	3000 cps.

Since at an energy of 13 eV primary currents of up to 50μ A have been obtained it is estimated that a polarised electron current of about 3×10^{-12} A has been obtained at this energy.

It was noticed that the cathode when new could produce a 2x or 3x increase in primary current, which fairly quickly deteriorated to a more constant value. On removal after several weeks operation it appeared that large areas of the cathode had probably stopped emitting altogether. This may be part of the cause of the angular asymmetry.

8.6 OPTIMUM OPERATING SETTINGS.

In order to compare the different results to determine the optimum operating conditions, a suitable parameter must be used. The polarisation value is not such a parameter since high polarisations occur where the cross-section is small giving low intensities. If the brightness is considered (see equation 2.1).

$$B = \frac{P^2 E}{r^2 \theta_1^2 E_0} \quad (2 - 1)$$

then allowance is made for the intensity and for the electron energies.

A difficulty which is encountered with this

parameter is that the scattered intensity N is proportional to the primary beam. Since the electron gun is operated under space charge conditions it is not sufficient to normalise all values to a fixed primary current. However a space charge limited diode satisfies.

$$i \propto E_0^{3/2}$$

By normalising the scattered intensity to a fixed primary current, and allowing for this additional factor, a suitable parameter is given by

$$B = \frac{C E}{r^2 \theta_1^2}$$

where

$$C = P^2 N E_0^{1/2}$$

The values of the scattering angle which maximises the parameter C is shown in table 9, for each scattering energy. Also shown are the corresponding polarisation values and the scattered intensity, N (in counts/sec/10 μ A).

Table 9 Tabulation of the optimum polarisation conditions.

energy (eV)	scattering angle θ	measured polarisation P (%)	N	C
6.5 \pm 0.5	85°	28.6 \pm 5.3	4970	1036
11.1 \pm 0.1	100°	44.6 \pm 5.9	1520	1009
13.1 \pm 0.1	95°	62.7 \pm 8.0	1630	2403
14.1 \pm 0.1	95°	67.2 \pm 8.2	1150	1950
15.1 \pm 0.1	100°	59.9 \pm 7.7	1150	1601
17.1 \pm 0.1	110°	47.0 \pm 5.8	1160	1061
19.1 \pm 0.1	100°	30.3 \pm 3.8	1290	516
22.1 \pm 0.1	110°	10.5 \pm 3.0	1390	72
29.1 \pm 0.1	75°	15.5 \pm 2.4	2400	313
34.1 \pm 0.1	70°	18.1 \pm 2.1	3220	618
39.1 \pm 0.1	60°	14.7 \pm 3.4	4230	575
44.1 \pm 0.1	60°	17.1 \pm 1.9	6220	1202

The values used for the scattered intensity in calculating C must be treated as approximate values only. This is because the lens system will not have identical transmission functions for all electron energies. However, since at each new energy the lens settings are set for maximum transmission comparable efficiencies are expected.

The general trend which can be seen from the table is that the conditions are better below a scattering energy of 17 eV. The best conditions would appear to be with a scattering energy of about 13 - 14 eV

at a scattering angle of 95° where an electron polarisation greater than 60% is measured.

Although both positive and negative polarisation values were measured none of the negative values corresponds to an optimum condition. However, since the polarisation direction is defined by the incident and scattered electron directions, by scattering through an angle $(-\theta)$ instead of an angle θ , the polarisation direction has changed sign but the magnitude is unaltered.

CONCLUSION.

A source of polarised electrons has been developed which can produce a polarisation of $(62.7 \pm 8.0)\%$ with an electron current estimated to be about 3×10^{-12} A. The operating conditions of the source are a mercury oven temperature about 114°C corresponding to a mercury partial pressure of 10^{-4} to 10^{-3} torr in the interaction region. Electrons of 13.1 eV energy are scattered elastically through 95° . To obtain the estimated polarised electron current a primary electron beam current of $50 \mu\text{A}$ is required. A greater polarisation of $(67.2 \pm 8.2)\%$ has been obtained but the estimated current is only 10^{-12} A. This source is relatively compact and can easily be rotated about an alkali beam allowing triplet scattering experiments to be attempted. It is expected that the background pressure of mercury is not a serious limitation on a further scattering process if a chopping technique is used.

Improvements of the source are limited. Possibly a different cathode material could maintain larger currents for a longer period. The mercury filter lens system could be improved to increase the transmission efficiency. The mercury density can only be increased by using a collimated supersonic beam reducing the scattering length otherwise depolarisation will occur. Using a collimated mercury beam the angular asymmetry could be checked out. The first two suggestions could probably increase the polarised current by a factor of ten.

ACKNOWLEDGEMENTS.

I would like to acknowledge the considerable support which I received from both my supervisors. The keen interest always shown by Professor H. Kleinpoppen in this project is greatly appreciated. The successful outcome of this experiment was made possible by Dr. D. Hils. His knowledge of experimental details, in particular those associated with Mott scattering at high voltage, was invaluable over most of the course of this project.

I am also indebted to Dr. K.A. Moran and Mr. B.J. Benson who were involved in this project in the early stages. I am grateful for the advice on technical problems readily offered by Mr. R.R. Harrison. To him much of the credit for the design of the turntable and the vacuum system is due.

This experiment received considerable technical support which was greatly appreciated. The departmental technicians, in particular Mr A.J. Duncan, were always willing to oblige and to offer advice. My thanks also go to the technical staff of the Shared Technical Services in the University, who manufactured many of the components used.

Financial support during the period of my studentship was provided by the Science Research Council.

APPENDIX I.

THE USES OF STOKES PARAMETERS TO DESCRIBE POLARISATION STATES BEFORE AND AFTER SCATTERING.

The Stokes parameters may be defined by

$$S_i = \text{Tr}(\rho \sigma_i) \quad i = 0, 1, 2, 3.$$

where ρ is the density matrix σ_0 is the 2×2 identity matrix, and σ_i ($i = 1, 2, 3$) are the components of the Pauli spin matrices given by

$$\sigma_1 = \begin{pmatrix} 0 & 1 \\ 1 & 0 \end{pmatrix} \quad \sigma_2 = \begin{pmatrix} 0 & -i \\ i & 0 \end{pmatrix} \quad \sigma_3 = \begin{pmatrix} 1 & 0 \\ 0 & -1 \end{pmatrix}$$

These parameters provide a useful way of describing a polarised beam state, and were first introduced in the last century by Stokes in connection with the polarisation of light.

The intensity of the beam is given by S_0 , and the polarisation components can be obtained from the Stokes parameters using

$$P_i = S_i/S_0 \quad i = 1, 2, 3 \quad (\text{A1} - 1)$$

For non-relativistic quantum mechanics, when spin is included, any suitable set of orthogonal axes may be used. However, in relativistic quantum mechanics an electron is specified by a four component spinor. The above formalism can be applied if the large components only are considered. The Stokes parameters are then understood on the basis that S_3 represents the longitudinal component of the polarisation and that S_1 and S_2 represent the transverse

polarisation components.

The Stokes parameters are invariant with respect to a change of basis states, in a manner analagous to a Minkowski 4 - vector under a Lorentz transformation, and so the name Stokes vector is often applied to the combination of (I_0, S_1) .

It can be shown (Byrne and Farago, 1971) that the Stokes vector before and after collision are linearly related through a transfer matrix, T.

$$\underline{s}^i = T \underline{s} \quad (A1 - 2)$$

The precise form of T is related to the scattering matrix M and the appropriate representation for the interaction obtainable from group theory.

APPENDIX II.

THE POTENTIAL VARIATION IN A BEAM OF CHARGED PARTICLES
DUE TO THE PRESENCE OF SPIN CHARGE.

In electron optics all charged particles passing through a long lens element at potential V (referred to the same point as the particle energy is referred to) are considered to possess an energy given by qV , where q is the charge on the particle. However if the beam is intense enough, the space through which the particle is travelling need not correspond to a potential of V , and the energy value obtained above is invalid.

Considering an electron beam of circular cross-section of radius R_0 moving symmetrically along the axis of a lens of radius k , which is at some potential V . If the electron beam is considered to be at a potential of V_0 , then the charge per unit length is

$$q = iV_0^{-\frac{1}{2}}(2e/m)^{-\frac{1}{2}} \quad (A2 - 1)$$

where i is the electron current and e/m is the charge to mass ratio of the electron.

Applying Gauss' Law and substituting from equation (A2 - 1)

$$\int E \cdot dS = q / \epsilon_0$$

Integrating this equation results in

$$E_r = iV_0^{-\frac{1}{2}}(2e/m)^{-\frac{1}{2}} \left(\frac{1}{2\pi\epsilon_0 r} \right) \quad (A2 - 2)$$

By integrating E from the edge of the beam to the lens surface equation (A2 - 2) gives

$$V - V_0 = \left(\frac{iV_0^{-\frac{1}{2}}}{2\pi\epsilon_0 (2e/m)^{\frac{1}{2}}} \right) \ln(R/R_0)$$

The potential depression, V, between the beam edge and the lens is

$$V = 3.04 \times 10^{-2} iV_0^{-\frac{1}{2}} \ln(R/R_0) \quad (\text{A2 - 3})$$

where i is the current in microamperes and V_0 is the electron beam energy in volts.

In a similar manner the potential variation within a circular electron beam is given by

$$V = 1.52 \times 10^{-2} iV_0^{-\frac{1}{2}} \quad (\text{A2 - 4})$$

where i and V_0 are the current in microamperes and the mean energy of the electrons. This potential variation results in an increase in the electron energy distribution of the beam as a whole.

It is worth while noting that the above derivations are dependent on the net charge per unit length, which has been assumed is only due to the electrons. If ions were to be formed further consideration is required.

The case of an electron beam, passing through a field free region, is considered when the electron energy is sufficiently high to ionise any atoms present. Since the ions are moving much slower than the electrons, the number of ions required to cancel the negative space charge of the electron beam is quite low. Equilibrium

conditions will exist when the rate of production of ions is balanced by the rate at which they leave the interaction region. This loss rate is governed, at low ion densities, by the drift velocity which the original atom may have possessed or, at high ion densities by the velocity acquired by the repulsive field produced by the ions themselves.

The rate of formation of the ions is

$$R_f = \sigma_1 V n_a i/e$$

where σ_1 is the ionisation cross-section

V is the volume of the interaction region

n_a is the atom density, and

i is the electron current.

The rate of loss of ions is

$$R = A n_i v_i$$

where n_i and v_i are ion density and velocity, respectively in the interaction region, and

A is the area through which the ions escape.

At equilibrium

$$\sigma_1 V n_a i/e = A n_i v_i \quad (A2 - 5)$$

In the first situation the velocity of the ions is about 1/4000 that of the velocity of the electrons present. For a 10 μ A electron beam current there is about 6×10^5 electrons/cm. To cancel the space charge depression will only require an ion density of about 100 ions/cm. The potential depression will diminish linearly with the atomic intensity increasing.

In the latter case the determination of v_i , which is dependent on n_i and the dimensions of the "field free"

region becomes very involved and shall not be solved here. However, a rough outline will be given.

Treating the ions as diffusing from a line of charge, the potential, set up by the ions, will be proportional to the charge, $n_i e$, of the ions. From this charge an expression for v_i could be obtained, which when substituted into equation (A2 - 5) results in

$$n_i \propto (i n_a \sigma_i)^{\frac{2}{3}}$$

The potential produced by the ion space charge will vary as $n_a^{\frac{2}{3}}$, and will be insignificant until n_a exceeds some critical value, after which, it will increase rapidly in magnitude.

APPENDIX III.

DETECTION OF INSTRUMENTAL ASYMMETRIES.

In the arrangement of the Mott spin analyser there are two detectors at scattering angles of 45° in the plane of scattering. These detectors will be mainly sensitive to instrumental asymmetries only, since at 45° the Sherman function is very low. The method used for calculating the polarisation values has assumed that

$$\frac{A(+)}{A(-)} = 1 \quad (5 - 7)$$

The detectors at 45° provide a check on the validity of equation (5 - 7)

Van Klinken (1965) has shown, (assuming Rutherford scattering) that for a beam hitting the gold foil off-centre by a distance y , and inclined at an angle δ to the normal of the foil, will result in an asymmetry given by

$$R = \frac{I_{\text{up}}}{I_{\text{down}}} \approx 1 - 4 \left(\delta - \frac{y}{h} \right) \frac{\sin \theta}{1 - \cos \theta}$$

where θ is the scattering angle being studied and h is the distance of either detector to the centre of the foil.

The deviation from 1 is given by B with

$$B \propto \frac{\sin \theta}{1 - \cos \theta}$$

Hence $B(45^\circ) = 4.4 B(120^\circ)$ if $h(45^\circ) = h(120^\circ)$

Any misalignment in the beam is 4 times more sensitive with the 45° detectors than with the 120° detectors.

Substituting for R in equation (5 - 7) results in

$$R = \frac{A(+)}{A(-)} = \frac{\left[1 - 4(\delta - y/h) \left(\frac{\sin \theta}{1 - \cos \theta} \right) \right]}{\left[1 - 4(\delta' - y/h) \left(\frac{\sin \theta}{1 - \cos \theta} \right) \right]}$$
$$= 1 - 4\left(\eta - \frac{x}{h}\right) \left(\frac{\sin \theta}{1 - \cos \theta} \right)$$

where $\eta = \delta - \delta'$

$x = y - y'$

Again it can be seen that this value will be about four times more sensitive at 45° than at 120° . By monitoring this ratio for the 45° detectors any instrumental asymmetries can be noticed and due allowance made in any values affected with instrumental asymmetries.

APPENDIX IV

USES OF FORMVAR*

AS A PROTECTIVE FILM AGAINST MERCURY ON DETECTORS.

The front gold contact on solid state detectors is easily attacked by any mercury present in a vacuum system, and in this experiment it can arise from the mercury diffusion pump being used, and more likely from the background mercury atmosphere due to the mercury beam in the main scattering chamber. Damage to this gold layer results in the detector having 'dead spots' and more seriously greatly increases the detector noise such that, if bad enough, saturation of the amplifier output occurs whenever the bias voltage is switched on, no matter at what level.

A method of coating the detectors with a thin film ($\sim 20 \mu\text{E}/\text{cm}^2$) of formvar by immersion in a solution of formvar in chloroform (Muggleton and Parsons, 1963) was tried and proved successful for the smaller (100 mm^2) detectors but the larger (300 mm^2) detectors were damaged. The chloroform attacking both the epoxy surrounding the detectors and lifting the silver contact from the gold film on the front. An alternative method of slow vacuum evaporation of formvar at about 100°C was tried (Hils and McGregor, 1973) and this proved entirely successful for detectors of any type of construction.

Detectors thus treated subsequently showed no signs of damage from mercury, with no noticeable deterioration in their resolution for 100 keV electrons.

* polyvinyl formal (Formvar 15/95E) supplied by Monsanto Corp. - used extensively in electron microscopy as a support film.

AS A SUBSTRATE.

Using the immersion method, described above, controllable films of formvar were deposited on glass slides. Marking out the size and shape of backing required with a knife, allowed it to be easily floated off when the glass slide was slowly lowered into a bath of water. The aluminium foilholder could be raised from underneath the film for mounting. The formvar film went taut as any adhering water evaporated from it. The film was then suitable as a substrate for subsequent evaporation of very thin gold films. These films proved to be sufficiently strong that there was little danger of bursting them whilst letting the apparatus up to air. For this reason all of our gold foils were subsequently backed with formvar.

Since the films could be made extremely thin ($20 \mu\text{g}/\text{cm}^2$) and were composed of light atoms ($Z \leq 8$) these films did not seriously influence the scattering signal from the gold.

REFERENCES.

- Bargmann, Michel, Telegdi, (1959), Phys. Rev. Letters, 2, 435.
- Baum & Koch (1969), Nucl. Instr. Methods. 71, 189.
- Baum, Lubell & Raith, (1971), Bullt. Am. Phys. Soc., 16, 586.
- Baum, Lubell & Raith, (1972), Phys. Rev. A., 5, 1073.
- Benson, (1970), M.Sc. Thesis - University of Stirling (unpublished).
- Böhning, (1968), Z. Physik, 208, 286.
- Busch, Campagne & Seigman, (1970), J. Appl. Phys., 41, 1044.
- Busch, Campagne & Seigman, (1971), J. Appl. Phys., 42, 1781.
- Byrne, (1971), J. Phys. B., 4, 940.
- Byrne & Farago, (1965), Proc. Phys. Soc. (London) A, 86, 801.
- Campbell, Brash & Farago, (1971), Phys. Letters, 36A, 449.
- Campbell, Brash & Farago, (1972), Proc. Roy. Soc. Edin. 70A, 165.
- Coiffer, (1967), Compt. Rend., 264, 454.
- Cooper, (1962), Phys. Rev., 128, 681.
- Drukarev & Ob'edkov, (1971) J.E.T.P., 61, 534.
- van Duinen & Aalders, (1968), Nucl. Phys., A115, 353.
- Duweke, Kirchner Reichert & Staudt, (1973), J. Phys. B. 6, 1208.
- Eckstein, (1970), Internal Report No. 1pp7/1 Institut für Plasmaphysik, Munich, (unpublished).
- Fano, (1969A), Phys. Rev., 178, 131.
- Fano, (1969B), Phys. Rev., 184, 250.
- Farago, (1956), Adv. in Electronics and Electron Phys. (L. Marton, Ed.), Academic Press, 21, 1.
- Firester, (1966), Rev. Sci. Instrum., 37, 1264.
- Franzen & Gupta, (1965), Phys. Rev. Letters, 15, 819.

- Gehenn, Haug, Wilmers & Deichsel, (1969), Z. angew. Physik, 28, 142.
- Heinzmann, Kessler & Lorenz, (1970A), Phys. Rev. Letters, 24, 87.
- Heinzmann, Kessler & Lorenz, (1970B), Z. Physik, 240, 42.
- Hils & McGregor, (1973), Rev. Sci. Instrum., 44, 911.
- Hughes, Long, Lubell, Posner & Raith, (1972), Phys. Rev. A, 5, 195.
- Jost, (1972), VI Yugoslav Symposium on Physics of Ionised Gases, Ed. M.V.Kurepa.
- Jost & Kessler, (1966), Z. Physik, 195, 1.
- Kessler, (1969), Rev. Mod. Phys., 41, 3.
- Kessler & Lorenz, (1970), Phys. Rev. Letters, 24, 87.
- Kleinpoppen, (1971), Phys. Rev. A, 3, 2015.
- van Klinken, (1965), Proefschrift, Rijksuniversiteit te Gronigen. (unpublished)
- Kuyatt, Simpson & Mielczarek, (1965), Phys. Rev., 138, A385.
- Long, Raith & Hughes, (1965), Phys. Rev. Letters, 15, 1.
- Lubell & Raith, (1969), Phys. Rev. Letters, 23, 211.
- McCusker, Hatfield & Walters, (1969), Phys. Rev. Letters, 22, 817.
- McCusker, Hatfield & Walters, (1972), Phys. Rev. A, 5, 177.
- Massey & Rona, (1941), Proc. Roy. Soc. A, 177, 341
- Meister, (1962), Z. Physik, 166, 468.
- Mott, (1929), Proc. Roy. Soc. A, 124, 426.
- Mott, (1932), Proc. Roy. Soc. A, 135, 429.
- Mott & Massey, (1965), The Theory of Atomic Collisions, 3rd Edition, Oxford University Press.
- Muggleton & Parsons, (1963), Rev. Sci. Instrum., 34, 804.
- Pierce, (1940), J. of Appl. Phys., 11, 548.
- Pierce, (1954), Theory and Design of Electron Beams, Van Nostrand.
- Raith, (1969), Atomic Physics, (B. Bederson, V.W. Cohen, & F.M.J. Pickanik, Editors) Plenum Press, 389.

- Regenfus & Sutsh, (1974), Z. Physik, 266, 319
- Reichert & Deichsel, (1967), Physics Letters, 25A, 560
- Shull, Chase & Myers, (1943), Phys. Rev., 63, 29
- Simpson & Kuyatt, (1963A), Rev. Sci. Instrum., 34, 265
- Simpson & Kuyatt, (1963B), J. of Research Nat. Bur.
Standards, 67C, 279
- Simpson & Martin, (1961), Rev. Sci. Instrum., 32, 801
- Wilmers, Haug & Deichsel, (1969), Z. angew Physik, 27, 204

Attention is drawn to the fact that the copyright of this thesis rests with its author.

This copy of the thesis has been supplied on condition that anyone who consults it is understood to recognise that its copyright rests with its author and that no quotation from the thesis and no information derived from it may be published without the author's prior written consent.